# SENSOR AND SENSORLESS SPEED CONTROL OF PERMANENT MAGNET SYNCHRONOUS MOTOR USING EXTENDED HIGH-GAIN OBSERVER

By

Abdullah Ahmad Alfehaid

A DISSERTATION

Submitted to
Michigan State University
in partial fulfillment of the requirements
for the degree of

Electrical Engineering–Doctor of Philosophy

2021

ABSTRACT

SENSOR AND SENSORLESS SPEED CONTROL OF PERMANENT MAGNET SYNCHRONOUS MOTOR USING EXTENDED HIGH-GAIN OBSERVER

By

Abdullah Ahmad Alfehaid

Control of the speed as well as shaping the speed transient response of a surface-mounted Permanent Magnet Synchronous Motor (PMSM) is achieved using the method of feedback linearization and extended high-gain observer. To recover the performance of feedback linearization, an extended high-gain observer is utilized to estimate both the speed of the motor and the disturbance present in the system. The observer is designed based on a reduced model of the PMSM, which is realized through the application of singular perturbation theory. The motor parameters are assumed uncertain and we only assume knowledge of their nominal values. The external load torque is also assumed to be unknown and time-varying, but bounded. Stability analysis of the output feedback system is given. Experimental results confirm the performance and robustness of the proposed controller. We also compare our proposed control method to the cascaded Proportional Integral (PI) speed controller. Then, we show the extension of this control method to solve the problem of sensorless control of PMSMs. The proposed sensorless control method is a back-emf based control scheme. Therefore, we design a high-gain back-emf observer in the α-β coordinates. Next, we transform the model of the PMSM to the d-q coordinates, which is performed using the estimated position, and close the loop around the currents with relatively fast PI controllers. After that, we reduce the model of the PMSM and design a third order Q-PLL extended high-gain observer as well as the speed feedback controller. Then, we perform a rigorous stability analysis of the closed loop system. Finally, we show simulation and experimental results to verify performance and robustness of the proposed controller.

Copyright by
ABDULLAH AHMAD ALFEHAID
2021

To my family

## ACKNOWLEDGMENTS

I would like to express my sincere appreciation to the following people:

To my mentor Dr. Hassan K. Khalil who patiently and excellently guided me through my research. Indeed, his advice and suggestions have been and will be of great help to me. His knowledge and passion for the subject is inspiring. He is truly an honest, a patient, and a humble person. I am honored to have been his student.

To Dr. Elias G. Strangas who offered his laboratory for conducting the experiments and for his valuable insights and assistance throughout the experiments.

To my dear parents Ahmad Alfehaid and Moodhy Alhomaidy who supported me, encouraged me, and believed in me. I sincerely thank them for teaching me the love of seeking knowledge.

And to my beloved wife Yara Almani who stood by me during my studies and created a comfortable atmosphere that allowed me to focus on my research. I could not have done it without you.

**TABLE OF CONTENTS**

## LIST OF TABLES

## LIST OF FIGURES

# CHAPTER 1

## Introduction

Permanent Magnet Synchronous Motors (PMSM) are increasingly used in industry and rapidly replacing induction and DC motors particularly in servo application such as CNC machines and robotic systems. PMSM are popular due to their efficiency, high power density, light weight, maintenance-free, and small size in comparison to DC and induction machines [1].

There are mainly two types of PMSMs: the *surface mounted permanent magnet machines* and the *interior magnet permanent magnet machines*. The predominant difference between the two is in the construction of the rotor. The surface mounted PMSMs are built with magnets mounted on the surface of the rotor while the interior magnet PMSMs are built with magnets embedded in the rotor. This structural difference leads to different mathematical models and hence leads to different control approaches. Throughout this work, only the surface mounted PMSM will be considered. Figure 1.1 shows a cross-sectional view of a four pole surface mounted PMSM [2].

PMSMs are not easy to control because they exhibit nonlinear dynamic behavior. The parameters of PMSMs are prone to temperature changes and variation in operating points, e.g the stator winding resistance can vary by as much as 200% of its nominal value and the rotor flux linkage can vary by as much as 20% of its nominal value [3]. Moreover, the load torque in many industrial applications is unknown, which adds more complication to the control problem. Addressing these challenges require robust control techniques, which have led to a variety of control approaches that have been successfully applied.

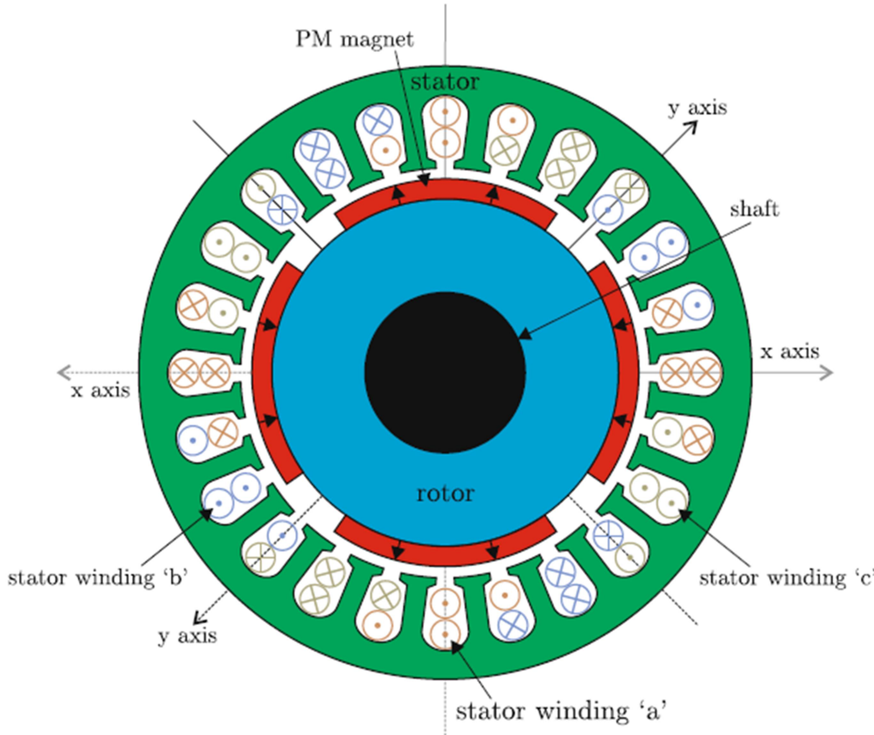


Figure 1.1. Cross-sectional view of a surface mounted PMSM [2].

High performance control of PMSM requires the Field Oriented Control (FOC) technique, which is realized by Park transformation. This transformation requires accurate knowledge of the rotor position of the motor and there are two main control techniques to achieve this transformation. The first control technique is using a position sensor and the second technique is controlling the motor without a position sensor, which is referred to as sensorless control. Typically, position sensors are employed to achieve FOC. However, there is an interest in eliminating the position sensor due to several factors that include cost, reduced wiring, which feeds noise to the system, increased reliability of the drive system, and size reduction. Therefore, it is sometimes desired to replace position sensors with mathematical tools that would achieve comparable results. By eliminating the position sensor, we introduce more complication to the problem of controlling the motor and thus sophisticated control methods are needed to design and analyze the controllers.

## 1.1 PMSM Control with Position Sensor

In industry, Proportional Integral (PI) controllers have been largely used in motor drive systems [4]. It is one of the simplest control techniques that offer good performance. However, PI controllers are not a good choice for speed control in applications where high performance and high precision are required.

Sliding mode Control (SMC) is becoming popular in PMSM drives due to its robustness to parameter variations. However, in the presence of disturbance and system parameter variation, the gains of the SMC are increased to guarantee robustness. This causes the system to exhibit a phenomenon called chattering. Improvements to SMC have taken place to reduce chattering such as using reaching laws and disturbance estimators. In [5] and [6], reaching laws are used to decrease chattering but this causes reduction in SMC robustness near the sliding surface and also increases the reaching time. In [6], an extended SM observer is used to estimate the disturbance and then cancel it in the control law. A key difference between this thesis and [6] is that the thesis includes the position measurement in the closed loop analysis as opposed to assuming the speed is measured. Furthermore, the proposed control method in this thesis is capable of shaping the transient response, whereas the work presented in [6] provides no means for shaping the transient response.

Adaptive control has been used to control the speed of PMSM. In [7], Model Reference Adaptive Control (MRAC) is used with disturbance estimator to avoid estimating each parameter of the motor separately. This work is similar to our work in two ways, 1) the disturbance is estimated and then canceled by the control law, 2) The transient response is shaped by the MRAC. However, our work is different in that we assume a time-varying non-vanishing disturbance that could depend on both states and time, and we do not assume that the speed is directly measured. In [7], the disturbance depends only on time and its derivative converges to zero as time tends to infinity.

Feedback linearization has also been used to control the speed of PMSM. In [8], feedback linearization is used with a PI controller to regulate the speed of PMSM. However, in real applications, feedback linearization, with or without PI controller, fails to shape the transient response in the presence of model uncertainty and unknown disturbance. Therefore, other tools must be used with feedback linearization to guarantee both stability and performance. In [9] and [10], feedback linearization is used with an extended observer to estimate speed and disturbance. Our work differs from [9] and [10] in that we reduce the model of the PMSM hence reducing the order of the observer. In comparison with [9], we design the controller based on the nominal parameters, and we do not use a PI controller in the speed loop. The work presented in [10] extends the observer with multiple states to estimate the disturbance while we extend the observer by only one state, thus requiring less computation.

Other control methods have been applied in speed control of PMSM such as fuzzy logic control with disturbance estimation [11] and [12], and predictive functional control with disturbance estimation [13]. Most of the recent work on PMSM control involves the use of disturbance estimation techniques to effectively increase the robustness of the control method. A wide range of different kinds of disturbance estimation techniques can be found in [14] and [15], and the references therein.

## 1.2 Sensorless Control of PMSM

In principle, there are two main approaches to sensorless position and speed estimation. The first approach is the fundamental excitation method where the back-EMF signals are estimated and then position and speed information are extracted by different mathematical means [16]-[26].The second approach is the signal injection method where high frequency signals, ideally much higher than the fundamental frequency, are injected in a predetermined fashion such that saliency features of the rotor are excited then exploited revealing estimates of position and speed [28]-[30]. This method has also been successfully applied for initial rotor position detection [31].

The major advantages of using the back-EMF method are its simplicity and it can easily be implemented on existing drive systems. However, a major drawback of this type is the loss of information at zero speed and signal corruption at very low speeds due to the smallness of signal to noise ration. On the other hand, the high frequency signal injection method typically works on all speed ranges unlike the back-EMF method. However, the disadvantages include induced vibration and acoustic noise, and increased power loss. Therefore, in [29]-[30] the back-emf based control method is combined with the high frequency injection method for a wider range speed control. When these methods are combined, the back-emf based control method is used for intermediate to high speed while the high frequency injection method is used when the motor operates in low speeds.

Our proposed controller uses the fundamental excitation method as a first step towards the estimation of position and speed of the rotor. To estimate the back-EMF signals, papers [16] and [17] use extended classical Luenberger observer, [18] uses the steady state algebraic expressions in the d-q coordinates, [19] and [20] use nonlinear observers, and [21]-[26] use sliding mode observers (SMO) with either reaching laws or low pass filters that are used to reduce chattering which adds complication to an already complex problem. We, on the other hand, estimate the back-EMF signals using extended high-gain observers in the $\alpha$-$\beta$ coordinates.

The high-gain observers are used to provide fast convergence rate.

We use a Quadrature Phase Locked Loop (Q-PLL) to estimate position and speed of the rotor as well as the disturbance from the back-EMF signals as opposed to estimating the position and speed via the arctangent function as in [19], [21] and [22], and the arccosine function as in [25]. Our Q-PLL is different than the Q-PLL used in [16]-[18], [24], and [26] in that we extend ours to estimate the disturbance while [16]-[18], [24], and [26] only estimate position and speed. To our knowledge, it seems to us that our proposed controller is first to extend the Q-PLL to estimate the disturbance.

In general, knowledge of the direction sign of the rotor's speed is essential for the stability of the Q-PLLs when operating in the positive and negative speeds. Attempts have been reported to solve this problem in [17] and [26]. Paper [17] uses a modified driving error signal yielding a sum-difference tangent function which risks division by zero when noise is present. Paper [26] also modifies the error signal using the double angle trigonometric identity, which shrinks the potential attraction region of the Q-PLL by half. We, on the other hand, simply use the sign of the speed reference.

Similar to [22], we use feedback linearization. However, we use a Q-PLL extended high-gain observer while [22] uses the arc tangent function to drive the observer. Also, we reduced the model of the motor based on the singular perturbation theory yielding a more accurate model than just assuming the quadrature current reference signal equal to the true quadrature current as in [22].

It can be seen that [16]-[26] lack closed loop analysis of the proposed control methods. The problem of analyzing the stability of the closed loop is not an easy task but very important.

We provide nonlinear analysis of the closed loop system which is made possible because we purposely design our system to be a multi-time scale one. Thus, we are able to use singular perturbation theory to show exponential stability of the equilibrium point of the closed loop system.

### 1.3 Mathematical Model of PMSM

The mathematical model of a surface mount PMSM in the two-phase-equivalent stator frame of reference, the α-β coordinates, is as follows [33]:

$$L\frac{di_\alpha}{dt} = -Ri_\alpha + k_m\omega\sin\left(n_p\theta\right) + u_\alpha \tag{1.1}$$

$$L\frac{di_\beta}{dt} = -Ri_\beta - k_m\omega\cos\left(n_p\theta\right) + u_\beta \tag{1.2}$$

$$J\frac{d\omega}{dt} = k_m\left(-i_\alpha\sin\left(n_p\theta\right) + i_\beta\cos\left(n_p\theta\right)\right) - B\omega - T_L \tag{1.3}$$

$$\frac{d\theta}{dt} = \omega \tag{1.4}$$

where $i_\alpha$ and $i_\beta$ are the two-phase equivalent stator currents, $u_\alpha$ and $u_\beta$ are the two-phase equivalent stator voltages, $\omega$ is the mechanical rotor speed, $\theta$ is the rotor position, $T_L$ is the external load, $R$ is the stator winding resistance, $L$ is the stator inductance and it is defined to be the sum of the magnetizing inductance and the leakage inductance of the stator, $n_p$ is the number of pole pairs, $k_m$ is the rotor magnetic flux linkage, $B$ is the coefficient of viscous friction, and $J$ is the moment of inertia of the rotor.

The relationship between the three phase voltages and their two-phase-equivalent voltages is given by,

$$\begin{bmatrix} u_\alpha \\ u_\beta \\ u_0 \end{bmatrix} = \Upsilon \begin{bmatrix} u_a \\ u_b \\ u_c \end{bmatrix}$$

where $u_a$, $u_b$, and $u_c$ are the three phase voltages, and $u_0$ is the zero-sequence voltage which is identically zero for a balanced three phase system. Also, $\Upsilon$ is the transformation matrix that relates the three phase components to their two phase equivalents and it is defined by

$$\Upsilon = \sqrt{\frac{2}{3}} \begin{bmatrix} 1 & -\frac{1}{2} & -\frac{1}{2} \\ 0 & \frac{\sqrt{3}}{2} & -\frac{\sqrt{3}}{2} \\ \frac{1}{\sqrt{2}} & \frac{1}{\sqrt{2}} & \frac{1}{\sqrt{2}} \end{bmatrix}$$

Similarly, the relationship between the three phase currents and their two-phase equivalent currents is governed by,

$$\begin{bmatrix} i_\alpha \\ i_\beta \\ i_0 \end{bmatrix} = \Upsilon \begin{bmatrix} i_a \\ i_b \\ i_c \end{bmatrix}$$

where $i_a$, $i_b$, and $i_c$ are the three phase currents, and $i_0$ is the zero-sequence current which is identically zero for a balanced three phase system.

The model of the PMSM shown above is highly nonlinear and is thus hard to control. However, it is much easier to control the motor in the rotor's frame of reference, the d-q coordinates, which is a rotating frame of reference. Figure 1.2 shows the relationship between the stator and the rotor frame of references. From Figure 1.2, the transformation from the α-β coordinates to the d-q coordinates is achieved by the following relationship,

$$\begin{bmatrix} u_d \\ u_q \end{bmatrix} = \begin{bmatrix} \cos(n_p\theta) & \sin(n_p\theta) \\ -\sin(n_p\theta) & \cos(n_p\theta) \end{bmatrix} \begin{bmatrix} u_\alpha \\ u_\beta \end{bmatrix}$$

and

$$\begin{bmatrix} i_d \\ i_q \end{bmatrix} = \begin{bmatrix} \cos(n_p\theta) & \sin(n_p\theta) \\ -\sin(n_p\theta) & \cos(n_p\theta) \end{bmatrix} \begin{bmatrix} i_\alpha \\ i_\beta \end{bmatrix}$$

where $u_d$ is the direct-axis input voltage, $u_q$ is the quadrature-axis input voltage, $i_d$ is the direct-axis current, and $i_q$ is the quadrature-axis current. Now, the system ( 1.1 )-( 1.4 ) can be rewritten in the rotor's frame of reference (d-q coordinates) as shown in ( 1.5 )-( 1.8 ).

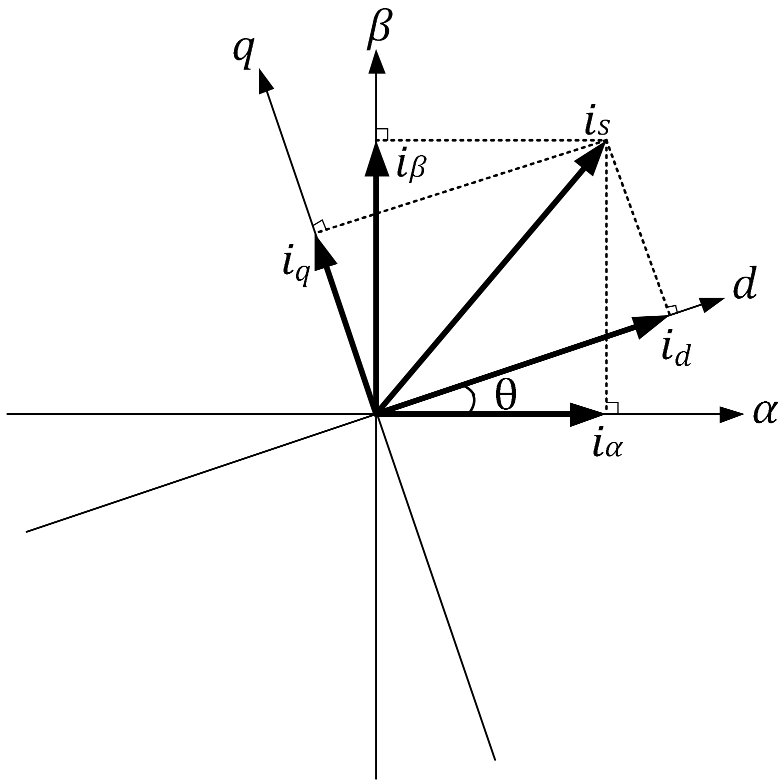


Figure 1.2. Relationship between the stator and the rotor frame of references.

$$L\frac{di_d}{dt} = -Ri_d + n_pL\omega i_q + u_d \qquad (1.5)$$

$$L\frac{di_q}{dt} = -Ri_q - n_pL\omega i_d - k_m\omega + u_q \qquad (1.6)$$

$$J\frac{d\omega}{dt} = k_m i_q - B\omega - T_L \qquad (1.7)$$

$$\frac{d\theta}{dt} = \omega \qquad (1.8)$$

The mathematical model of the PMSM in the rotor's frame of reference is still nonlinear; however, it is easier to control. Controlling the motor in this frame of reference is called Field Oriented Control (FOC) because stator currents are projected onto the rotor's magnetic field. This transformation reveals a very important piece of information that $i_q$ is the only torque producing current as seen in ( 1.7 ). Hence, the current $i_d$ should be regulated to zero to increase the efficiency of the system.

The mathematical model of the PMSM is subject to practical constraints. The stator voltages and currents cannot exceed certain limits; that is,

$$u_d{}^2 + u_q{}^2 \leq V_{max}{}^2$$

and

$$i_d{}^2 + i_q{}^2 \leq I_{max}{}^2$$

where $V_{max}$ and $I_{max}$ are the maximum stator voltage and current, respectively. In practical settings, these constraints are imposed on the model by the electrical ratings of both the motor and the inverter that is used to drive the motor. It is very important not to violate these limitations otherwise it would cause serious damage to the motor as well as to the inverter. Therefore, the controller design must account for these limitations.

The mathematical model of the PMSM possesses a very important feature. Typically, the electrical time constant is much smaller than the mechanical time constant. Subsequently, the electrical states are much faster than the mechanical states. Thus, the mathematical model of the PMSM is a two-time-scale system. It will be shown in the following chapters how singular perturbation theory can be utilized to take advantage of this feature in order to reduce the model of the PMSM.

## 1.4 Preliminaries

### 1.4.1 Performance Recovery of Feedback Linearization

Consider the following single-input-single-output nonlinear system in the normal form[32]:

$$\dot{x} = Ax + B[b(x, w) + a(x, w)u], \ y = Cx \tag{1.9}$$

where $x \in \mathbb{R}^n$ is the state, $u \in \mathbb{R}$ is the control input, $y \in \mathbb{R}$ is the measured output, $w$ is the disturbance input and it belongs to a known compact set $\mathcal{W} \subset \mathbb{R}^\ell$, $a(x, w) \geq a_0 > 0$, and $A$, $B$, and $C$ are defined by

$$A = \begin{bmatrix} 0 & 1 & 0 & \cdots & 0 \\ 0 & 0 & 1 & \cdots & 0 \\ \vdots & \vdots & \ddots & \ddots & \vdots \\ 0 & 0 & \cdots & 0 & 1 \\ 0 & 0 & \cdots & \cdots & 0 \end{bmatrix} \in \mathbb{R}^{n \times n}, B = \begin{bmatrix} 0 \\ 0 \\ \vdots \\ 0 \\ 1 \end{bmatrix} \in \mathbb{R}^n$$

$$C = \begin{bmatrix} 1 & 0 & \cdots & \cdots & 0 \end{bmatrix} \in \mathbb{R}^{1 \times n}$$

The objective here is to design an output feedback controller that not only stabilizes the origin $x = 0$ but also drives the system trajectories to closely match that of a target system. A natural choice for the target system would be:

$$\dot{x}^\star = (A - BK)x^\star, y = Cx^\star$$

where $K$ is chosen such that $(A - BK)$ is Hurwitz and $x^\star$ is the state of the target system whose trajectories meet the desired transient response.

The control objective can be met using the method of feedback linearization. Let us first consider the case where all the state variables of the system are available for measurement and the functions $a(x, w)$ and $b(x, w)$ are exactly known; then via feedback linearization a state feedback control $u$ that achieves the objectives is given by

$$u = \frac{-b(x, w) - Kx}{a(x, w)}$$

In practice; however, this control input may not be implementable or it may not deliver satisfactory performance due to two problems. First, some states of the system may not be accessible for measurement; or simply, we choose not to measure them due to technical or economic reasons. Second, only the nominal models of $a(\cdot)$ and $b(\cdot)$ are known. To solve these problems and recover the performance of feedback linearization, extended state observers are usually utilized. In particular, the following extended high-gain observer is used:

$$\begin{aligned} \dot{\hat{x}} &= A\hat{x} + B\left[\hat{\sigma} + \hat{b}(\hat{x}) + \hat{a}(\hat{x})u\right] + \begin{bmatrix} \frac{\rho_1}{\varepsilon} & \cdots & \frac{\rho_n}{\varepsilon^n} \end{bmatrix}^T (y - C\hat{x}) \\ \dot{\hat{\sigma}} &= \frac{\rho_{n+1}}{\varepsilon^{n+1}}(y - C\hat{x}) \end{aligned} \qquad (1.10)$$

where $\hat{x}$ is the estimate of $x$, $\hat{a}(x)$ and $\hat{b}(x)$ are nominal values of $a(x, \mathcal{w})$ and $b(x, \mathcal{w})$, respectively, $\hat{\sigma}$ is the estimate of the disturbance $\sigma$, defined by

$$\sigma = b(x, \mathcal{w}) - \hat{b}(x) + \big(a(x, \mathcal{w}) - \hat{a}(x)\big)u,$$

$\varepsilon > 0$ is a small parameter, and $\rho_1, \ldots, \rho_{n+1}$ are constants chosen such that the polynomial

$$s^{n+1} + \rho_1 s^n + \cdots + \rho_{n+1}$$

is Hurwitz. Under the assumption that $\hat{a}(\hat{x}) \geq a_0 > 0$, the control input $u$ can now be taken as:

$$u = \frac{-\hat{\sigma} - \hat{b}(\hat{x}) - K\hat{x}}{\hat{a}(\hat{x})}$$

High-gain observers are known to exhibit peaking in the estimation variables which might lead to instability of the closed loop system [34]. Therefore, to protect the system from the peaking phenomenon, the control law $u$ is saturated outside a compact set, that is,

$$u = Msat\left(\frac{-\hat{\sigma} - \hat{b}(\hat{x}) - K\hat{x}}{M\hat{a}(\hat{x})}\right)$$

where $sat(\cdot)$ is the saturation function and it is defined as $sat(z) = min\{1, |z|\}sign(z)$, and the saturation level $M$ is given by,

$$M > \max_{x \in \Omega_c, \mathcal{w} \in \mathcal{W}} \left| \frac{-b(x, \mathcal{w}) + Kx}{a(x, \mathcal{w})} \right|$$

where $\Omega_c$ is a compact set given by,

$$\Omega_c = \{x^T P x \leq c\}$$

and $x^T P x$ is a Lyapunov function in which $P = P^T > 0$ is the solution of the Lyapunov equation $P(A - BK) + (A - BK)^T P = -Q$ for some $Q = Q^T > 0$. The constant $c$ can be chosen large enough such that any given compact subset of $\mathbb{R}^n$ is included in the interior of $\Omega_c$. Under this control law, it is shown in [32] that the control law recovers the performance of feedback linearization in the presence of both model uncertainty and unknown disturbance. Moreover, the control law stabilizes the origin $x = 0$ in the case when the disturbance is constant

### 1.4.2 Quadrature Phase-Locked-Loop

One of the tools that are used in back-EMF based sensorless control of PMSM is the Q-PLL (Quadrature Phase-Locked-Loop) which we will use later in Chapter 3 when we expand our sensored case control method to the sensorless case. Therefore, in this context, a Q-PLL is used here as an observer to estimate the rotor's position and speed of the PMSM. A Q-PLL is basically a feedback loop system that mainly consists of two parts. The first part is the error generator and the second part is the error compensator. Figure 1.3 shows the basic construction of the Q-PLL.

In steady-state, the back-EMF signals of the PMSM in the alpha-beta coordinates are ideally sinusoidal signals having the same amplitude and frequency with a 90 degrees phase shift between them. For simplicity; let us assume that we have an online measurement of two sinusoidal signals and they are defined by

$$x_\alpha = \sin\big(\theta(t)\big)$$

$$x_\beta = -\cos\big(\theta(t)\big)$$

where $\theta(t)$ is an unknown continuous time-varying function. The question here is there a way to estimate $\theta(t)$ and its time derivative $\dot{\theta}(t) = \omega(t)$? Well, it turns out there are multiple ways to estimate $\theta(t)$ and $\omega(t)$ and one of these ways is using a Q-PLL.

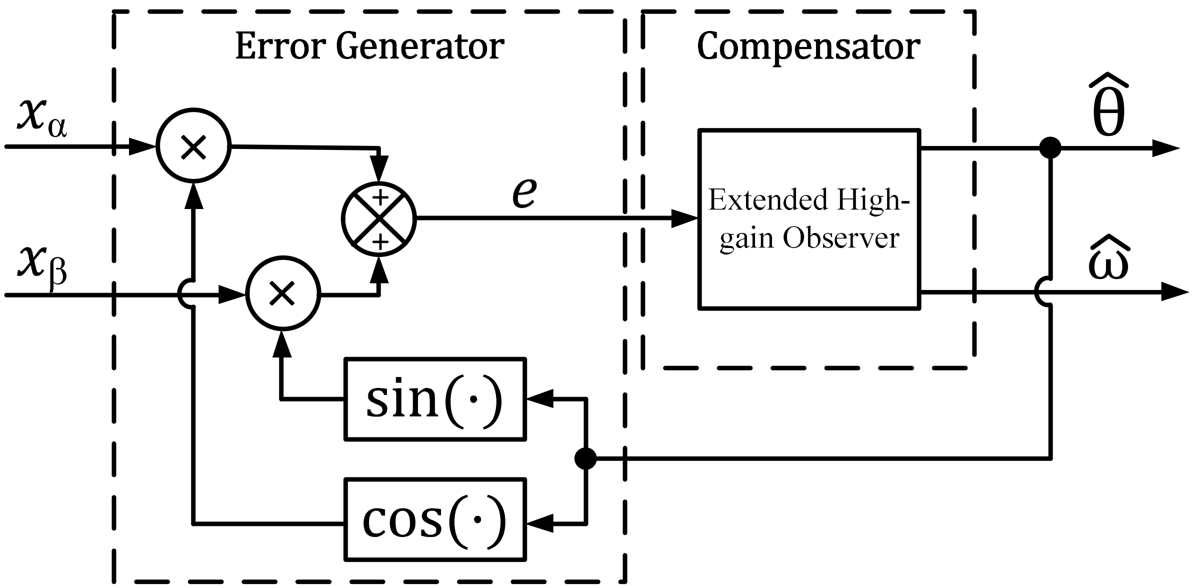


Figure 1.3. Q-PLL high-gain observer

First, let us look at the error generator part in Figure 1.3 which is very simple but effective. The error generator makes use of the trigonometric identity

$$\sin(x - y) = \sin(x)\cos(y) - \cos(x)\sin(y)$$

So, let $e$ be the generated error signal defined by

$$e = x_\alpha \cos(\hat{\theta}) + x_\beta \sin(\hat{\theta})$$

where $\hat{\theta}$ is an estimate of $\theta$. By substituting $x_\alpha$ and $x_\beta$ we arrive at

$$e = \sin(\theta)\cos(\hat{\theta}) - \cos(\theta)\sin(\hat{\theta})$$

which simplifies to

$$e = \sin(\theta - \hat{\theta})$$

It can be seen that we can control the error by steering $\hat{\theta}$ which is accomplished by using a compensator. The compensator can be a simple one such as a PI controller. However, here, we will use a high-gain observer because it offers fast convergence rate that can be achieved with little tuning effort. The Q-PLL high-gain observer can be constructed as

$$\frac{d\hat{\theta}}{dt} = \hat{\omega} + \frac{\rho_1}{\varepsilon} e$$

$$\frac{d\hat{\omega}}{dt} = \frac{\rho_2}{\varepsilon^2} e$$

that is

$$\frac{d\hat{\theta}}{dt} = \hat{\omega} + \frac{\rho_1}{\varepsilon} \sin(\theta - \hat{\theta})$$

$$\frac{d\hat{\omega}}{dt} = \frac{\rho_2}{\varepsilon^2} \sin(\theta - \hat{\theta})$$

where $\hat{\omega}$ is the estimate of $\omega$, $\rho_1$ and $\rho_2$ are positive constants, and $\varepsilon$ is a small positive parameter that directly controls the speed of estimation.

We can study the stability of this system using singular perturbation theory. Therefore, we make the following change of variables

$$\eta_1 = \frac{1}{\varepsilon}(\theta - \hat{\theta})$$

$$\eta_2 = \omega - \hat{\omega}$$

which leads to the following singularly perturbed system

$$\varepsilon\dot{\eta} = A\eta + B\psi + \varepsilon E\dot{\omega}$$

where $\eta = \begin{bmatrix} \eta_1 \\ \eta_2 \end{bmatrix}$, $A = \begin{bmatrix} -\rho_1\beta & 1 \\ -\rho_2\beta & 0 \end{bmatrix}$, $B = \begin{bmatrix} \rho_1 \\ \rho_2 \end{bmatrix}$, $\psi = -\left[\frac{\sin(\varepsilon\eta_1)}{\varepsilon\eta_1} - \beta\right]\eta_1$, and $E = \begin{bmatrix} 0 \\ 1 \end{bmatrix}$. $\beta > 0$ is a constant chosen such that

$$\left[\frac{\sin(\varepsilon\eta_1)}{\varepsilon\eta_1} - \beta\right] > 0$$

With the assumption that $\dot{\omega}$ is bounded by a constant independent of $\varepsilon$, the boundary layer of this system is written as

$$\varepsilon\dot{\eta} = A\eta + B\psi$$

It can be easily verified by linearization that this boundary layer has an exponentially stable equilibrium point at the origin. We can further analyze the system using nonlinear tools which tells us more about the stability of the system away from the equilibrium point. Towards that end, we augment the output equation $y = C\eta$ where $C = [1 \quad 0 \quad 0]$ to the boundary layer. This boundary layer can now be represented as in Figure 1.4 which shows a negative feedback connection of the transfer function

$$\Gamma(\varepsilon s) = \frac{\rho_1(\varepsilon s) + \rho_2}{(\varepsilon s)^2 + \beta(\rho_1(\varepsilon s) + \rho_2)}$$

and the nonlinearity $\psi$ which belongs to the sector $[\beta, \infty]$. This system structure is a textbook example of how Popov's criterion can be applied. The transfer function $\Gamma(\varepsilon s)$ is strictly positive real if and only if $\rho_1$, and $\rho_2$ are chosen positive and the following inequality is satisfied

$$\beta{\rho_1}^2 - \rho_1 > 0$$

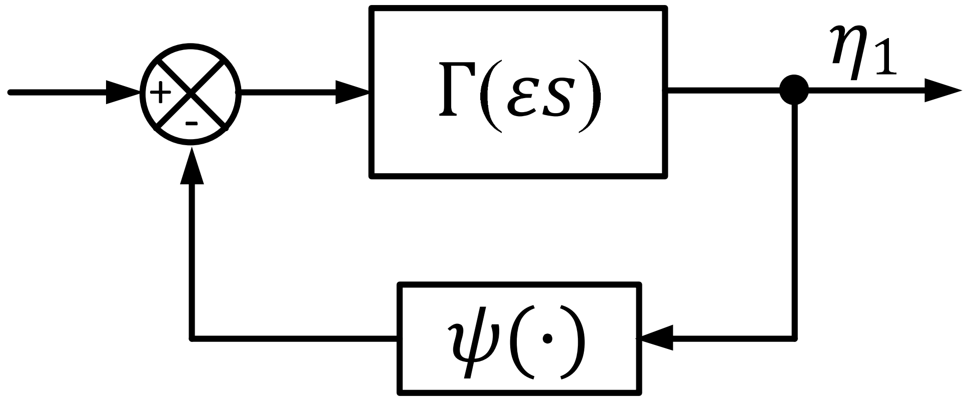


Figure 1.4. Block diagram of the boundary layer of the Q-PLL

We Use the Kalman-Yakubovic-Popov lemma [34], Lemma 6.3] to obtain a quadratic Lyapunov function; that is,

$$V(\eta) = \frac{1}{2}\eta^T P\eta$$

where $P$ is the positive definite symmetric solution of the Kalman-Yakubovic-Popov equations

$$PA + A^T P = -N^T N - \zeta P$$

$$PB = C^T$$

In which $\zeta > 0$. It can be shown that the time derivative of $V$ along the boundary layer satisfies

$$\varepsilon\dot{V}(\eta) \leq -\frac{1}{2}\zeta\lambda_{min}(P)\|\eta\|^2$$

which shows exponential stability of the boundary layer. Take

$$W(\eta) = \frac{1}{2}\eta^T P\eta$$

for the full system which has a time derivative satisfying

$$\varepsilon\dot{W}(\eta) \le -\frac{1}{2}\zeta\lambda_{min}(P)\|\eta\|^2 + \varepsilon\eta^T PE\dot{\omega} \le -\frac{1}{2}\zeta\lambda_{min}(P)\|\eta\|^2 + \varepsilon k\|\eta\|$$

where $k$ is an upper bound of $\|PE\||\dot{\omega}|$. Hence,

$$\varepsilon\dot{W}(\eta) \le -\frac{1}{4}\zeta\lambda_{min}(P)\|\eta\|^2, \qquad \forall\ \|\eta\| \ge \frac{4\varepsilon k}{\zeta\lambda_{min}(P)}$$

Consider the set

$$\Omega = \left\{W \le \frac{c}{\varepsilon^2}\right\}$$

where $c > 0$. Then,

$$\left\{\|\eta\|^2 \le \frac{c}{\varepsilon^2\lambda_{max}(P)}\right\} \subset \left\{W \le \frac{c}{\varepsilon^2}\right\} \subset \left\{\|\eta\|^2 \le \frac{c}{\varepsilon^2\lambda_{min}(P)}\right\}$$

Therefore, $\Omega$ is positively invariant when

$$\frac{c}{\varepsilon^2\lambda_{max}(P)} \ge \left(\frac{4\varepsilon k}{\zeta\lambda_{min}(P)}\right)^2$$

which is true for sufficiently small $\varepsilon$. Now, all trajectories starting in $\Omega$ stay in $\Omega$ for all future time. However, we want the trajectories to satisfy the sector condition which is satisfied for $\theta - \hat{\theta} \le \gamma < \pi$, where $\gamma$ depends on $\beta$. Equivalently, $|\eta_1| < \frac{\gamma}{\varepsilon}$. The maximum of $|\eta_1|$ over $\Omega$ is given by

$$\sqrt{\frac{2c}{\varepsilon}}\left\|[1 \quad 0]P^{-1/2}\right\|$$

Therefore, choosing $c$ large enough to satisfy

$$\sqrt{\frac{2c}{\varepsilon}}\left\|\begin{bmatrix}1 & 0\end{bmatrix}P^{-1/2}\right\| < \gamma$$

ensures that the sector condition is satisfied. Eventually, all trajectories starting in $\Omega$ will enter a set of the form

$$\Omega_1 = \{W \leq \varepsilon^2 c_1\}$$

where $c_1 > 0$. $\Omega_1$ is positively invariant for

$$\frac{\varepsilon^2 c_1}{\lambda_{max}(P)} \geq \left(\frac{4\varepsilon k}{\zeta\lambda_{min}(P)}\right)^2$$

which is satisfied by choosing $c_1$ large enough.

We should note that the previous discussion is only preliminary for readers who are not familiar with Q-PLLs. When Q-PLLs are used in sensorless control of PMSM, the back-EMF signals are first estimated then passed to the Q-PLL. Also, the back-EMF signals are ideally pure sinusoidal only in steady state. Therefore, during transient there will be other components involved from both the transient response of the PMSM subsystem and from the back-EMF observer which adds complication to the problem.

## CHAPTER 2

Up to this point, we have shown different types of control approaches that have been applied in the past to solve the problem of controlling the speed of PMSMs. We have also introduced and described the mathematical model of the PMSM. In this chapter we propose a new control method that solves the problem of controlling the speed of PMSMs with the use of a position sensor. First, we close the loop around the currents with relatively fast PI controllers. Then, we reduce the model of the PMSM and design a third order extended high-gain observer as well as the speed feedback controller. After that, we perform stability analysis of the closed loop system. Then, we show simulation and experimental results to verify the performance and robustness of the proposed controller. Finally, comparison between the proposed control method and the cascaded Proportional Integral (PI) speed controller is given based on experimental results. The new proposed control approach is based on the control technique that was described in section 1.4.

### Speed Control with a Position Sensor

The goal is to design an output feedback controller that can achieve the following objectives:

1) Regulating the speed of the PMSM to a reference signal $\omega_{ref}$ in the presence of both bounded external load $T_L$ and parameters uncertainty.
2) The ability to shape the transient response of the speed.

The aforementioned objectives can be realized using the method described in [32] with two different approaches. The first approach is a direct application of the method described in chapter 1 and it is based on the complete model of the PMSM. The second approach is based on a reduced mathematical model of the PMSM that is obtained by utilizing the singular perturbation method; consequently, requiring a lower order extended high-gain observer. In both cases the rotor position $\theta$ and the three phase currents $i_a$. $i_b$, and $i_c$ are measured, thus $i_d$ and $i_q$ are known.

## 2.1 Proposed Control Algorithm

The proposed control algorithm consists of three main parts, fast inner current loops, speed and disturbance estimation using the measured position via an extended high-gain observer, and speed shaping and regulation via feedback linearization. The block diagram of the control algorithm is shown in Figure 2.1. The inner current loops will be designed purposely to be fast which will further increase the time scale separation between the electrical and mechanical subsystems. This allows the system to be reduced via singular perturbation theory. As a result, a reduced order extended high-gain observer is designed, which is easier to implement.

### 2.1.1 Current Loops

The fast current loops are made possible by the smallness of the electrical time constant $\tau_e = \frac{L}{R}$ and the use of PI controllers for $i_d$ and $i_q$. The current PI controllers are used here to provide means to regulate the currents and to further increase the time scale separation between the fast dynamics of the electrical subsystem and the mechanical subsystem. The design of the current PI controllers starts by defining the current tracking errors as:

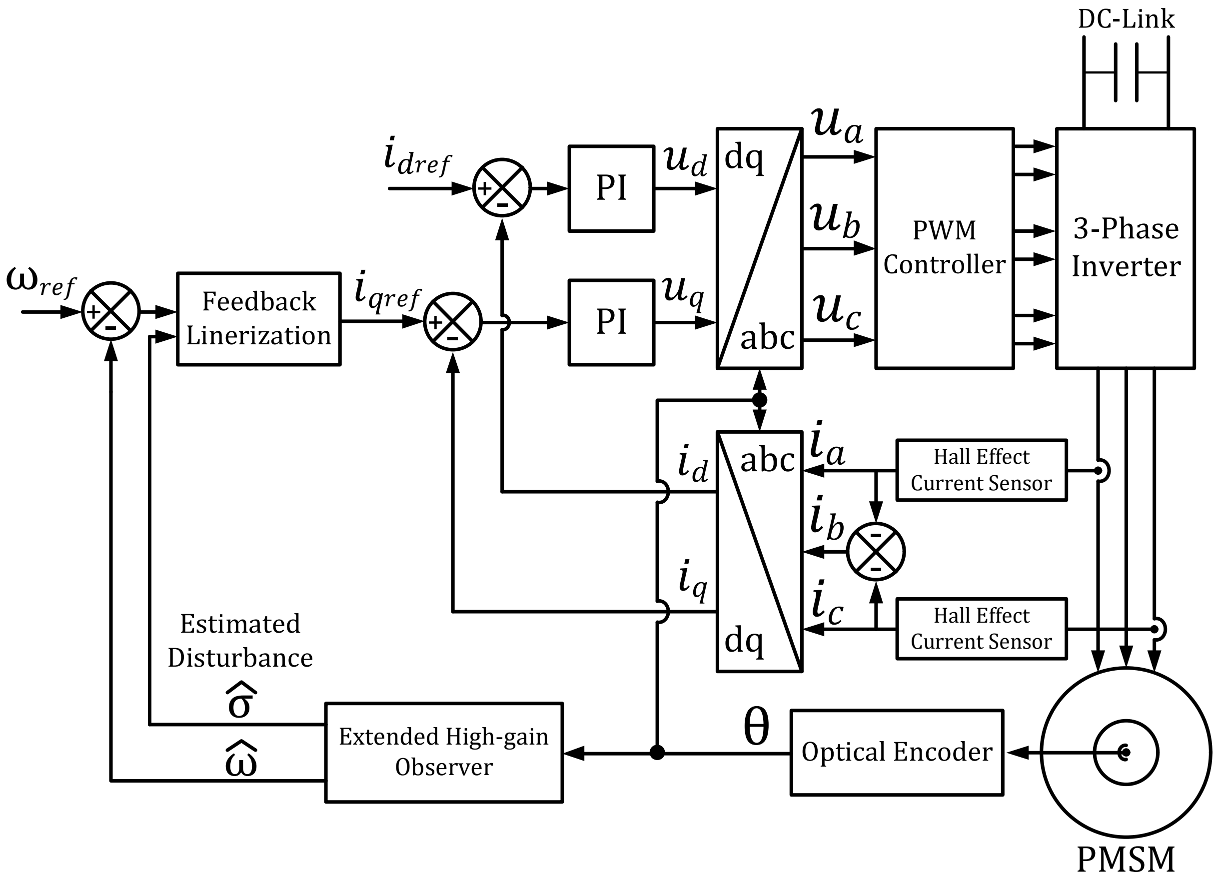


Figure 2.1. Block diagram of the proposed control algorithm.

$$e_d = i_{d_{ref}} - i_d \tag{2.1}$$

$$e_q = i_{q_{ref}} - i_q \tag{2.2}$$

where $e_d$ and $e_q$ are the direct and quadrature current-tracking errors, respectively; $i_{d_{ref}}$ and $i_{q_{ref}}$ are the direct and quadrature current reference signals, respectively. $i_{d_{ref}}$ is assumed constant. The control inputs $u_d$ and $u_q$ are chosen as follows:

$$\begin{aligned} u_d &= k_p e_d + x_d \\ u_q &= k_p e_q + x_q \end{aligned} \tag{2.3}$$

with

$$x_d = k_i \int_0^t e_d(\acute{t})d\acute{t} \tag{2.4}$$

$$x_q = k_i \int_0^t e_q(\acute{t})d\acute{t} \tag{2.5}$$

where $\acute{t}$ is a dummy integration variable, $k_p$ is the proportional gain, $k_i$ is the integral gain, and $x_d$ and $x_q$ are the integrals of $e_d$ and $e_q$, respectively. Substituting $u_d$ and $u_q$ into ( 1.5 ) and ( 1.6 ) yields the following current tracking error equations:

$$\tau \frac{de_d}{dt} = -e_d + \frac{1}{R+k_p}\left(Ri_{d_{ref}} - x_d\right) - \tau\left[n_p\omega\left(i_{q_{ref}} - e_q\right)\right] \tag{2.6}$$

$$\tau \frac{de_q}{dt} = -e_q + \frac{1}{R+k_p}\left(Ri_{q_{ref}} + k_m\omega - x_q\right) + \tau\left[\frac{di_{q_{ref}}}{dt} + n_p\omega\left(i_{d_{ref}} - e_d\right)\right] \tag{2.7}$$

where $\tau = \frac{L}{R+k_p}$ is the time constant of the current tracking errors. $\tau$ can be made much smaller than $\tau_e = \frac{L}{R}$ by increasing the proportional gain $k_p$ of the PI controller; and therefore increasing the time separation between the electrical and mechanical subsystems. This will help in reducing the model of the PMSM and thus reducing the order of the extended high-gain observer.

### 2.1.2 PMSM Model Reduction

By the proper choice of the current controller gains $k_p$ and $k_i$, $e_{i_d}$ and $e_{i_q}$ are made fast and they will reach quasi-steady-state much faster than other state variables in the system. This induces a two time scale system, with fast and slow dynamics, which gives us an advantage and invites the use of the singular perturbation method [34] to reduce the model and then design the extended high-gain observer.

The quasi-steady-state of the fast variables $e_{i_d}$ and $e_{i_q}$, obtained by setting $\tau = 0$ in ( 2.6 ) and ( 2.7 ) is,

$$e_d = \frac{1}{R + k_p}\left(Ri_{d_{ref}} - x_d\right) \tag{2.8}$$

$$e_q = \frac{1}{R + k_p}\left(Ri_{q_{ref}} + k_m\,\omega - x_q\right) \tag{2.9}$$

Substitute ( 2.2 ) into ( 1.7 ) to obtain the equation:

$$\frac{d\omega}{dt} = \frac{k_m}{J}\left(i_{q_{ref}} - e_q\right) - \frac{B}{J}\omega - \frac{1}{J}T_L \tag{2.10}$$

where $i_{q_{ref}}$ is viewed as the control input. Now, ( 2.4 ), ( 2.5 ), ( 2.8 ), ( 2.9 ), and ( 2.10 ) are used to arrive at the following slow dynamics of the system:

$$\frac{dx_d}{dt} = \frac{k_i}{R + k_p}\left(Ri_{d_{ref}} - x_d\right) \tag{2.11}$$

$$\frac{dx_q}{dt} = \frac{k_i}{R + k_p}\left(Ri_{q_{ref}} + k_m\,\omega - x_q\right) \tag{2.12}$$

$$\frac{d\omega}{dt} = \alpha i_{q_{ref}} - \gamma\omega + \mu x_q - \frac{1}{J}T_L \tag{2.13}$$

where $\alpha = \frac{k_m k_p}{J(R+k_p)}$ , $\gamma = \frac{{k_m}^2}{J(R+k_p)} + \frac{B}{J}$ , $\mu = \frac{k_m}{J(R+k_p)}$.

### 2.1.3 Feedback Linearization under State Feedback

The method of feedback linearization is used here to regulate the speed of the PMSM to a reference signal $\omega_{ref}$. It also provides means to shape the transient response of the speed. The speed tracking error is defined as

$$e_\omega = \omega_{ref} - \omega \tag{2.14}$$

where $\omega_{ref}$ is the speed reference signal. Using ( 2.13 ) and ( 2.14 ) we obtain the following:

$$\frac{de_\omega}{dt} = \frac{d\omega_{ref}}{dt} + \gamma\omega_{ref} - \alpha i_{q_{ref}} - \gamma e_\omega - \mu x_q + \frac{1}{J}T_L \qquad (2.15)$$

It is desired to match the transient response of the speed tracking error to that of the following target system

$$\frac{de_\omega{}^\star}{dt} = -k_\omega e_\omega{}^\star \qquad (2.16)$$

where $k_\omega > 0$. If the speed $\omega$ were available for measurement and the external load $T_L$ were exactly known, the state feedback control law that achieves the objectives would have been given by

$$i_{q_{ref}} = \frac{1}{\alpha}\left[\frac{d\omega_{ref}}{dt} + \gamma\omega_{ref} + (k_\omega - \gamma)e_\omega - \mu x_q + \frac{1}{J}T_L\right]$$

$$\triangleq \bar{\psi}\left(e_\omega, x_q, \omega_{ref}, \frac{d\omega_{ref}}{dt}, T_L\right) \qquad (2.17)$$

The closed-loop system formed of ( 2.11 ), ( 2.12 ), ( 2.15 ), and ( 2.17 ) is given by

$$\dot{\xi} = A_1\xi \qquad (2.18)$$

where $\xi = \left[x_d - Ri_{d_{ref}}, x_q - \bar{x}_q, e_\omega\right]^T$, $\bar{x}_q$ satisfies the equation

$$\frac{d\bar{x}_q}{dt} = \frac{k_i}{(R + k_p)}\left[R\bar{\psi}\left(0, \bar{x}_q, \omega_{ref}, \frac{d\omega_{ref}}{dt}, T_L\right) + k_m\omega_{ref} - \bar{x}_q\right]$$

and

$$A_1 = \begin{bmatrix} -\dfrac{k_i}{R+k_p} & 0 & 0 \\ 0 & -\dfrac{k_i}{k_p} & -\dfrac{k_i}{k_m k_p}\left({k_m}^2 - RJ\left(k_\omega - \dfrac{B}{J}\right)\right) \\ 0 & 0 & -k_\omega \end{bmatrix} \tag{2.19}$$

The matrix $A_1$ is Hurwitz.

### 2.1.4 Feedback Linearization under Output Feedback

Since the external load $T_L$ is assumed unknown and only the nominal parameters of the PMSM are known, equation ( 2.13 ) is rewritten as:

$$\frac{d\omega}{dt} = \hat{\alpha} i_{q_{ref}} - \hat{\gamma}\omega + \hat{\mu} x_q + \sigma \tag{2.20}$$

where $\hat{\alpha}$, $\hat{\gamma}$ and $\hat{\mu}$ are the nominal values of $\alpha$, $\gamma$ and $\mu$, and $\sigma$ is the disturbance, which is defined by

$$\sigma = (\alpha - \hat{\alpha}) i_{q_{ref}} - (\gamma - \hat{\gamma})\omega + (\mu - \hat{\mu}) x_q - \frac{1}{J} T_L$$

The assumption here is that the rotor position is directly measured and the speed of the PMSM is not available for measurement. Therefore, the measured rotor position is used to drive an extended high-gain observer that estimates both the speed of the motor $\omega$ and the disturbance $\sigma$. The extended high-gain observer, formed using ( 1.8 ) and ( 2.20 ), is given by

$$\frac{d\hat{\theta}}{dt} = \hat{\omega} + \frac{\rho_1}{\varepsilon}\left(\theta - \hat{\theta}\right) \tag{2.21}$$

$$\frac{d\hat{\omega}}{dt} = \hat{\alpha} i_{q_{ref}} - \hat{\gamma}\hat{\omega} + \hat{\mu} x_q + \hat{\sigma} + \frac{\rho_2}{\varepsilon^2}\left(\theta - \hat{\theta}\right) \tag{2.22}$$

$$\frac{d\hat{\sigma}}{dt} = \frac{\rho_3}{\varepsilon^3}\left(\theta - \hat{\theta}\right) \tag{2.23}$$

where $\hat{\theta}$, $\hat{\omega}$, and $\hat{\sigma}$ are the estimates of $\theta$, $\omega$, and $\sigma$, respectively, $\rho_1$, $\rho_2$, and $\rho_3$ are chosen such that

$$s^3 + \rho_1 s^2 + \rho_2 s + \rho_3 = 0 \quad (2.24)$$

is Hurwitz, and $\varepsilon > 0$ is a small parameter. If we have not used the singular perturbation method to reduce the model, the order of the extended high-gain observer would have been 4, which would be harder to implement.

To formulate the output feedback controller, we need to rewrite the speed tracking error in its nominal form which can be obtained using ( 2.14 ) and ( 2.20 ) as

$$\frac{de_\omega}{dt} = \frac{d\omega_{ref}}{dt} + \hat{\gamma}\omega_{ref} - \hat{\alpha} i_{q_{ref}} - \hat{\gamma} e_\omega - \hat{\mu} x_q - \sigma$$

Since the objective here is to drive the speed tracking error trajectory to match that of the target system ( 2.16 ), the output feedback control law is taken as

$$i_{q_{ref}} = \frac{1}{\hat{\alpha}}\left[\frac{d\omega_{ref}}{dt} + \hat{\gamma}\omega_{ref} + (k_\omega - \hat{\gamma})\hat{e}_\omega - \hat{\mu} x_q - \hat{\sigma}\right]$$

$$\triangleq \psi\left(\hat{e}_\omega, x_q, \hat{\sigma}, \omega_{ref}, \frac{d\omega_{ref}}{dt}\right) \quad (2.25)$$

where $\hat{e}_\omega$ is the speed tracking error estimate, defined by $\hat{e}_\omega = \omega_{ref} - \hat{\omega}$. It can be verified that

$$\psi\left(e_\omega, x_q, \sigma, \omega_{ref}, \frac{d\omega_{ref}}{dt}\right) = \bar{\psi}\left(e_\omega, x_q, \omega_{ref}, \frac{d\omega_{ref}}{dt}, T_L\right) \quad (2.26)$$

To protect the system from the peaking phenomenon of high-gain observers [34],the control law ( 2.25 ) is saturated outside the compact set $\Omega_1 = \{V_1 = \xi^T P_1 \xi \leq c_1\}$ where $P_1 = P_1^T > 0$ is the solution of the Lyapunov equation $P_1A_1 + A_1^T P_1 = -Q_1$ for some $Q_1 = Q_1^T > 0$, and $c_1 > 0$ is chosen such that $\xi(0)$ is in the interior of $\Omega_1$ and

$$\max_{\xi \epsilon \Omega_1} \left| \bar{\psi}\left(e_\omega, x_q, \omega_{ref}, \frac{d\omega_{ref}}{dt}, T_L\right) \right| < i_{q_{max}} \tag{2.27}$$

where $i_{q_{max}}$ is the limit of $|i_q|$. The above inequality is possible if

$$\left| \bar{\psi}\left(0, \bar{x}_q, \omega_{ref}, \frac{d\omega_{ref}}{dt}, T_L\right) \right| < i_{q_{max}}$$

which restricts $\omega_{ref}$, and $T_L$. The control law is then given by

$$i_{q_{ref}} = M sat\left( \frac{\psi\left(\hat{e}_\omega, x_q, \hat{\sigma}, \omega_{ref}, \frac{d\omega_{ref}}{dt}\right)}{M} \right) \tag{2.28}$$

where $M = i_{q_{max}}$.

## 2.2 Closed Loop analysis

***Theorem 2.1:*** *Consider the closed loop system formed of the PMSM model* ( 1.5 )-( 1.8 )*, the PI current controllers* ( 2.3 )*, the extended high-gain observer* ( 2.21 )-( 2.23 )*, and the speed controller* ( 2.28 )*. Assume that*

1) $\omega_{ref}$, $\frac{d\omega_{ref}}{dt}$, *and* $\frac{d^2\omega_{ref}}{dt^2}$ *are bounded*
2) $T_L$ *and* $\frac{dT_L}{dt}$ *are bounded*
3) $\left|\frac{\alpha - \hat{\alpha}}{\hat{\alpha}}\right| < 1$

*4) $\xi(0)$ is in the interior of $\Omega_1$ and the initial states $i_d(0)$, $i_q(0)$, $\hat{\theta}(0)$, $\hat{\omega}(0)$, and $\hat{\sigma}(0)$ are bounded.*

*Then, there exist positive constants $\lambda_1$ and $\lambda_2$ such that for all $\varepsilon \le \lambda_1$ and $\frac{\tau}{\varepsilon} \le \lambda_2$, the trajectories of the closed loop system are bounded for all $t \ge 0$, and*

$$|e_\omega{}^{\star}(t) - e_\omega(t)| \to 0 \text{ as } \varepsilon \to 0 \text{ and } \frac{\tau}{\varepsilon} \to 0 \text{ for all } t \ge 0 \qquad (2.29)$$

***Proof:*** The closed-loop system is represented as a three-time-scale singularly perturbed system. The state variables are taken as

$$\xi_1 = x_d - Ri_{d_{ref}}, \quad \xi_2 = x_q - \bar{x}_q, \quad \xi_3 = e_\omega,$$

$$\eta_1 = \frac{1}{\varepsilon^2}\left(\theta - \hat{\theta}\right), \quad \eta_2 = \frac{1}{\varepsilon}(\omega - \hat{\omega}),$$

$$\eta_3 = (\alpha - \hat{\alpha})M\phi_\varepsilon\left(\frac{\psi\left(\hat{e}_\omega, x_q, \hat{\sigma}, \omega_{ref}, \frac{d\omega_{ref}}{dt}\right)}{M}\right) - (\gamma - \hat{\gamma})\omega + (\mu - \hat{\mu})x_q - \frac{1}{J}T_L - \hat{\sigma}$$

$$z_1 = i_d - \frac{1}{R + k_p}\left(k_p i_{d_{ref}} + x_d\right)$$

$$z_2 = i_q - \frac{1}{R + k_p}\left[k_p M\phi_\varepsilon\left(\frac{\psi\left(\hat{e}_\omega, x_q, \hat{\sigma}, \omega_{ref}, \frac{d\omega_{ref}}{dt}\right)}{M}\right) - k_m\,\omega + x_q\right]$$

$$\xi = \begin{bmatrix}\xi_1\\ \xi_2\\ \xi_3\end{bmatrix}, \eta = \begin{bmatrix}\eta_1\\ \eta_2\\ \eta_3\end{bmatrix}, z = \begin{bmatrix}z_1\\ z_2\end{bmatrix}$$

where $\phi_\varepsilon$ is an odd function defined by

$$\phi_\varepsilon(y) = \begin{cases} y & for\ 0 \le y \le 1 \\ y + \dfrac{y-1}{\varepsilon} - \dfrac{y^2-1}{2\varepsilon} & for\ 1 \le y \le 1+\varepsilon \\ 1 + \dfrac{\varepsilon}{2} & for\ y \ge 1+\varepsilon \end{cases}$$

which is a continuously differentiable nondecreasing function with a locally Lipschitz derivative and bounded uniformly in $\varepsilon$ on any bounded interval of $\varepsilon$. Furthermore, the function $\phi_\varepsilon$ satisfies $|sat(y) - \phi_\varepsilon(y)| \le \frac{\varepsilon}{2}$ and $|\phi'_\varepsilon(y)| \le 1\ \forall\ y \in \mathbb{R}$.

For $\xi \epsilon \Omega_1$, the closed-loop system is described by

$$\dot{\xi} = A_1\xi + E_1 z + B_1 f_1(\cdot) + \varepsilon B_2 f_2(\cdot) \tag{2.30}$$

$$\varepsilon\dot{\eta} = A_2\eta - B_3\rho_3\Delta\eta_1 + \varepsilon[B_3 f_3(\cdot) + B_4 f_4(\cdot)] + B_4 b z_2 \tag{2.31}$$

$$\tau\dot{z} = -z - \frac{\tau}{\varepsilon}\frac{\rho_3}{\hat{\alpha}}\phi'_\varepsilon(\cdot)B_5\eta_1 - \varepsilon\frac{k_p}{R+k_p}B_5 f_2(\cdot) + \tau g(\cdot) \tag{2.32}$$

where $A_1$ is defined by ( 2.19 ),

$$E_1 = \begin{bmatrix} -k_i & 0 \\ 0 & -k_i \\ 0 & -\frac{k_m}{J} \end{bmatrix}, \quad B_1 = \frac{1}{R+k_p}\begin{bmatrix} 0 \\ k_i R \\ -\frac{k_m k_p}{J} \end{bmatrix}, \quad B_2 = \frac{k_p}{R+k_p}\begin{bmatrix} 0 \\ -k_i \\ -\frac{k_m}{J} \end{bmatrix}$$

$$A_2 = \begin{bmatrix} -\rho_1 & 1 & 0 \\ -\rho_2 & 0 & 1 \\ -\rho_3 & 0 & 0 \end{bmatrix}, \quad B_3 = \begin{bmatrix} 0 \\ 0 \\ 1 \end{bmatrix}, \quad B_4 = \begin{bmatrix} 0 \\ 1 \\ 0 \end{bmatrix}, B_5 = \begin{bmatrix} 0 \\ 1 \end{bmatrix}, b = \frac{k_m}{J},$$

$g(\cdot) = \begin{bmatrix} g_1(\cdot) \\ g_2(\cdot) \end{bmatrix}$, and $\Delta = \frac{\alpha - \hat{\alpha}}{\hat{\alpha}}\phi'_\varepsilon\left(\frac{\psi\left(\hat{e}_\omega, x_q, \hat{\sigma}, \omega_{ref}, \frac{d\omega_{ref}}{dt}\right)}{M}\right)$.

The functions $f_1$ to $f_4$ and $g_1$ and $g_2$ are given in Appendix A. The functions $f_1$ and $f_2$ are globally bounded, and $f_1$ vanishes at $\eta = 0$. The functions $f_3$ and $g$ satisfy a bound of the form

$k_a + k_b\|\eta\| + k_c\|z\|$, while $f_4$ satisfies a bound of the form $k_a + k_b\|\eta\|$ where $k_a$, $k_b$, and $k_c$ are positive constants.

For $\tau \ll \varepsilon \ll 1$, The system ( 2.30 )-( 2.32 ) is singularly perturbed with three-time-scales. In the fastest time scale, the boundary layer model is $\tau\dot{z} = -z$, which is obtained by setting $\frac{\tau}{\varepsilon} = 0$, $\tau = 0$, and $\varepsilon = 0$ on the right-hand side of ( 2.32 ). The quasi-steady-state of this model is $z = 0$. In the intermediate time scale, the boundary layer model is

$$\varepsilon\dot{\eta} = A_2\eta - B_3\rho_3\Delta\eta_1 \tag{2.33}$$

which is obtained by setting $\varepsilon = 0$ and $z = 0$ on the right-hand side of the $\dot{\eta}$-equation. This system can be represented as a negative feedback connection of the transfer function

$$\Gamma(\varepsilon s) = \frac{\rho_3}{(\varepsilon s)^3 + \rho_1(\varepsilon s)^2 + \rho_2(\varepsilon s) + \rho_3}$$

and the time varying gain $\Delta(\cdot)$. Since $\left|\frac{\alpha-\hat{\alpha}}{\hat{\alpha}}\right| < 1$ and $|\phi_\varepsilon'(\cdot)| \le 1$, $|\Delta| < 1$. Because the poles of the transfer function $\Gamma(\varepsilon s)$ are real and negative, $\max_\omega|\Gamma(j\varepsilon\omega)| \le 1$. The circle criterion [34] shows that the origin of ( 2.33 ) is globally exponentially stable. By applying a loop transformation and using the Kalman-Yakubovich-Popov lemma [34, Lemma 6.3] we obtain a quadratic Lyapunov function $V_2(\eta) = \eta^T P_2 \eta$ whose derivative with respect to ( 2.33 ) is bounded from above by $-\left(\frac{\lambda}{\varepsilon}\right)V_2(\eta)$ for some positive constant $\lambda$, independent of $\varepsilon$. In the slowest time scale, the slow model is $\dot{\xi} = A_1\xi$, which is obtained by setting $\varepsilon = 0$ and $\eta = 0$ on the right-hand side of ( 2.30 ).

Consider the set

$$\Omega = \Omega_1 \times \{W(\eta, z) \leq \varepsilon^2 c_2\}$$

where $W(\eta, z) = \eta^T P_2 \eta + \frac{1}{2} z^T z$. Similar to arguments used in the analysis of high-gain observer [34], it can be shown that, by choosing $c_2 > 0$ large enough, the set $\Omega$ is positively invariant for sufficiently small $\varepsilon$ and $\frac{\tau}{\varepsilon}$. This is done by showing that $\dot{V}_1 < 0$ on the boundary of $\Omega_1$, and $\dot{W} < 0$ on the boundary $W(\eta, z) = \varepsilon^2 c_2$.

At the initial time, $(\eta(0), z(0))$ could be outside the set $\{W(\eta, z) \leq \varepsilon^2 c_2\}$ but would move rapidly toward the set and will reach it within an interval $[0, T(\varepsilon)]$, where $\lim_{\varepsilon \to 0} T(\varepsilon) = 0$. Because the initial state $\xi(0)$ is in the interior of $\Omega_1$, choosing $\varepsilon$ small enough ensures $\xi$ does not leave $\Omega_1$, and by the end of this interval $(\xi, \eta, z)$ would be in the positively invariant set $\Omega$.

The limit ( 2.29 ) follows from the continuous dependence of the solutions of differential equations on parameters [34, Theorem 9.1] and exponential stability of the subsystem

$$\dot{\xi} = A_1 \xi. \qquad \blacksquare$$

***Theorem 2.2:*** *Under the assumptions of Theorem 2.1, suppose $\omega_{ref}$ and $T_L$ are constant. Then, there exist positive constants $\lambda_3$ and $\lambda_4$ such that for $\varepsilon < \lambda_3$ and $\frac{\tau}{\varepsilon} < \lambda_4$,* $\lim_{t \to \infty} e_\omega(t) = 0$.

***Proof:*** We have already shown in the proof of Theorem 2.1 that the trajectories of the system enter the positively invariant set $\Omega$ wherein $\left\| \begin{matrix} \eta \\ z \end{matrix} \right\| = O(\varepsilon)$. Inside $\Omega$, the saturation is not active; hence $M\phi_\varepsilon(\psi/M) = Msat(\psi/M) = \psi$. When $\omega_{ref}$ and $T_L$ are constant, it can be shown that the system has an equilibrium point at $(\bar{\xi}, \bar{\eta}, \bar{z})$, where

$\bar{\xi}_1 = -\frac{Ln_p\omega_{ref}(B\omega_{ref}+T_L)}{k_m}$, $\bar{\xi}_2 = Ln_p\omega_{ref}i_{d_{ref}}$, $\bar{\xi}_3 = \bar{\eta}_1 = \bar{\eta}_2 = 0$, $\bar{\eta}_3 = \frac{\tau n_p k_m \omega_{ref} i_{d_{ref}}}{J}$,

$\bar{z}_1 = \frac{\tau n_p\omega_{ref}(B\omega_{ref}+T_L)}{k_m}$, and $\bar{z}_2 = -\tau n_p\omega_{ref}i_{d_{ref}}$.

At this equilibrium point $e_\omega = \xi_3 = 0$. We now show that the equilibrium point is exponentially stable and every trajectory in $\Omega$ converges to it as time tends to infinity. Towards that end, we shift the equilibrium point to the origin by the change of variables

$$\tilde{\xi} = \xi - \bar{\xi}, \quad \tilde{\eta} = \eta - \bar{\eta}, \quad \tilde{z} = z - \bar{z}$$

The transformed system is given by

$$\dot{\tilde{\xi}} = A_1\tilde{\xi} + E_1\tilde{z} + B_1\tilde{f}_1(\cdot)$$

$$\varepsilon\dot{\tilde{\eta}} = H\tilde{\eta} + B_4 b\tilde{z}_2 + \varepsilon\left[B_3\tilde{f}_3(\cdot) + B_4\tilde{f}_4(\cdot)\right]$$

$$\tau\dot{\tilde{z}} = -\tilde{z} - \frac{\tau}{\varepsilon}\frac{\rho_3}{\hat{\alpha}}B_5\tilde{\eta}_1 + \tau\tilde{g}(\cdot)$$

where $H = A_2 - \rho_3\left(\frac{\alpha-\hat{\alpha}}{\hat{\alpha}}\right)B_3C_3$, in which $C_3 = [1 \quad 0 \quad 0]$. As shown in the proof of Theorem 2.1, $H$ is Hurwitz for $\left|\frac{\alpha-\hat{\alpha}}{\hat{\alpha}}\right| < 1$. The functions $\tilde{f}$ and $\tilde{g}$ are obtained from $f$ and $g$ by subtracting their values at the equilibrium point. A composite Lyapunov function for this three-time-scale singularly perturbed system is taken as

$$V = \tilde{\xi}^T P_1\tilde{\xi} + \tilde{\eta}^T P_3\tilde{\eta} + \frac{1}{2}\tilde{z}^T\tilde{z}$$

where $P_3$ is the positive definite symmetric solution of the Lyapunov equation

$$P_3H + H^TP_3 = -I.$$

The time derivative of $V$ satisfies the inequality

$$\dot{V} \leq -\begin{bmatrix} \|\tilde{\xi}\| \\ \|\tilde{\eta}\| \\ \|\tilde{z}\| \end{bmatrix}^T \begin{bmatrix} k_1 & -k_2 & -k_3 \\ -k_2 & \left(\frac{1}{\varepsilon} - k_4\right) & -\left(k_5 + \frac{k_6}{\varepsilon}\right) \\ -k_3 & -\left(k_5 + \frac{k_6}{\varepsilon}\right) & \left(\frac{1}{\tau} - k_7\right) \end{bmatrix} \begin{bmatrix} \|\tilde{\xi}\| \\ \|\tilde{\eta}\| \\ \|\tilde{z}\| \end{bmatrix}$$

where $k_1$ to $k_7$ are positive constants independent of $\tau$ and $\varepsilon$. The matrix of this quadratic form is positive definite for sufficiently small ε and $\frac{\tau}{\varepsilon}$. Hence, the origin is exponentially stable. Moreover, the forgoing inequality is valid in Ω; hence all trajectories in Ω converge to the origin as t tends to infinity. ■

### 2.3 Simulations and Experimental Results

The performance of the proposed control method is evaluated through conducting various simulations and experiments under different conditions such as parameter variation and external load. The nominal parameters of the used surface mount PMSM are shown in Table 1.

Three main sets of simulations and experiments have been conducted. The first set of simulations and experiments is carried out using the nominal parameters of the motor with no external load. In this set, we show the operation of the motor under a speed reference profile which includes speed reversal. The first set includes the use of three different values of the constant $k_\omega$, namely, $k_\omega = 2.5$, $k_\omega = 5$, and $k_\omega = 10$. The second set explores the effect of both uncertainty in the parameters and decreasing ε on the performance of the proposed control method. We achieve uncertainty in the parameters by varying the motor's parameters in the controller. Finally, the third set investigates the effect of the external load and the influence of decreasing ε on the robustness of the control method.

| Parameter | Value |
|---|---|
| Rated Voltage | 200 $VAC_{L\text{-}L}$ |
| Rated Current | 5.1 A |
| Rated Torque | 3.18 N.m |
| Rated Speed | 3000RPM |
| Inductance $\boldsymbol{L}$ | 4.47 mH |
| Per Phase Winding Resistance $\boldsymbol{R}$ | 0.835 Ω |
| Torque Constant $\boldsymbol{k_m}$ | 0.859 $V \cdot s$ |
| Number of Pole Pairs $\boldsymbol{n_p}$ | 4 |
| Viscosity Coefficient $\boldsymbol{B}$ | 0.0011 $\frac{N \cdot m \cdot s}{rad}$ |
| Moment of Inertia $\boldsymbol{J}$ | 0.0036 $Kg \cdot m^2$ |

Table 2.1. Nominal parameters of the used PMSM.

The PI controllers of the inner current loops are designed such that the currents $i_d$ and $i_q$ are relatively fast. The proportional and integral gains of the PI current controllers that are found to satisfy the criterion above are: $k_p = 25$, and $k_i = 1200$. In all cases $i_{d_{ref}} = 0$.

There are two aspects that must be taken into account when designing the parameter $\varepsilon$ of the extended high-gain observer. First, the assumption $\tau \ll \varepsilon \ll 1$ must hold. Second, $\varepsilon$ should be chosen so that the best compromise between fast convergence and minimal noise amplification is achieved. With $\tau = 1.73 * 10^{-4}$, the value of $\varepsilon$ that satisfies both criteria was found to be $0.005$. In addition, the roots of the polynomial ( 2.24 ) of the extended high gain observer are all assigned at $-1$. Therefore, $\rho_1 = 3$, $\rho_2 = 3$, and $\rho_3 = 1$. These parameters are used in both the simulation and the experiment. The simulations are all performed using MATLAB-Simulink.

### 2.3.1 Experimental Setup

The experiments were performed in the Electric Machines and Drives Laboratory (EMDL) at Michigan State University (MSU). Figure 2.2 shows the block diagram of the experiment. The host computer is used to perform multiple functions such as, providing user interface, plotting measured quantities of interest in real-time, and building the proposed controller's programs on LabVIEW. The host PC is also used to deploy the controller's programs on the Target PC. The target PC uses the National Instruments' real-time operating system (RTOS) to execute the controller's programs in real-time. The target PC communicates with the inverter and the incremental encoder through the NI PCIe-7852R card which is a real-time multifunction Data Acquisition (DAQ) card.

Two modules of the NI PCIe-7852R card are utilized in the experiment: 1)-the 16-bit Analog to Digital Converter (ADC) module, and the Field Programmable Gate Array (FPGA) module. The ADC is used to measure the phase currents, temperature of the IGPT's that are used in the inverter, and the DC-link voltage. The FPGA, on the other hand, is used to interface the incremental encoder and provide switching signals to the inverter via a Pulse Width Modulation (PWM) controller circuit. The FPGA module on the NI PCIe-7852R runs on an on-board 40MHz oscillator.

The incremental encoder, as shown in Figure 2.2, is connected to the shaft of the PMSM which is also directly connected to the Induction Motor. The connection between the PMSM and the induction motor is made with a jaw coupler that is cushioned with a rubber spider. Here, the induction motor is used to apply load on the PMSM to assess the proposed controller's ability to cope with external disturbance. The induction motor is driven with a Texas Instruments' RDK-ACIM board.

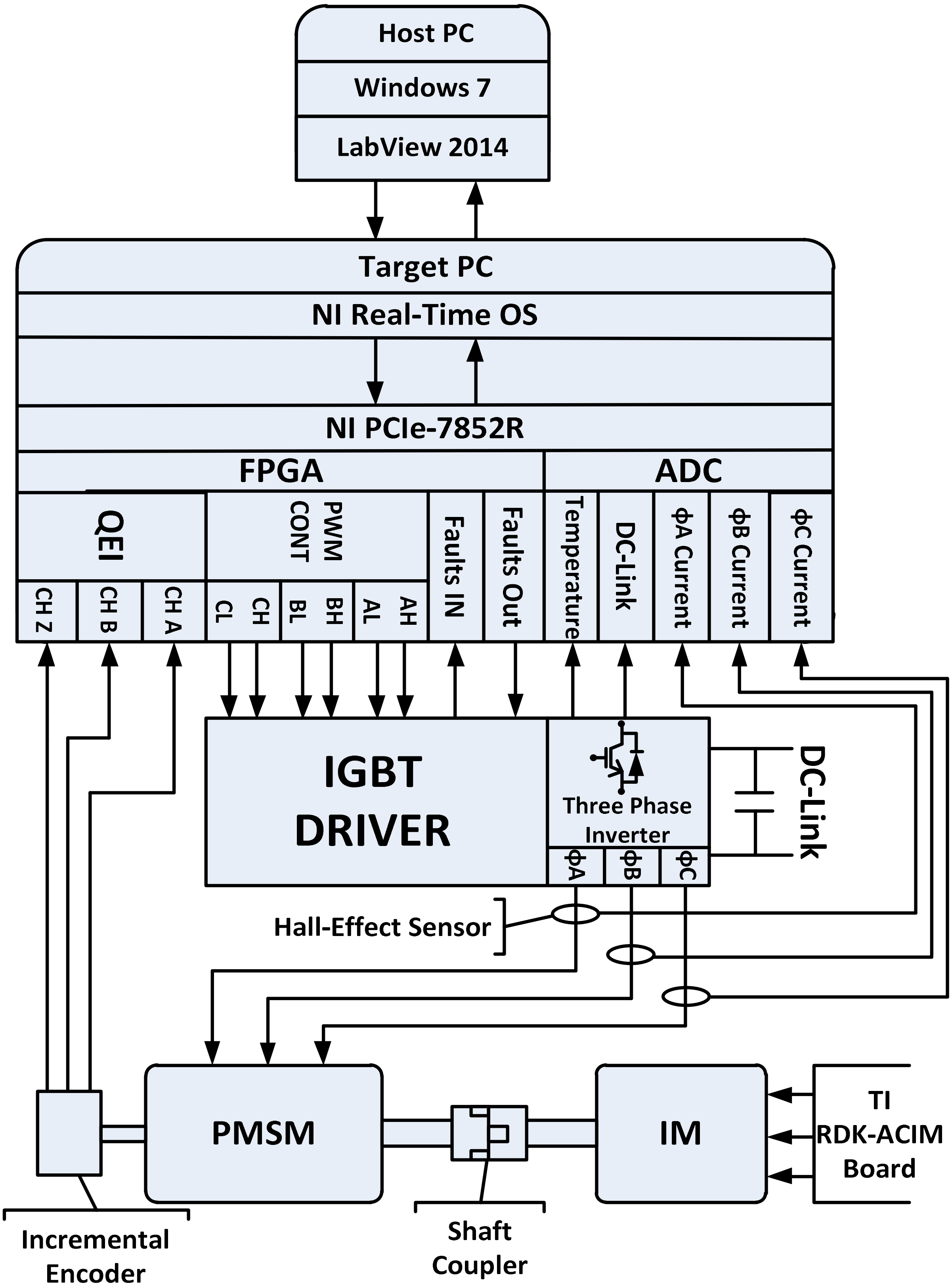


Figure 2.2. Block diagram of the experimental setup.

The control algorithm is implemented with a $10kHz$ sampling frequency. The Hall Effect current sensors have a maximum bandwidth of 150kHz at -1db. The position of the motor's shaft is measured with a $2500PPR$ incremental encoder. All the reported speeds from the experiment are estimated using a separate high-gain observer that is independent of the feedback loop. Figure 2.3 shows a picture of the experimental setup.

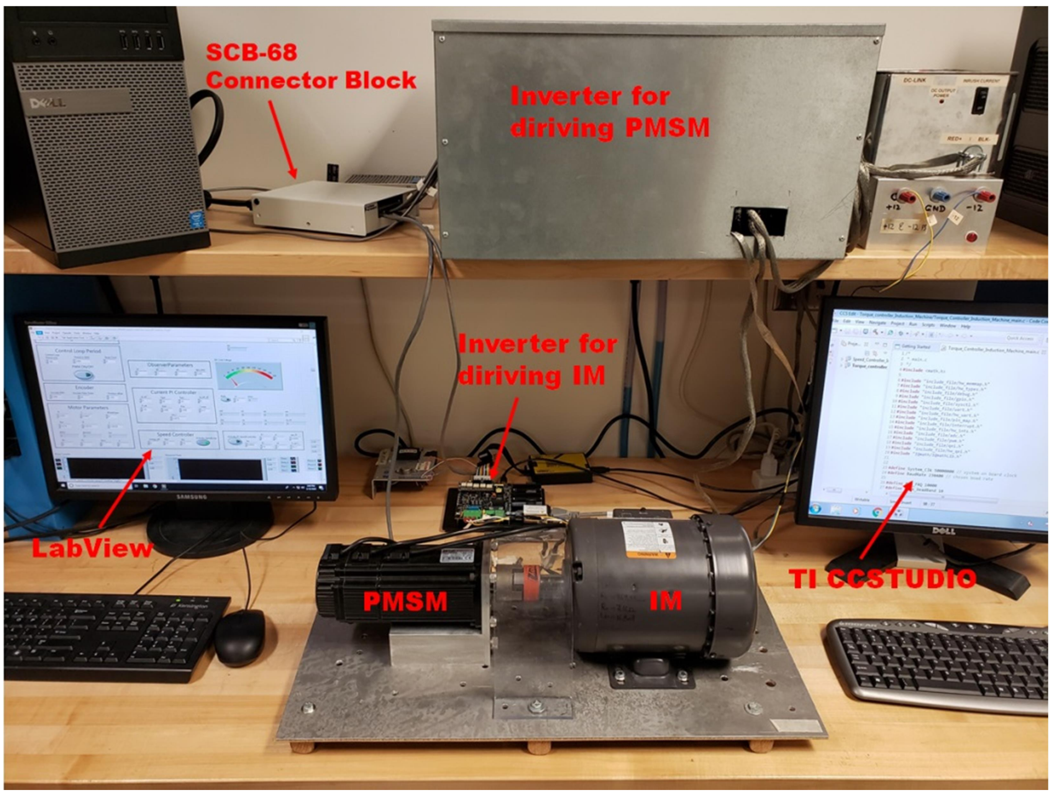


Figure 2.3. Picture of the experimental setup.

### 2.3.2 Simulation & Experiment I

In this case, the nominal parameters, which are shown in Table 2.1, are used in the controller and no external load is applied to the motor. The motor in this case is at standstill when the following speed profile is applied

$$\omega_{ref} = 100u(t) - 200u(t-5) + 100u(t-10)$$

where

$$u(t) = \begin{cases} 0 & t < 0 \\ 1 & t \geq 0 \end{cases}$$

The speed profile is a series of steps that will show operation of the motor for different speed references including speed reversal. Even though Theorem 2.1 requires $\omega_{ref}$ to be twice differentiable, the series of steps of $\omega_{ref}$ can be viewed as a change of initial conditions. Figures 2.4(a), 2.5(a), and 2.6(a) show the speed reference signal $\omega_{ref}$, the desired target $\omega^{\star} = \omega_{ref} - e_{\omega}{}^{\star}$, and the speed of the motor from both the simulation and the experiment for the three values of $k_{\omega}$: $k_{\omega} = 2.5$, $k_{\omega} = 5$, and $k_{\omega} = 10$, respectively. It can be seen that the proposed control method was able to regulate the speed and shape the transient response of the speed to the desired trajectory.  It can also be seen that there is an excellent agreement between simulation and experimental results.  Figures 2.4(b), 2.5(b), and 2.6(b) show the deviation error between the target speed and the motor speed of the simulation and the experiment. These deviation errors further show the high performance property of the proposed control method. The results from simulation show a maximum of 0.2% deviation error during the transient period and a zero steady state error. On the other hand, the maximum experimental deviation error is about 4% during the transient period and less than 0.6% during the steady state. These simulations and experiments show the effectiveness of the proposed control method in regulating and shaping the transient response of the speed.

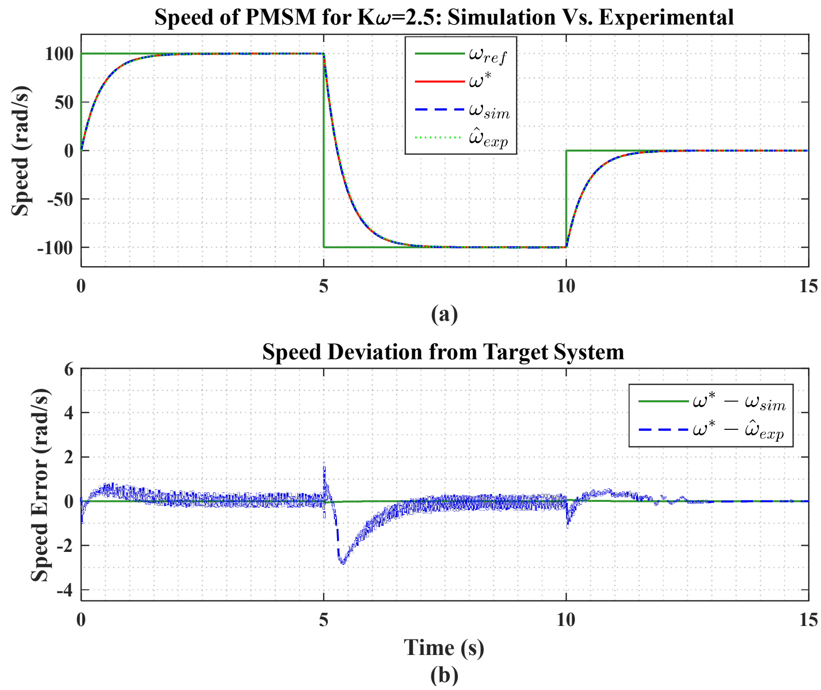


Figure 2.4. (a) Simulation and experimental speed of PMSM when $k_\omega = 2.5$ and using the nominal parameters, (b) Simulation and experimental speed deviation from target speed.

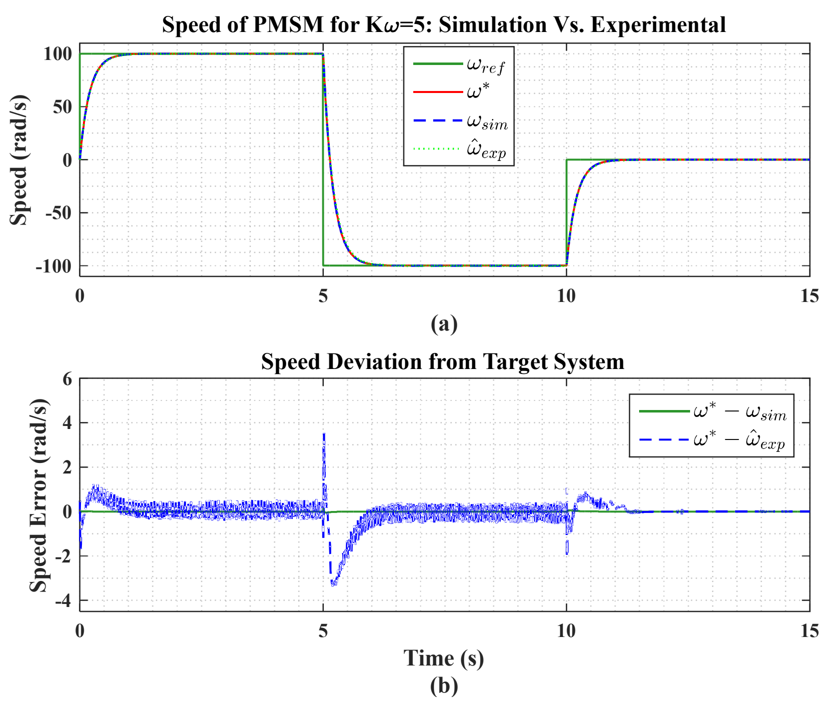


Figure 2.5. (a) Simulation and experimental speed of PMSM when $k_\omega = 5$ and using the nominal parameters, (b) Simulation and experimental speed deviation from target speed.

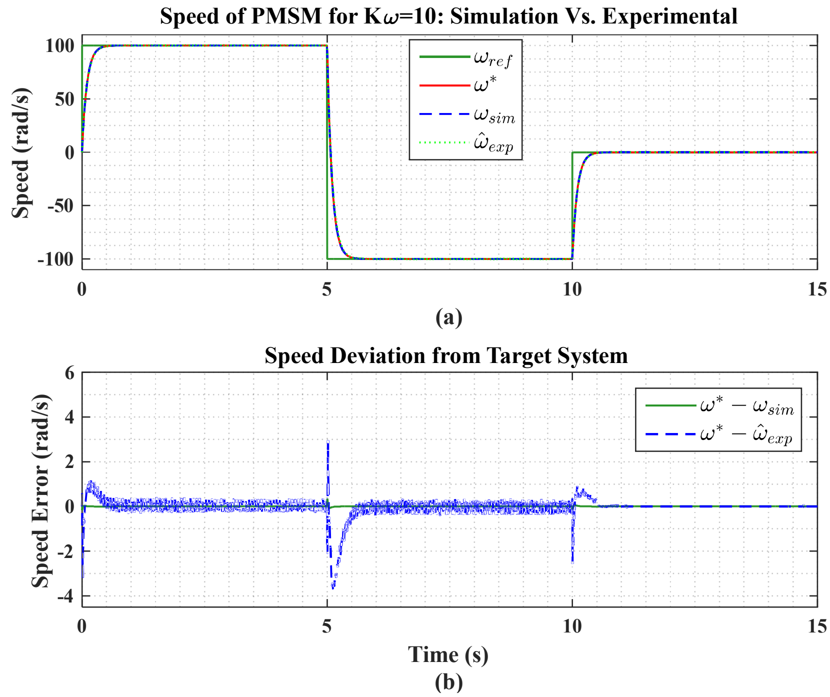


Figure 2.6. (a) Simulation and experimental speed of PMSM when $k_\omega = 10$ and using the nominal parameters, (b) Simulation and experimental speed deviation from target speed.

### 2.3.3 Simulation & Experiment II

In this case, the effect of varying the nominal parameters on the proposed control method is investigated. In all experiments of this section, the PMSM is at full stop when a speed step reference of $100\,rad/sec$ is applied at $t = 0$. Also, in all experiments the PMSM is not externally loaded. There are 18 experiments that have been conducted for this investigation and they are summarized in Table 2.2.

Table 2.2 shows the maximum experimental transient deviation error for $k_\omega = 5$ and for two values of $\varepsilon$. It can be seen from Table 2.2 that perturbing the winding resistance $R$ and the coefficient of viscous friction $B$ have minimum to no effect on the performance of the proposed control method when compared to the case when no parameters perturbation is present. On the other hand, decreasing the moment of inertia $J$ affects the performance of the proposed control method the most while moderate effect is caused when the torque constant $k_m$ is perturbed. It can also be seen that when $\varepsilon$ is decreased, the maximum transient deviation error is also decreased which has been predicted in Theorem 2.1. Figures 2.7 and 2.8 show samples of the speed when $J$ and $k_m$ are varied from their nominal values.

Figures 2.7(a) and 2.8(b) show simulation and experimental results when the nominal value of the moment of inertia $J$ was decreased by 50% and the nominal value of the torque constant $k_m$ was increased by 25%, respectively. Both figures show the commanded speed, the desired target system, and the speed of the motor for $k_\omega = 5$ and $\varepsilon = 0.005$. In both cases, the proposed control method was able to regulate the speed, and to a great extent, shape the transient response to the desired trajectory despite parameter uncertainties.

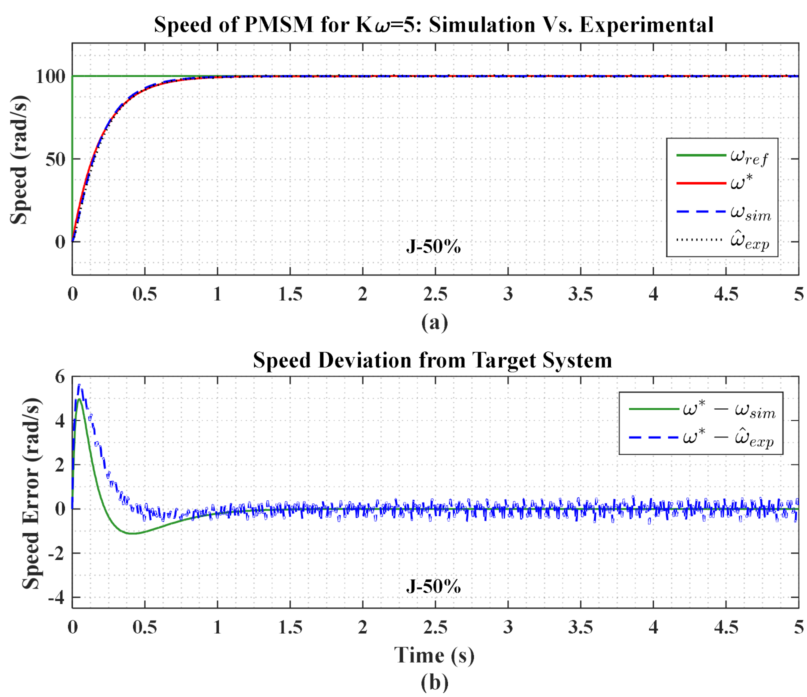


Figure 2.7. (a) Simulation and experimental speed of PMSM for $k_\omega = 5$ and when the moment of inertia $J$ is decreased by 50%, (b) Simulation and experimental speed deviation from target speed when the moment of inertia $J$ is decreased by 50%.

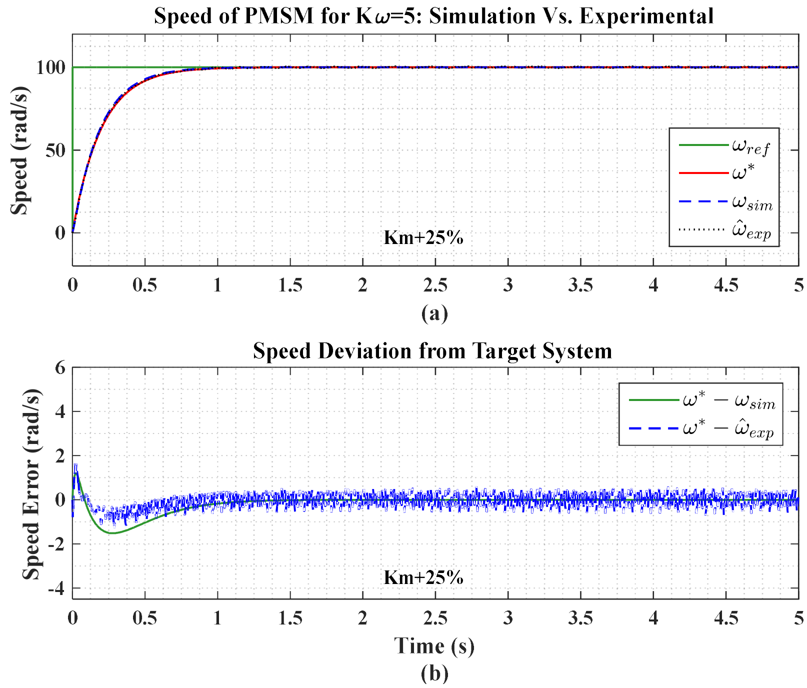


Figure 2.8. (a) Simulation and experimental speed of PMSM for $k_\omega = 5$ and when the torque constant $k_m$ is increased by 25%, (b) Simulation and experimental speed deviation from target speed when the torque constant $k_m$ is increased by 25%.

| Perturbation | | | | Maximum Experimental Transient Deviation Error | |
|---|---|---|---|---|---|
| $k_m$ | $J$ | $R$ | $B$ | $\varepsilon = 0.01$ | $\varepsilon = 0.005$ |
| 0% | 0% | 0% | 0% | 2.07% | 1.63% |
| +25% | 0% | 0% | 0% | 3.7% | 1.78% |
| −25% | 0% | 0% | 0% | 3.11% | 1.65% |
| 0% | +50% | 0% | 0% | 4.62% | 2.61% |
| 0% | −50% | 0% | 0% | 9.13% | 5.57% |
| 0% | 0% | +200% | 0% | 2.35% | 1.70% |
| 0% | 0% | −100% | 0% | 2.26% | 1.67% |
| 0% | 0% | 0% | +50% | 2.13% | 1.71% |
| 0% | 0% | 0% | −50% | 2.18% | 1.74% |

Table 2.2. Maximum Experimental Transient Deviation Error

Figure 2.7(b) and 2.8(b) show the deviation error between the target speed and the motor speed for simulation and experimental results when the nominal value of the moment of inertia $J$ was decreased by 50% and the nominal value of the torque constant $k_m$ was increased by 25%, respectively. These deviation errors further show the high performance property of the proposed control method. The results from simulation show a maximum of 4.9% deviation error during the transient period while the maximum experimental deviation error from the target system is about 5.57% during the transient period. However, the experimental deviation error in the steady state is less than 0.5%. The maximum deviation error occur when the nominal value of the moment of inertia $J$ is decreased by 50%.

It can also be observed that simulation and experimental results are very close to one another that they almost overlap. The deviation errors further show the extent of this agreement. The agreement between simulation and experimental results is a very important feature to have since it allows development and testing of the controller in simulation before testing it in real life applications. This also has the potential of replicating many circumstances that are otherwise impossible to do in real life or that they will cost money and resources. This experiment shows the effectiveness of the proposed control method in shaping the transient response and regulating the speed of the motor despite varying the parameters.

### 2.3.4 Simulation & Experiment III

This case investigates the effectiveness of the proposed control method when the PMSM is externally loaded. The PMSM, in this case, is regulated at a constant speed of $100\ rad/sec$. Then, a step of external load of about $2N \cdot m$ was applied at $\mathrm{t} = 3\mathrm{s}$ and removed at $\mathrm{t} = 7\mathrm{s}$. Figure 2.9(a) and (b) show the PMSM's speed from the experiment before and after the external load was applied for $k_\omega = 5$ and $k_\omega = 10$, respectively. In addition, both plots show the effect of reducing $\varepsilon$ on the performance of the proposed controller against the external disturbance.

It can be seen that at the moment the external load was applied the speed of the motor in all cases briefly dropped but recovered quickly and the speed is maintained at $100\ rad/sec$. At the moment the external load was applied; however, the cases where $\varepsilon = 0.005$ show a maximum speed loss of about 7% while the cases where $\varepsilon = 0.01$ show a maximum speed loss of about 15%. This result is expected since a smaller $\varepsilon$ leads to a faster disturbance estimation and thus faster controller reaction. Similar behavior can also be observed at the moment when the external load was removed.

This experiment shows the effectiveness of the proposed control method in the presence of external disturbance. The robustness of the proposed control method against external disturbance is due to estimating the disturbance and cancelling it in the control law.

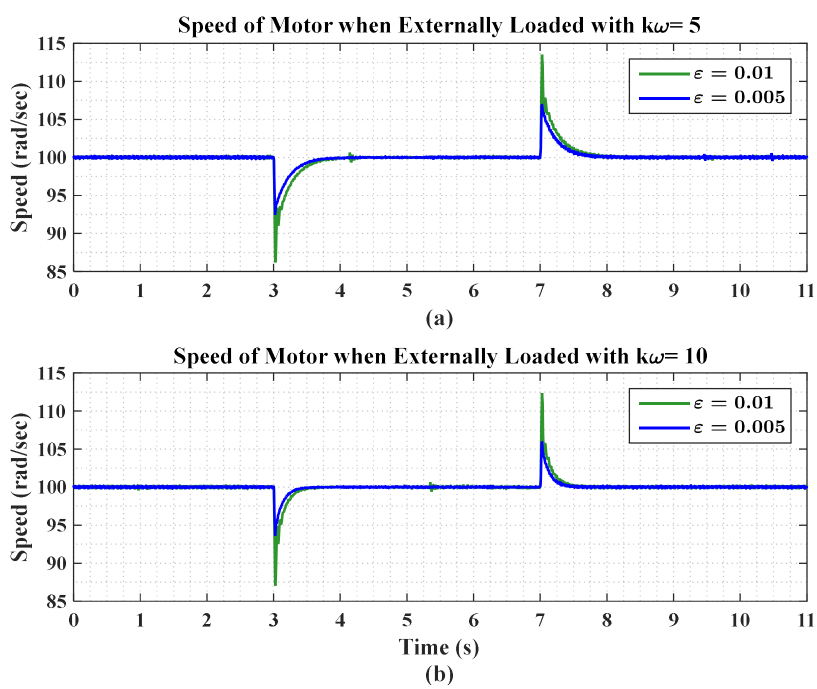


Figure 2.9. Speed of PMSM before and after the external load was applied.

## 2.4 Comparison with the PI Speed Controller

### 2.4.1 Description of the PI Speed Controller

Since this paper introduces a new method to control the speed of PMSMs, it is natural to compare it with the most widely used speed control method in industrial and commercial electrical drive systems.

Nearly all speed control methods of electrical drive systems that are used currently in the industry utilize cascaded PI controllers [36][4]. There are several versions and variation of the cascaded PI speed control of electric motors that can be found in [1], [3], [4], and [36]. Here, we have chosen to compare our speed control method with the version that is presented in [4] and [36] since they are  most recent and both claimed that the control method that they have presented is the most used speed control method in electrical drive systems. The main difference between the version of the cascaded PI speed controller in [4] and [36], and the versions presented in [1] and [3] is that in [4] and [36] the cross coupling between the current equations is cancelled by using nonlinear feedback through the control inputs $u_d$ and $u_q$ leaving the mathematical model of the PMSM linear.

All of these references except [36] assumed the speed is directly measured when presenting the cascaded PI controller and a speed observer was not discussed. In [36] a speed estimator is described to have a position differentiator in series with a low-pass filter. Thus, the speed estimator constitutes a high-pass filter from the measured position to the estimated speed. Figure 2.10 shows the complete cascaded PI speed controller that is used here for comparison.

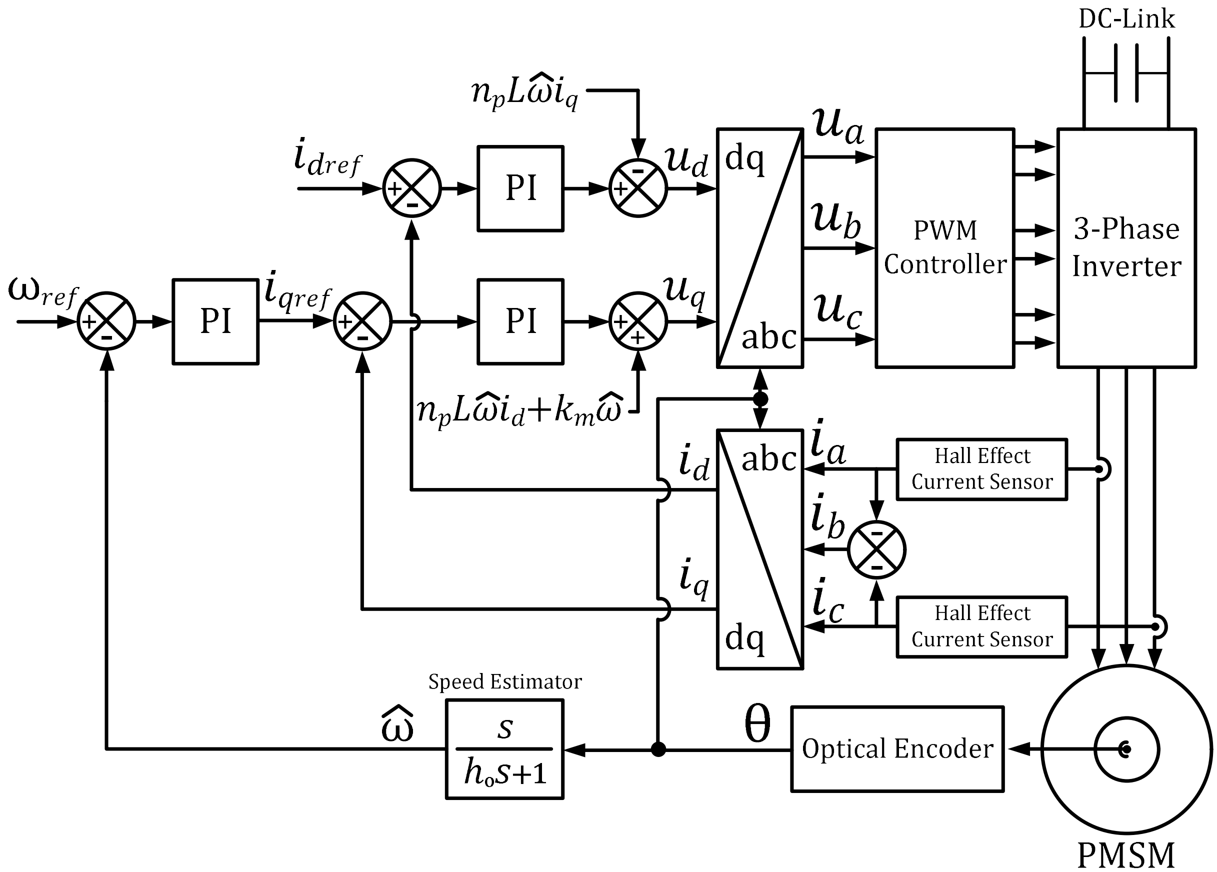


Figure 2.10. Block diagram of the PI speed controller.

The development of the cascaded PI controller is straightforward. The direct and quadrature voltages are given by

$$u_d = k_p e_d + x_d - n_p L \widehat{\omega} i_q$$

$$u_q = k_p e_q + x_q + n_p L \widehat{\omega} i_d + k_m \widehat{\omega}$$

where $e_d$, $e_q$, $x_d$, and $x_q$are defined as in ( 2.1 ), ( 2.2 ), ( 2.4 ), and ( 2.5 ), respectively. The quadrature current reference $i_{q_{ref}}$ is the output of the PI speed control loop and is given by

$$i_{q_{ref}} = h_p\left(\omega_{ref} - \widehat{\omega}\right) + h_i \int_0^t \left(\omega_{ref}(\acute{t}) - \widehat{\omega}(\acute{t})\right) d\acute{t}$$

where $h_p$ and $h_i$ are the proportional and integral gains of the PI speed controller, respectively. Furthermore, the speed estimate $\widehat{\omega}$ is defined by

$$\widehat{\omega} = \frac{s}{h_o s + 1}[\theta]$$

where $h_o$ is the speed estimator time constant. It can be seen that decreasing $h_o$ decreases the simultaneous speed estimation error but on the other hand increases quantization noise of the optical encoder. It should be noted that the decoupling of the current equations is exact only when the true parameters of the machine are accurately known.

### 2.4.2 Experimental Setup and Tuning

The performance of the proposed control method is further evaluated here by comparing it to the PI speed controller through two experiments. The first experiment is conducted to show the speed tracking ability of the proposed controller in comparison to the PI speed controller. The second experiment is performed to test the robustness of the proposed controller against external load in comparison to the PI speed controller. These experiments are exactly conducted for both controllers. This will allow us to draw a final conclusion about the performance of the proposed control method in comparison to the PI speed controller. The nominal parameters of the used surface-mounted PMSM are shown in Table 2.1.

The PI controllers of the inner current loops are designed such that the currents $i_d$ and $i_q$ are relatively fast. The proportional and integral gains of the PI current controllers that are found to satisfy the criterion above are: $k_p = 20$, and $k_i = 2500$. In all cases $i_{d_{ref}} = 0$. These values are used for both controllers. For the proposed controller, we choose $\varepsilon = 0.001$ and the roots of the polynomial ( 2.24 ) of the extended high gain observer are all assigned at $-1$. Therefore, $\rho_1 = 3$, $\rho_2 = 3$, and $\rho_3 = 1$. Also, we choose the gain $k_\omega = 60$.

There were over 80 experiment runs conducted to fine tune the cascaded PI speed controller. Only about 30% of these experiment runs were considered. The remaining 70% were discarded because they were too oscillatory, they have slow responses, or an unacceptable performance when an external load was applied. Only three pairs of the speed PI gains were selected out of the considered 30%. They were selected based on overshoot and disturbance rejection, so for example; out of all transient responses that have an overshoot ≤2% we selected the one that has the best disturbance rejection. A summary of the selected tuning gains are shown in Table 2.3. The estimator time constant $h_o$=0.0032 was found to provide fast convergence and an acceptable noise amplification.

| Gain Pair # | Overshoot % | $h_p$ | $h_i$ |
|---|---|---|---|
| 1 | ≤2% | 1 | 1 |
| 2 | ≤5% | 1 | 10 |
| 3 | ≤10% | 1 | 30 |

Table 2.3. PI speed controller tuning parameters.

### 2.4.3 Experimental Results

#### 2.4.3.1 Experiment I

In this case, the nominal parameters, which are shown in Table 1, are used in the proposed controller and no external load is applied to the motor. The motor in this case is at standstill when the following speed profile is applied,

$$\omega_{ref} = \begin{cases} \frac{1}{2} z_1 t^2 & for \quad 0 \le t < t_1 \\ a_f t + C_1 & for \quad t_1 \le t < t_2 \\ -\frac{1}{2} z_1 t^2 + z_2 t + C_2 & for \quad t_2 \le t < t_3 \\ C_3 & for \quad t_3 \le t \end{cases}$$

where $z_1 = 310719$, $z_2 = 21554$, $a_f = 1554$, $C_1 = -3.884$, $C_2 = -647.6$, $C_3 = 100$, $t_1 = 0.005$, $t_2 = 0.0644$, and $t_3 = 0.0694$. The speed profile is designed to be relatively fast and the maximum required acceleration does not exceed the motor's capability.

Figure 2.11(a) shows the speed reference signal $\omega_{ref}$, the speed of the motor $\omega$ when the proposed controller is used, and the speed of the motor $\omega_{PI}$ when the cascaded PI controller is used with different pairs of PI gains. It can be seen that the proposed controller was able to control the speed of the motor to closely track the reference speed while the PI speed controller was not able to perform as well as the proposed controller. Figure 2.11(b) shows the speed tracking error between the speed reference $\omega_{ref}$ and the motor speed for both controllers. This figure further shows the performance difference between the proposed controller and the cascaded PI speed controller.

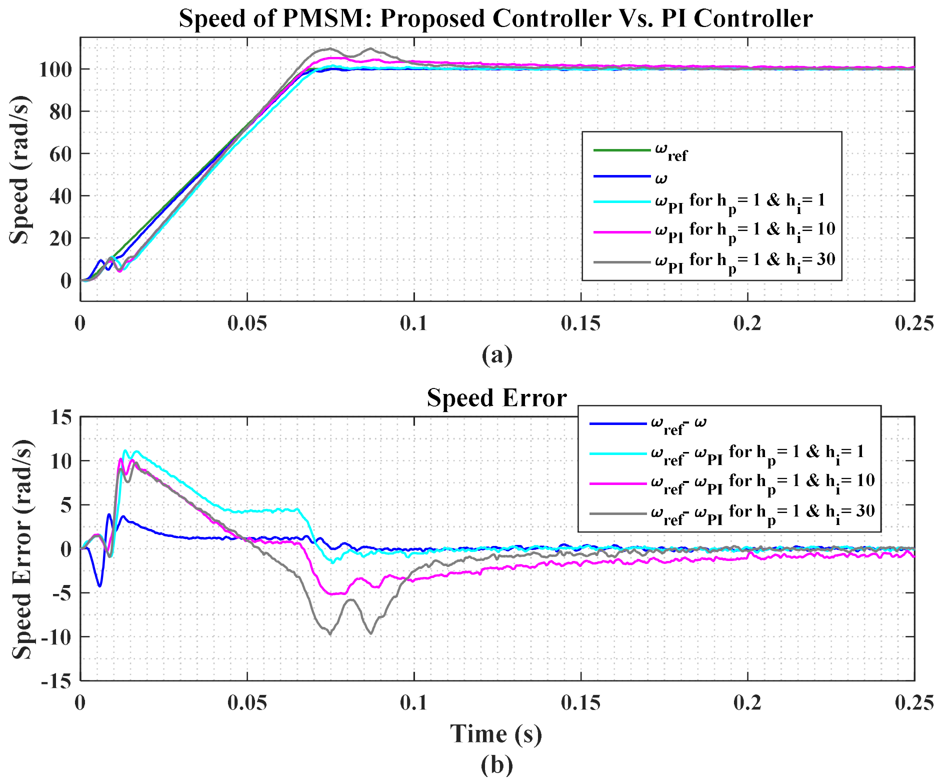


Figure 2.11. (a) Experimental speed of PMSM, (b) Experimental speed deviation from reference speed.

### 2.4.3.2 Experiment II

This case investigates the effectiveness of both the proposed control method and the PI speed controller when the PMSM is externally loaded with a step disturbance as well as a time-varying disturbance. The PMSM, in both of these case, is regulated at a constant speed of 100 rad/sec. Then, the external load is applied.

Figure 2.12(a) shows the speed of the motor $\omega$ when the proposed controller is used, and the speed of the motor $\omega_{PI}$ when the PI speed controller is used with different pairs of PI gains when the load is applied to the PMSM. The load is a step of about $2N \cdot m$ which was applied at $\mathrm{t} = 10\mathrm{s}$ and removed at $\mathrm{t} = 20\mathrm{s}$. It can be seen that at the moment the load was applied, the speed of the motor in all cases dropped then recovered and the speed was maintained at $100\, rad/sec$. This behavior is expected from the proposed controller because there is an integral action that results when the proposed controller is used in the presence of constant disturbance which leads to zero steady state error. Similarly, the PI speed controller relies on the integrator part of the PI controller to yield zero steady state error. There is however difference in how much the speed drops at the moment the load was applied and also how fast the speed is recovered. One can see that the step disturbance caused the speed of the motor to drop about 2.5% when the proposed controller is used while it caused the speed to drop about 5% when the PI speed controller is used. It can also be seen that the proposed controller was able to recover the speed relatively fast while the PI controller requires high integrator gain to achieve similar recovery time. Similar behavior was observed at the moment when the external load was removed which is shown in Figure 2.12(b).

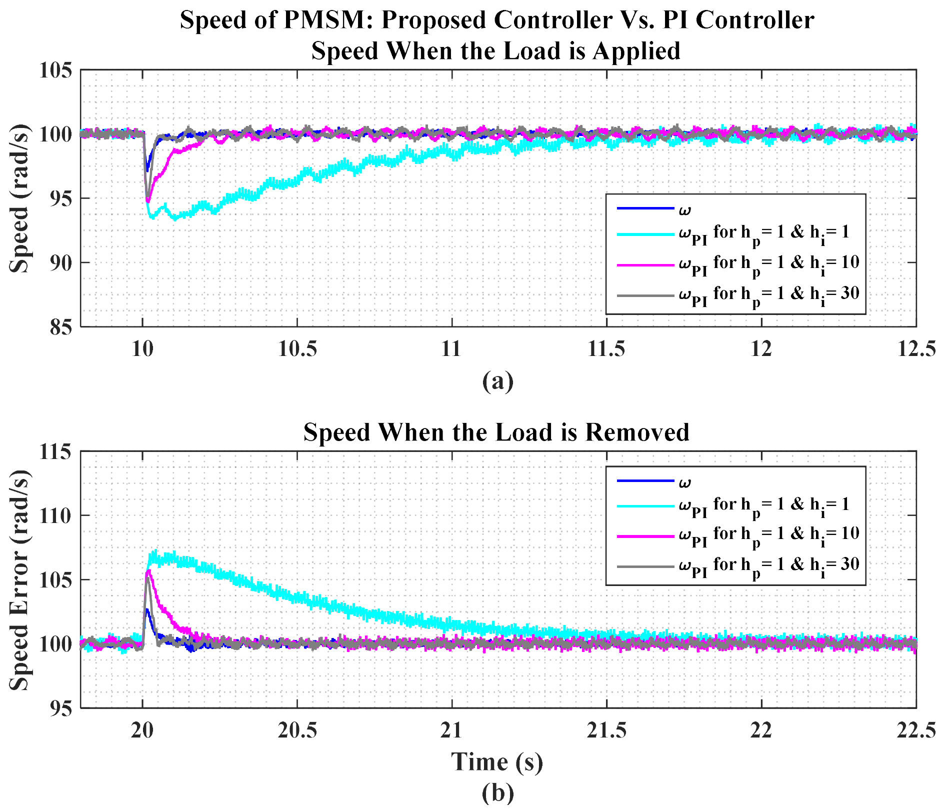

Figure 2.12. Speed of PMSM before and after the external load was applied.

Figure 2.13 shows the speed of the motor $\omega$ when the proposed controller is used, and the speed of the motor $\omega_{PI}$ when the PI speed controller is used with different pairs of PI gains when a time-varying load is applied to the PMSM. The load is about $1 + 0.75\sin(50 * (t - 10))$ which was applied at $\mathrm{t} = 10\mathrm{s}$. It can be seen that the proposed controller was able to keep the peak-to-peak steady state error less than $3.5\mathrm{rad/s}$ while the smallest peak-to-peak steady state error resulting from using the PI speed controller is about $5.5\mathrm{rad/s}$.

Both experiments show the effectiveness of the proposed control method in the presence of external disturbance. The robustness of the proposed control method against external disturbance is due to estimating the disturbance and cancelling it in the control law. On the other hand, the PI speed controller's robustness depends on dominating the effect of disturbance and thus requiring very high controller gains which affects the transient response. This poses a compromise between transient response and robustness against external load which does not exist in the proposed controller.

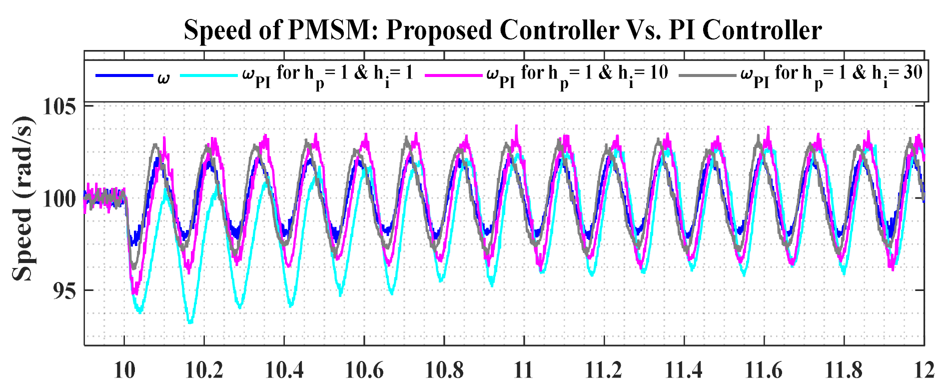

Figure 2.13. Speed of PMSM when the time-varying external load was applied.

## 2.5 Conclusion

A high performance control method has been introduced to regulate and shape the transient response of the speed of a PMSM to match that of a target system. We use an extended high-gain observer, which is driven by the measured rotor position, to estimate both the speed of the motor and the disturbance. Then, these estimates are used in a feedback linearization law to shape and regulate the speed of the motor. The extended high-gain observer is designed based on a reduced model of the system. The model is reduced by creating fast current loops which allow us to utilize singular perturbation theory.

Performance and robustness of the proposed control method are confirmed by demonstrating extensive simulation and experimental results that includes different operating conditions. The results also show that there is a very close agreement between simulation and experimental data which is a very important aspect from the design point of view. It allows development and testing of the controller in simulation before testing it in real life applications.

Finally, we have compared the performance of the proposed control method to the PI speed controller. The experimental results showed that the proposed control method is superior to the PI speed controller in three different ways. First, the PI speed controller required much more tuning effort than the proposed control method. Second, the proposed controller performed much better tracking a speed reference signal than the PI speed controller. Third, the proposed controller showed more robustness to external load than the PI speed controller.

# CHAPTER 3

In Chapter 2, we have introduced a new method to control the speed of surface mount PMSMs. In this Chapter, we will show the extension of this control method to solve the problem of sensorless control of PMSMs. The proposed sensorless control method is a back-emf based control scheme. Therefore, we will first revisit the model of the PMSM in the α-β coordinates and identify the back-emf signals. Then, we will design the back-emf observer in the same coordinates. Next, we transform the model of the PMSM to the d-q coordinates, which is performed using the estimated position, and close the loop around the currents with relatively fast PI controllers. After that, we reduce the model of the PMSM and design a third order Q-PLL extended high-gain observer as well as the speed feedback controller. Then, we perform a rigorous stability analysis of the closed loop system. Finally, we show simulation and experimental results to verify performance and robustness of the proposed controller.

## Speed Control without a Position Sensor

The goal is to design an output feedback controller that can achieve the following objectives:

1) Regulating the speed of the PMSM to a reference signal $\omega_{ref}$ using only current sensors without a position sensor, in the presence of both bounded external load $T_L$ and parameters uncertainty.
2) The ability to shape the transient response of the speed; when the absolute values of the motor and command speeds are above a certain value, to match that of a target system.

Since the proposed sensorless control method is back-emf based, let us rewrite the mathematical model of the PMSM to identify the induced EMF signals

$$L\frac{di_\alpha}{dt} = -Ri_\alpha + V_\alpha + u_\alpha \tag{3.1}$$

$$L\frac{di_\beta}{dt} = -Ri_\beta + V_\beta + u_\beta \tag{3.2}$$

$$J\frac{d\omega}{dt} = k_m\left(-i_\alpha \sin\left(n_p\theta\right) + i_\beta \cos\left(n_p\theta\right)\right) - B\omega - T_L \tag{3.3}$$

$$\frac{d\theta}{dt} = \omega \tag{3.4}$$

where $V_\alpha$ and $V_\beta$ are the two-phase equivalent induced EMF signals, which are defined by

$$V_\alpha = k_m\omega \sin\left(n_p\theta\right) \tag{3.5}$$

$$V_\beta = -k_m\omega \cos\left(n_p\theta\right) \tag{3.6}$$

The back-emf signals $V_\alpha$ and $V_\beta$ appear explicitly in the mathematical model of the PMSM in the α-β coordinates. These signals can be considered as disturbance inputs into the current equations ( 3.1 ) and ( 3.2 ). The electric subsystem of the PMSM is in a standard structure that is suitable for a class of disturbance observers; especially extended high-gain observers, which can be directly used without complex manipulation of the equations. Therefore, this model will be used for the estimation of the back-emf signals as a first step towards the estimation of the position and speed of the motor.

### 3.1 Proposed Control Algorithm

As indicated above, our proposed control scheme is an extension of the control method that was introduced in Chapter 2 to the position sensorless case and it is a back-emf based control strategy. Figure 3.1 shows the block diagram of the proposed control scheme.

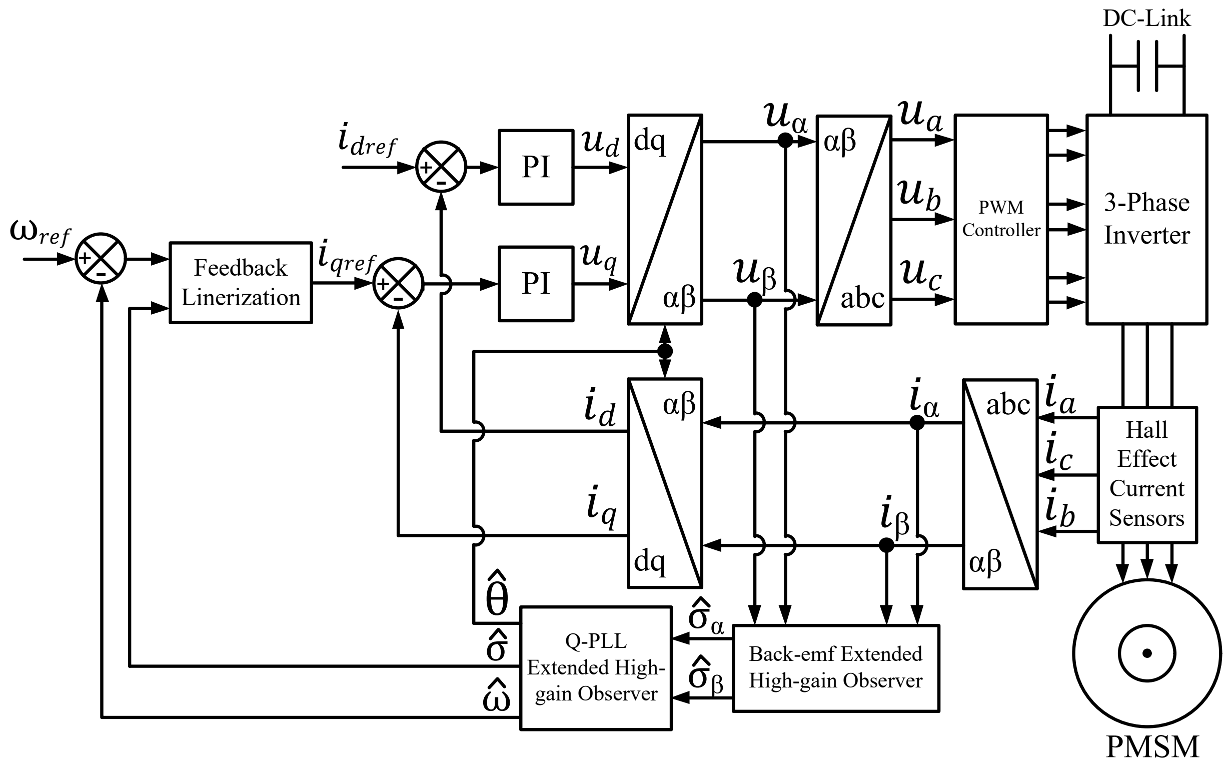


Figure 3.1. Block diagram of the proposed sensorless control algorithm.

The measured currents are used to drive the back-emf extended high-gain observer. The estimated back-emf signals $\hat{\sigma}_\alpha$ and $\hat{\sigma}_\beta$ are fed to a third order Q-PLL (Quadrature Phase Lock Loop) that is designed based on a reduced d-q model of the PMSM and formulated to operate as an extended high-gain observer. The Q-PLL estimates the position and the speed of the rotor as well as the disturbance that is present in the speed equation. The estimated position is then used to transform the currents $i_\alpha$ and $i_\beta$ from the stationary α-β coordinates to the rotating d-q coordinates for the field oriented control technique. We close the loop around the d-q currents with PI controllers that are designed to be relatively fast. As a result, the time separation between the electric subsystem and the mechanical subsystem of the PMSM is increased. Thus, we induce a two-time scale system which facilitates the reduction of the system using singular perturbation theory. Finally, the estimated speed and the estimated disturbance are used in a feedback linearization law to generate a control reference signal for the torque producing current $i_q$. Hence, the output feedback controller that would achieve the objectives is accomplished.

### 3.1.1 Back-emf Extended High-Gain Observer

The electrical subsystem of the mathematical model of the PMSM in the α-β coordinates ( 3.1 ) and ( 3.2 ) is used to design the back-emf extended high-gain observer. Before we proceed to design the back-emf observer, we first need to rewrite the electrical subsystem in the nominal form since we have assumed that the true parameters are not exactly known. Let $\hat{R}$ and $\hat{L}$ be respectively the nominal values of $R$ and $L$, then the nominal model of the electric subsystem takes the following form:

$$\frac{di_\alpha}{dt} = -\frac{\hat{R}}{\hat{L}} i_\alpha + \frac{1}{\hat{L}} u_\alpha + \sigma_\alpha \tag{3.7}$$

$$\frac{di_\beta}{dt} = -\frac{\hat{R}}{\hat{L}} i_\beta + \frac{1}{\hat{L}} u_\beta + \sigma_\beta \tag{3.8}$$

where $\sigma_\alpha$ and $\sigma_\beta$ are the disturbances, which are defined by

$$\sigma_\alpha = \frac{1}{L} V_\alpha - \left(\frac{R}{L} - \frac{\hat{R}}{\hat{L}}\right) i_\alpha + \left(\frac{1}{L} - \frac{1}{\hat{L}}\right) u_\alpha \tag{3.9}$$

$$\sigma_\beta = \frac{1}{L} V_\beta - \left(\frac{R}{L} - \frac{\hat{R}}{\hat{L}}\right) i_\beta + \left(\frac{1}{L} - \frac{1}{\hat{L}}\right) u_\beta \tag{3.10}$$

The definition of the disturbances $\sigma_\alpha$ and $\sigma_\beta$ include the back-emf signals as well as perturbation terms. The perturbation terms are present because of our assumption that we only know the nominal model of the system. The perturbation terms can be viewed as state dependent noise and their sizes depend on how close the nominal values $\hat{R}$ and $\hat{L}$ to the true values $R$ and $L$.

Now, the back-emf extended high–gain observer can be designed based on ( 3.7 ) and ( 3.8 ) as

$$\frac{d\hat{\imath}_\alpha}{dt} = -\frac{\hat{R}}{\hat{L}}\hat{\imath}_\alpha + \frac{1}{\hat{L}}u_\alpha + \hat{\sigma}_\alpha + \frac{h_1}{\mu}(i_\alpha - \hat{\imath}_\alpha) \tag{3.11}$$

$$\dot{\hat{\sigma}}_\alpha = \frac{h_2}{\mu^2}(i_\alpha - \hat{\imath}_\alpha) \tag{3.12}$$

$$\frac{d\hat{\imath}_\beta}{dt} = -\frac{\hat{R}}{\hat{L}}\hat{\imath}_\beta + \frac{1}{\hat{L}}u_\beta + \hat{\sigma}_\beta + \frac{h_1}{\mu}(i_\beta - \hat{\imath}_\beta) \tag{3.13}$$

$$\dot{\hat{\sigma}}_\beta = \frac{h_2}{\mu^2}(i_\beta - \hat{\imath}_\beta) \tag{3.14}$$

where $\hat{\imath}_\alpha$ and $\hat{\imath}_\beta$ are respectively the estimates of $i_\alpha$ and $i_\beta$, and $\hat{\sigma}_\alpha$ and $\hat{\sigma}_\beta$ are respectively the estimates of the disturbances $\sigma_\alpha$ and $\sigma_\beta$.The constants $h_1 > 0$ and $h_2 > 0$, and $\mu$ is a positive small parameter which satisfies the inequality $0 < \mu \ll 1$.

### 3.1.2 Current Loops

Field oriented control requires that the mathematical model of the PMSM ( 1.1 )-( 1.4 ) to be transformed from the stationary α-β coordinates to the rotating d-q coordinates. This transformation is achieved using the following Park transformation

$$\begin{bmatrix} i_d \\ i_q \end{bmatrix} = T(\hat{\theta}) \begin{bmatrix} i_\alpha \\ i_\beta \end{bmatrix}, \text{ and } \begin{bmatrix} u_d \\ u_q \end{bmatrix} = T(\hat{\theta}) \begin{bmatrix} u_\alpha \\ u_\beta \end{bmatrix}$$

where $\hat{\theta}$ is the estimated position, $i_d$ and $i_q$ are respectively the estimates of the direct-axis and quadrature-axis currents, $u_d$ and $u_q$ are respectively the direct-axis and the quadrature-axis input voltages, and

$$T(\hat{\theta}) = \begin{bmatrix} \cos(n_p\hat{\theta}) & \sin(n_p\hat{\theta}) \\ -\sin(n_p\hat{\theta}) & \cos(n_p\hat{\theta}) \end{bmatrix}$$

is the Park transformation operator. This transformation is normally done using the position $\theta$ of the rotor as in Chapter 2. However, $\theta$ here is not available for measurement and we perform the transformation using the estimated position $\hat{\theta}$. Therefore, the mathematical model of the PMSM in the estimated d-q coordinates, which is derived in Appendix B1, is given by

$$\frac{di_d}{dt} = -\frac{R}{L}i_d + \frac{k_m}{L}\omega\sin(n_p[\theta - \hat{\theta}]) + n_p\frac{d\hat{\theta}}{dt}i_q + \frac{1}{L}u_d \tag{3.15}$$

$$\frac{di_q}{dt} = -\frac{R}{L}i_q - \frac{k_m}{L}\omega\cos(n_p[\theta - \hat{\theta}]) - n_p\frac{d\hat{\theta}}{dt}i_d + \frac{1}{L}u_q \tag{3.16}$$

$$\frac{d\omega}{dt} = \frac{k_m}{J}\left(-i_d\sin(n_p[\theta - \hat{\theta}]) + i_q\cos(n_p[\theta - \hat{\theta}])\right) - \frac{B}{J}\omega - \frac{1}{J}T_L \tag{3.17}$$

$$\frac{d\theta}{dt} = \omega \tag{3.18}$$

Now, we close the loops around the electric subsystem ( 3.15 ) and ( 3.16 ) with relatively fast PI controllers. Define the current tracking errors as

$$e_d = i_{d_{ref}} - i_d \tag{3.19}$$

$$e_q = i_{q_{ref}} - i_q \tag{3.20}$$

where $e_d$ and $e_q$ are the direct and quadrature errors, $i_{d_{ref}}$ and $i_{q_{ref}}$ are the direct and quadrature current reference signals. We set $i_{d_{ref}} = 0$ since $i_d$ does not produce torque. The control inputs $u_d$ and $u_q$ are taken as

$$u_d = k_p e_d + x_d$$
$$u_q = k_p e_q + x_q \tag{3.21}$$

with

$$x_d = k_i \int_0^t e_d(\acute{t}) d\acute{t} \tag{3.22}$$

$$x_q = k_i \int_0^t e_q(\acute{t}) d\acute{t} \tag{3.23}$$

where $\acute{t}$ is a dummy integration variable, $k_p$ and $k_i$ are respectively the proportional and integral gains, and $x_d$ and $x_q$ are the integrals of $e_d$ and $e_q$, respectively. For convenience, $k_p$ and $k_i$ are taken to be the same for both the direct and quadrature current loops. Substituting $u_d$ and $u_q$ into ( 3.15 ) and ( 3.16 ) and using ( 3.19 ) and ( 3.20 ) we obtain the following current tracking error dynamics:

$$\tau \frac{de_d}{dt} = -e_d + \frac{1}{R + k_p}\left[-k_m \omega \sin\left(n_p\left[\theta - \hat{\theta}\right]\right) - x_d\right] - \tau n_p \frac{d\hat{\theta}}{dt}\left(i_{q_{ref}} - e_q\right) \tag{3.24}$$

$$\begin{aligned} \tau \frac{de_q}{dt} &= -e_q + \frac{1}{R + k_p}\left[R i_{q_{ref}} + k_m \omega \cos\left(n_p\left[\theta - \hat{\theta}\right]\right) - x_q\right] \\ &\quad + \tau\left[n_p \frac{d\hat{\theta}}{dt}\left(i_{d_{ref}} - e_d\right) + \frac{d i_{q_{ref}}}{dt}\right] \end{aligned} \tag{3.25}$$

where $\tau = \frac{L}{R+k_p}$ is the time constant of the current tracking errors; $\tau$ can be made small by increasing the proportional gain $k_p$ of the PI controllers. This will help increase the time separation between the electric and the mechanical subsystems of the PMSM.

### 3.1.3 Model Reduction

As indicated above, by the smallness of $\tau$, the electric subsystem ( 3.24 ) and ( 3.25 ) is made faster than the mechanical subsystem. Therefore, $e_d$ and $e_q$ will reach quasi-steady-state much faster than other state variables in the system.

The quasi-steady-state values of $e_d$ and $e_q$ are obtained by setting $\tau = 0$ in ( 3.24 ) and ( 3.25 ), which yields

$$\overline{e_d} = \frac{1}{R + k_p}\left[-k_m\omega \sin\left(n_p[\theta - \hat{\theta}]\right) - x_d\right] \tag{3.26}$$

$$\overline{e_q} = \frac{1}{R + k_p}\left[Ri_{q_{ref}} + k_m\omega \cos\left(n_p[\theta - \hat{\theta}]\right) - x_q\right] \tag{3.27}$$

where $\overline{e_d}$ and $\overline{e_q}$ are the quasi-steady-state of $e_d$ and $e_q$, respectively. The model is reduced by substituting ( 3.26 ) and ( 3.27 ) into ( 3.17 ) and into the differential form of ( 3.22 ) and ( 3.23 ), which yields

$$\frac{dx_d}{dt} = \frac{k_i}{R + k_p}\left[-k_m\omega \sin\left(n_p[\theta - \hat{\theta}]\right) - x_d\right] \tag{3.28}$$

$$\frac{dx_q}{dt} = \frac{k_i}{R + k_p}\left[Ri_{q_{ref}} + k_m\omega \cos\left(n_p[\theta - \hat{\theta}]\right) - x_q\right] \tag{3.29}$$

$$\begin{aligned}\frac{d\omega}{dt} &= \alpha_1\left[k_p i_{q_{ref}} + x_q\right]\cos\left(n_p[\theta - \hat{\theta}]\right) - \alpha_2\omega \\ &-\alpha_1 x_d \sin\left(n_p[\theta - \hat{\theta}]\right) - \frac{1}{J}T_L\end{aligned} \tag{3.30}$$

where $\alpha_1 = \frac{k_m}{J(R+k_p)}$, and $\alpha_2 = \frac{{k_m}^2}{J(R+k_p)} + \frac{B}{J}$. We view $i_{q_{ref}}$ as the control input for the speed equation ( 3.30 ) and it will be used for the formulation of the feedback linearization law.

### 3.1.4 Q-PLL Extended High-Gain Observer

Because we have assumed that only the nominal parameters of the PMSM are known and that the external load $T_L$ is unknown, we rewrite ( 3.30 ) as

$$\frac{d\omega}{dt} = \hat{\alpha}_1 k_p i_{q_{ref}} + \hat{\alpha}_1 x_q - \hat{\alpha}_2 \omega + \alpha_1 \left[cos\left(n_p\left[\theta - \hat{\theta}\right]\right) - 1\right] \left[k_p i_{q_{ref}} + x_q\right] \\ -\alpha_1 x_d \, sin\left(n_p\left[\theta - \hat{\theta}\right]\right) + \sigma \tag{3.31}$$

where $\hat{\alpha}_1$ and $\hat{\alpha}_2$ are the nominal values of $\alpha_1$ and $\alpha_2$, and $\sigma$ is the disturbance that is defined by

$$\sigma = (\alpha_1 - \hat{\alpha}_1) \left[k_p i_{q_{ref}} + x_q\right] - (\alpha_2 - \hat{\alpha}_2)\omega - \frac{1}{J} T_L$$

Equation ( 3.31 ) with $\sigma = 0$ is identical to the equation that would have been obtained had $\theta$ been known (i.e $\theta = \hat{\theta}$), there were no uncertainty in $\alpha_1$ and $\alpha_2$, and there were no load disturbance $T_L$.

Now, we design the Q-PLL extended high-gain observer based on ( 3.18 ) and ( 3.31 ) and driven by the estimated back-emf signals $\hat{\sigma}_\alpha$ and $\hat{\sigma}_\beta$. The observer is taken as

$$\frac{d\hat{\theta}}{dt} = \hat{\omega} + \frac{\rho_1}{\varepsilon} e \tag{3.32}$$

$$\frac{d\hat{\omega}}{dt} = \hat{\alpha}_1 k_p i_{q_{ref}} + \hat{\alpha}_1 x_q - \hat{\alpha}_2 \hat{\omega} + \hat{\sigma} + \frac{\rho_2}{\varepsilon^2} e \tag{3.33}$$

$$\frac{d\hat{\sigma}}{dt} = \frac{\rho_3}{\varepsilon^3} e \tag{3.34}$$

where $\hat{\omega}$ and $\hat{\sigma}$ are respectively the estimates of $\omega$, and $\sigma$, $\varepsilon$ is a positive small parameter that is chosen such that $\tau \ll \varepsilon \ll 1$, $\rho_1$, $\rho_2$, and $\rho_3$ are positive constants, and $e$ is the driving error of the observer and it is constructed by

$$e = \begin{cases} \dfrac{\hat{L}}{n_p \hat{k}_m \omega_{ref}} \left[\hat{\sigma}_\alpha \cos\left(n_p \hat{\theta}\right) + \hat{\sigma}_\beta \sin\left(n_p \hat{\theta}\right)\right] & for \left|\omega_{ref}\right| > \omega_b \\ \dfrac{\operatorname{sign}\left(\omega_{ref}\right) \hat{L}}{n_p \hat{k}_m \delta} \left[\hat{\sigma}_\alpha \cos\left(n_p \hat{\theta}\right) + \hat{\sigma}_\beta \sin\left(n_p \hat{\theta}\right)\right] & for \left|\omega_{ref}\right| \le \omega_b \end{cases}$$

where $\omega_b$ is some positive constant that determines the speed at which the choice of $e$ is selected, $\delta$ is a positive number that is used to keep the gain of the observer under a certain limit, and $\omega_{ref}$ is the speed reference signal. The purpose of dividing by $\omega_{ref}$ is to normalize the driving error signal so the gain variation of the observer is minimized since the back-EMF signals are proportional to the speed of the rotor.

In a very short time $O(\mu)$, within which $\hat{\sigma}_\alpha$ and $\hat{\sigma}_\beta$ reach their quasi steady state and can be approximated by ( 3.5 ) and ( 3.6 ), respectively, when parameter uncertainty is neglected, $e$ simplifies to

$$e = \begin{cases} \dfrac{L}{n_p k_m \omega_{ref}} \left[\dfrac{k_m}{L} \omega \sin\left(n_p \left[\theta - \hat{\theta}\right]\right)\right] & for \left|\omega_{ref}\right| > \omega_b \\ \dfrac{\operatorname{sign}\left(\omega_{ref}\right) L}{n_p k_m \delta} \left[\dfrac{k_m}{L} \omega \sin\left(n_p \left[\theta - \hat{\theta}\right]\right)\right] & for \left|\omega_{ref}\right| \le \omega_b \end{cases}$$

Since the proposed controller is meant for controlling the speed of the motor in both positive and negative directions, the sign of the true rotor speed must be known for the stability of the Q-PLL. For this reason we multiply by $\operatorname{sign}\left(\omega_{ref}\right)$.

The analysis of the closed loop system; which will be presented in section 3.2, shows that the simplified boundary layer of the Q-PLL extended high-gain observer can be represented as a negative feedback connection of the transfer function

$$\Gamma(\varepsilon s) = \frac{\frac{k_m}{\hat{k}_m}\frac{\omega}{\omega_{ref}}(\rho_1(\varepsilon s)^2 + \rho_2(\varepsilon s) + \rho_3)}{(\varepsilon s)^3 + \frac{k_m}{\hat{k}_m}\frac{\omega}{\omega_{ref}}\beta(\rho_1(\varepsilon s)^2 + \rho_2(\varepsilon s) + \rho_3)}$$

and the nonlinearity

$$S = \left[\frac{sin\left(n_p\left[\theta - \hat{\theta}\right]\right)}{n_p\left[\theta - \hat{\theta}\right]} - \beta\right]$$

We use the circle criterion [34] to show exponential stability of this boundary layer. As a result, the transfer function $\Gamma(\varepsilon s)$ is required to be SPR (Strictly Positive Real) and the nonlinearity $S > 0$ which are achieved by choosing positive constants $\rho_1$, $\rho_2$, and $\rho_3$ to satisfy the following inequalities

$$\begin{gathered} \rho_2 < a{\rho_1}^2 \\ \rho_3 \le \frac{{\rho_2}^2}{2\rho_1} \\ \frac{sin\left(n_p\left[\theta - \hat{\theta}\right]\right)}{n_p\left[\theta - \hat{\theta}\right]} > \beta \end{gathered} \tag{3.35}$$

where $a > 0$ is a known lower bound of $\beta\frac{k_m}{\hat{k}_m}\frac{\omega}{\omega_{ref}}$ with $\beta > 0$. The inequalities ( 3.35 ) are derived in Appendix B3.

### 3.1.5 Feedback Linearization under State Feedback

In this section we show the state feedback speed controller that stabilizes the slow subsystem ( 3.28 )-( 3.30 ) and shapes the transient response. This state feedback assumes perfect knowledge of $\theta$, $\omega$ and $\sigma$. Define the speed tracking error as

$$e_\omega = \omega_{ref} - \omega \tag{3.36}$$

The speed tracking error dynamics is found by taking the time derivative of ( 3.36 ) and using ( 3.31 ) which yields

$$\frac{de_\omega}{dt} = \frac{d\omega_{ref}}{dt} + \hat{\alpha}_2\omega_{ref} - \hat{\alpha}_1 k_p i_{q_{ref}} - \hat{\alpha}_1 x_q - \hat{\alpha}_2 e_\omega - \sigma \tag{3.37}$$

We desire the transient response of the speed tracking error to match that of the following target system

$$\frac{de_\omega{}^\star}{dt} = -k_\omega e_\omega{}^\star \tag{3.38}$$

where $k_\omega > 0$. The state feedback speed control law that achieves the objectives is given by

$$i_{q_{ref}} = \frac{1}{\hat{\alpha}_1 k_p}\left[\frac{d\omega_{ref}}{dt} + \hat{\alpha}_2\omega_{ref} + (k_\omega - \hat{\alpha}_2)e_\omega - \hat{\alpha}_1 x_q - \sigma\right]$$

$$\triangleq \psi\left(e_\omega, x_q, \sigma, \omega_{ref}, \frac{d\omega_{ref}}{dt}\right) \tag{3.39}$$

With $\theta = \hat{\theta}$ the closed-loop system formed of ( 3.28 ), ( 3.29 ), ( 3.37 ), and ( 3.39 ) is given by

$$\dot{\xi} = A_1\xi \tag{3.40}$$

where $\xi = \left[x_d, x_q - \bar{x}_q, e_\omega\right]^T$, $\bar{x}_q$ is the steady state value when $e_\omega = 0$ which satisfies the equation

$$\frac{d\bar{x}_q}{dt} = \frac{k_i}{(R + k_p)}\left[R\psi\left(0, \bar{x}_q, \sigma, \omega_{ref}, \frac{d\omega_{ref}}{dt}\right) + k_m\omega_{ref} - \bar{x}_q\right]$$

and

$$A_1 = \begin{bmatrix} -\frac{k_i}{R+k_p} & 0 & 0 \\ 0 & -\frac{k_i}{k_p} & -\frac{k_i}{k_m k_p}\left({k_m}^2 - RJ\left(k_\omega - \frac{B}{J}\right)\right) \\ 0 & 0 & -k_\omega \end{bmatrix} \quad (3.41)$$

The matrix $A_1$ is Hurwitz.

### 3.1.6 Feedback Linearization under Output Feedback

In this section, we derive the output feedback speed controller using the estimated speed and disturbance. The speed tracking error is obtained using ( 3.31 ) and ( 3.36 )

$$\frac{de_\omega}{dt} = \frac{d\omega_{ref}}{dt} + \hat{\alpha}_2\omega_{ref} - \hat{\alpha}_1 k_p i_{q_{ref}} - \hat{\alpha}_1 x_q - \hat{\alpha}_2 e_\omega - \sigma \quad (3.42)$$

Since we desire the transient response of the speed tracking error to match ( 3.38 ), the speed controller can be taken as

$$i_{q_{ref}} = \frac{1}{\hat{\alpha}_1 k_p}\left[\frac{d\omega_{ref}}{dt} + \hat{\alpha}_2\omega_{ref} + (k_\omega - \hat{\alpha}_2)\hat{e}_\omega - \hat{\alpha}_1 x_q - \hat{\sigma}\right]$$

$$\triangleq \psi\left(\hat{e}_\omega, x_q, \hat{\sigma}, \omega_{ref}, \frac{d\omega_{ref}}{dt}\right) \quad (3.43)$$

where $\hat{e}_\omega = \omega_{ref} - \widehat{\omega}$.

The peaking phenomenon of the high-gain observer is suppressed by saturating the controller outside the compact set $\Omega_1 = \{\xi^T P_1 \xi \leq c_1\}$ where $P_1 = P_1^T > 0$ is the solution of the Lyapunov equation $P_1 A_1 + A_1^T P_1 = -Q_1$ for some $Q_1 = Q_1^T > 0$, $c_1 > 0$ is chosen such that $\xi(0)$ is in the interior of $\Omega_1$ and

$$\max_{\xi \epsilon \Omega_1} \left| \psi \left( e_\omega, x_q, \sigma, \omega_{ref}, \frac{d\omega_{ref}}{dt} \right) \right| < i_{q_{max}} \tag{3.44}$$

where $i_{q_{max}}$ is the limit of $|i_q|$. The above inequality is possible if

$$\left| \psi \left( 0, \bar{x}_q, \sigma, \omega_{ref}, \frac{d\omega_{ref}}{dt} \right) \right| < i_{q_{max}}$$

which restricts $\omega_{ref}$, and $T_L$. The control law is then given by

$$i_{q_{ref}} = Msat \left( \frac{\psi \left( \hat{e}_\omega, x_q, \hat{\sigma}, \omega_{ref}, \frac{d\omega_{ref}}{dt} \right)}{M} \right) \tag{3.45}$$

where $M = i_{q_{max}}$.

### 3.2 Closed Loop Analysis

Analyzing the stability of the closed loop system of the proposed sensorless control is not an easy task because it is highly nonlinear and there are twelve states. However, since the system was designed to be a multi-time scale one, we will use the singular perturbation theory to study the stability of the closed loop system. To simplify the closed loop analysis, we will assume exact knowledge of the inductance $L$ and the resistance $R$. However, the effects of all parameter uncertainty will be investigated in the simulations and experiments part of this chapter.

***Theorem 3.1:*** *Consider the closed loop system formed of the PMSM model* ( 3.1 )-( 3.4 )*, the back-EMF extended high-gain observer* ( 3.11 )-( 3.14 )*, the PI current controllers* ( 3.21 )*, the Q-PLL extended high-gain observer* ( 3.32 )-( 3.34 )*, and the speed controller*( 3.45 )*. Assume that*

*1)* $\omega_{ref}$, $\frac{d\omega_{ref}}{dt}$, *and* $\frac{d^2\omega_{ref}}{dt^2}$ *are bounded*

*2)* $T_L$ *and* $\frac{dT_L}{dt}$ *are bounded*

*3)* $\frac{k_m}{\hat{k}_m}\frac{\omega}{\omega_{ref}} > a > 0$

*4)* $\frac{1}{2}\zeta\lambda_{min}(P_2) - \frac{\rho_3 k_m \lambda_{max}(P_2)\omega}{\hat{k}_m\omega^\star}\left|\frac{k_m}{\hat{k}_m}\frac{\hat{J}}{J} - 1\right| > 0$

*5)* $\frac{sin(n_p[\theta-\hat{\theta}])}{n_p[\theta-\hat{\theta}]} > \beta$

*6)* $\xi(0)$ *is in the interior of* $\Omega_1$ *and the initial states* $i_\alpha(0)$, $i_\beta(0)$, $\hat{\imath}_\alpha(0)$, $\hat{\imath}_\beta(0)$, $\hat{\sigma}_\alpha(0)$, $\hat{\sigma}_\beta(0)$, $\hat{\omega}(0)$, *and* $\hat{\sigma}(0)$ *are bounded*

*Then, there exist positive constants* $\lambda_1$, $\lambda_2$ *and* $\lambda_3$ *such that for* $\varepsilon < \lambda_1$, $\frac{\tau}{\varepsilon} < \lambda_2$, *and* $\frac{\mu}{\varepsilon} < \lambda_3$, *the trajectories of the closed loop system are bounded for all* $t \geq 0$, *and*

$$|e_\omega{}^\star(t) - e_\omega(t)| \to 0 \text{ as } \varepsilon \to 0, \frac{\tau}{\varepsilon} \to 0, \text{ and } \frac{\mu}{\varepsilon} \to 0 \text{ for all } t \geq 0 \tag{3.46}$$

***Proof:*** The closed-loop system is represented as a three-time-scale singularly perturbed system. The state variables are taken as

$$\xi_1 = x_d\,,\ \ \xi_2 = x_q - \bar{x}_q\,,\ \ \xi_3 = e_\omega\,,\ \ \eta_1 = \frac{1}{\varepsilon^2}\left(\theta - \hat{\theta}\right) - \frac{1}{\varepsilon^2 n_p} sin^{-1}\left(\mu n_p \frac{h_1}{h_2}\omega\right),$$

$$\eta_2 = \frac{1}{\varepsilon}(\omega - \hat{\omega})\,,$$

$$\eta_3 = (\alpha_1 - \hat{\alpha}_1)\left[k_p M \phi_\varepsilon\left(\frac{\psi(\cdot)}{M}\right) + x_q\right] - (\alpha_2 - \hat{\alpha}_2)\omega - \frac{1}{J}T_L - \hat{\sigma},$$

$$z_\alpha = -i_\alpha + \frac{k_m}{R+k_p}\omega\, sin(n_p\theta) + \frac{1}{R+k_p}\left[x_d\, cos(n_p\hat{\theta}) - x_q\, sin(n_p\hat{\theta})\right]$$

$$-\frac{k_p}{R+k_p}M\phi_\varepsilon\left(\frac{\psi(\hat{\cdot})}{M}\right)sin(n_p\hat{\theta}),$$

$$z_\beta = -i_\beta - \frac{k_m}{R+k_p}\omega\, cos(n_p\theta) + \frac{1}{R+k_p}\left[x_d\, sin(n_p\hat{\theta}) + x_q\, cos(n_p\hat{\theta})\right]$$

$$+\frac{k_p}{R+k_p}M\phi_\varepsilon\left(\frac{\psi(\hat{\cdot})}{M}\right)cos(n_p\hat{\theta}),$$

$$v_{\alpha 1} = \frac{1}{\mu}\frac{L}{\varepsilon^2 k_m}(i_\alpha - \hat{\imath}_\alpha),\;\; v_{\alpha 2} = \frac{L}{\varepsilon^2 k_m}\left(\frac{k_m}{L}\omega\, sin(n_p\theta) - \hat{\sigma}_\alpha\right),$$

$$v_{\beta 1} = \frac{1}{\mu}\frac{L}{\varepsilon^2 k_m}(i_\beta - \hat{\imath}_\beta),\;\; v_{\beta 2} = \frac{L}{\varepsilon^2 k_m}\left(-\frac{k_m}{L}\omega\, cos(n_p\theta) - \hat{\sigma}_\beta\right),$$

$$\xi = \begin{bmatrix}\xi_1\\ \xi_2\\ \xi_3\end{bmatrix},\quad \eta = \begin{bmatrix}\eta_1\\ \eta_2\\ \eta_3\end{bmatrix},\quad z = \begin{bmatrix}z_\alpha\\ z_\beta\end{bmatrix},\quad v = \begin{bmatrix}v_{\alpha 1}\\ v_{\alpha 2}\\ v_{\beta 1}\\ v_{\beta 2}\end{bmatrix}$$

where $\phi_\varepsilon$ is an odd function defined by

$$\phi_\varepsilon(y) = \begin{cases} y & for\ 0 \le y \le 1 \\ y + \dfrac{y-1}{\varepsilon} - \dfrac{y^2-1}{2\varepsilon} & for\ 1 \le y \le 1+\varepsilon \\ 1 + \dfrac{\varepsilon}{2} & for\ y \ge 1+\varepsilon \end{cases}$$

which is a continuously differentiable nondecreasing function with a locally Lipschitz derivative and bounded uniformly in $\varepsilon$ on any bounded interval of $\varepsilon$. Furthermore, the function $\phi_\varepsilon$ satisfies $|sat(y) - \phi_\varepsilon(y)| \le \frac{\varepsilon}{2}$ and $|\phi_\varepsilon'(y)| \le 1\ \forall\ y \in \mathbb{R}$.

For $\xi \epsilon \Omega_1$, the closed-loop system is described by

$$\dot{\xi} = A_1\xi + f_1(\cdot) + \varepsilon f_2(\cdot) \tag{3.47}$$

$$\varepsilon\dot{\eta} = A_2\eta + B_1S_1 + B_2S_2 + f_3(\cdot) + \frac{\mu}{\varepsilon}f_4(\cdot) + \varepsilon f_5(\cdot) + \mu f_6(\cdot) \qquad (3.48)$$

$$\tau\dot{z} = -z + \frac{\tau}{\varepsilon}f_7(\cdot) + \varepsilon f_8(\cdot) + \tau f_9(\cdot) \qquad (3.49)$$

$$\mu\dot{v} = A_3v + \frac{r_2k_m}{J}B_3z + \frac{\mu}{\varepsilon}f_{10}(\cdot) + \varepsilon f_{11}(\cdot) + \mu f_{12}(\cdot) \qquad (3.50)$$

where $r_2 = \frac{\mu}{\varepsilon^2}$, $A_1$ is defined by ( 3.41 ),

$$A_2 = \begin{bmatrix} -\beta\frac{k_m}{\hat{k}_m}\frac{(\omega_{ref}-\xi_3)}{\omega_{ref}}\rho_1 & 1 & 0 \\ -\beta\frac{k_m}{\hat{k}_m}\frac{(\omega_{ref}-\xi_3)}{\omega_{ref}}\rho_2 & 0 & 1 \\ -\beta\frac{k_m}{\hat{k}_m}\frac{(\omega_{ref}-\xi_3)}{\omega_{ref}}\rho_3 & 0 & 0 \end{bmatrix}, \quad A_3 = \begin{bmatrix} -h_1 & 1 & 0 & 0 \\ -h_2 & 0 & 0 & 0 \\ 0 & 0 & -h_1 & 1 \\ 0 & 0 & -h_2 & 0 \end{bmatrix}, \quad B_1 = \begin{bmatrix} \frac{k_m}{\hat{k}_m}\frac{(\omega_{ref}-\xi_3)}{\omega_{ref}}\rho_1 \\ \frac{k_m}{\hat{k}_m}\frac{(\omega_{ref}-\xi_3)}{\omega_{ref}}\rho_2 \\ \frac{k_m}{\hat{k}_m}\frac{(\omega_{ref}-\xi_3)}{\omega_{ref}}\rho_3 \end{bmatrix},$$

$$B_2 = \begin{bmatrix} 0 \\ 0 \\ 1 \end{bmatrix}, \quad B_3 = \begin{bmatrix} 0 & 0 \\ sin^2(n_p\theta) & -\frac{1}{2}sin(2n_p\theta) \\ 0 & 0 \\ -\frac{1}{2}sin(2n_p\theta) & cos^2(n_p\theta) \end{bmatrix}, \quad S_1 = -\left[\frac{sin(\varepsilon^2n_p\eta_1)}{\varepsilon^2n_p\eta_1} - \beta\right]\eta_1,$$

$$S_2 = -\frac{\rho_3k_m(\omega_{ref}-\xi_3)}{\hat{k}_m\omega_{ref}}\left(\frac{\alpha_1}{\hat{\alpha}_1} - 1\right)\phi'_\varepsilon\left(\frac{\psi(\hat{\cdot})}{M}\right)\frac{sin(\varepsilon^2n_p\eta_1)}{\varepsilon^2n_p}$$

$A_2$ and $A_3$ are Hurwitz matrices by design. The functions $f_1(\cdot)$ to $f_{12}(\cdot)$, which are given in Appendix B4, are bounded by

$\|f_1(\cdot)\| \le k_b\|z\| + k_d$, $\|f_2(\cdot)\| \le k_d$, $\|f_3(\cdot)\| \le k_b\|z\| + k_a\|v\|$, $\|f_4(\cdot)\| \le k_b\|z\| + k_d$,

$\|f_5(\cdot)\| \le k_c\|\eta\| + k_b\|z\| + k_a\|v\| + k_d$, $\|f_6(\cdot)\| \le \frac{\varepsilon}{\mu}k_c\|\eta\| + \frac{\varepsilon}{\mu}k_d$,

$\|f_7(\cdot)\| \le k_c\|\eta\| + k_a\|v\| + k_d$, $\|f_8(\cdot)\| \le k_d$, $\|f_9(\cdot)\| \le k_d + k_a\|v\| + k_c\|\eta\| + k_b\|z\|$,

$\|f_{10}(\cdot)\| \le k_c\|\eta\| + k_a\|v\| + k_d$, $\|f_{11}(\cdot)\| \le \varepsilon k_c\|\eta\| + \frac{\mu}{\varepsilon}k_d$,

$\|f_{12}(\cdot)\| \le k_a\|v\| + k_b\|z\| + k_c\|\eta\| + k_d$.

Moreover, $f_1$ vanishes at $\mu = 0$, $\eta = 0$, and $z = 0$ and $f_3$ vanishes at $z = 0$ and $v = 0$.

For $\tau \ll \varepsilon \ll 1$, the system ( 3.47 )-( 3.50 ) is singularly perturbed with three-time-scales. In the fastest time-scale, the boundary layer model is

$$\tau \dot{z} = -z$$

$$\mu \dot{v} = A_3 v + \frac{r_2 k_m}{J} B_4 z$$

which is exponentially stable by design and it was obtained by setting $\mu = 0$, $\tau = 0$, $\varepsilon = 0$, $\frac{\mu}{\varepsilon} = 0$, and $\frac{\tau}{\varepsilon} = 0$ on the right-hand side of ( 3.49 ) and ( 3.50 ). The quasi-steady-state of this model is $z = 0$ and $v = 0$. In the next time-scale, the boundary layer model is

$$\varepsilon \dot{\eta} = A_2 \eta + B_1 S_1 + B_2 S_2 \qquad (3.51)$$

which was obtained by setting $\mu = 0$, $\varepsilon = 0$, $\frac{\mu}{\varepsilon} = 0$, $v = 0$, and $z = 0$ on the right-hand side of ( 3.48 ). This boundary layer has equilibrium points at $\eta_1 = \frac{m\pi}{\varepsilon^2 n_p}$ and $\eta_2 = \eta_3 = 0$ where $m \epsilon \mathbb{Z}$. For odd values of $m$, it can be easily shown by linearization that the corresponding equilibrium points of the boundary layer ( 3.51 ) are unstable. For even values of $m$, however, it is sufficient to study the equilibrium point that corresponds to $m = 0$, because not only does shifting the equilibrium point by $\frac{m\pi}{\varepsilon^2 n_p}$ leads to the same boundary layer but also to the same closed loop system. This is due to the fact that $\eta_1$ only appears as an argument of the sine and cosine functions throughout the closed loop system.

With $m = 0$ and the output equation $y = C\eta$ where $C = [1 \quad 0 \quad 0]$, the boundary layer system ( 3.51 ) can be represented as a negative feedback connection of the transfer function

$$\Gamma(\varepsilon s) = \frac{\frac{k_m}{\hat{k}_m}\frac{\omega}{\omega^\star}(\rho_1(\varepsilon s)^2 + \rho_2(\varepsilon s) + \rho_3)}{(\varepsilon s)^3 + \frac{k_m}{\hat{k}_m}\frac{\omega}{\omega^\star}\beta(\rho_1(\varepsilon s)^2 + \rho_2(\varepsilon s) + \rho_3)}$$

and the nonlinearity $S_1$. The nonlinearity $B_2 S_2$ is considered as disturbance to the boundary layer of $\dot{\eta}$-equation. The transfer function $\Gamma(\varepsilon s)$ is strictly positive real if and only if $\rho_1$, $\rho_2$, and $\rho_3$ are chosen positive and the following inequalities are satisfied

$$\rho_2 < a{\rho_1}^2$$

$$\rho_3 \leq \frac{{\rho_2}^2}{2\rho_1}$$

where $a > 0$ is a known lower bound of $\beta \frac{k_m}{\hat{k}_m}\frac{\omega}{\omega_{ref}}$ with $\beta > 0$. The nonlinear function $S_1$ belongs to the sector $[\beta, \infty]$ provided the following sector condition holds

$$\frac{sin(\varepsilon^2 n_p \eta_1)}{\varepsilon^2 n_p \eta_1} > \beta \text{ or equivalently rewritten as } \frac{sin(n_p[\theta - \hat{\theta}])}{n_p[\theta - \hat{\theta}]} > \beta \qquad (3.52)$$

We use the circle criterion [34] to show that the origin of the boundary layer of ( 3.51 ) is exponentially stable. We Use the Kalman-Yakubovic-Popov lemma [34, Lemma 6.3] to obtain a quadratic Lyapunov function; that is,

$$V_2(\eta) = \frac{1}{2}\eta^T P_2 \eta \qquad (3.53)$$

where $P_2$ is the positive definite symmetric solution of the Kalman-Yakubovic-Popov equations

$$P_2 A_2 + {A_2}^T P_2 = -N^T N - \zeta P_2$$
$$P_2 B_1 = C^T$$

where $\zeta > 0$. It can be shown that the time derivative of ( 3.53 ) along the boundary layer ( 3.51 ) satisfies

$$\varepsilon\dot{V}_2(\eta) \leq -\left[\frac{1}{2}\zeta\lambda_{min}(P_2) - \frac{\rho_3 k_m \lambda_{max}(P_2)\omega}{\hat{k}_m\omega^\star}\left|\frac{k_m\hat{J}}{\hat{k}_m J} - 1\right|\right]\|\eta\|^2$$

which shows exponential stability of the boundary layer ( 3.51 ) provided that

$$\frac{1}{2}\zeta\lambda_{min}(P_2) - \frac{\rho_3 k_m \lambda_{max}(P_2)\omega}{\hat{k}_m\omega^\star}\left|\frac{k_m\hat{J}}{\hat{k}_m J} - 1\right| > 0$$

Finally, the slow subsystem reduces to $\dot{\xi} = A_1\xi$ which is exponentially stable and was obtained by setting $\eta = 0$, $z = 0$, $\mu = 0$, and $\varepsilon = 0$ in ( 3.47 ).

Consider the set

$$\Omega = \Omega_1 \times \{W(\eta, z, v) < \ell^2 c_2\}$$

where $\ell = \max\left(\varepsilon, \frac{\tau}{\varepsilon}\right)$ and $W(\eta, z, v) = \eta^T P_2 \eta + \frac{1}{2} z^T z + r_1 v^T P_3 v$ in which $P_3 = P_3^T > 0$ is the solution of the Lyapunov equation $P_3 A_3 + A_3^T P_3 = -Q_3$ for some $Q_3 = Q_3^T > 0$. Similar to arguments used in the analysis of high-gain observers [34], it can be shown that, by choosing $c_2 > 0$ large enough, the set $\Omega$ is positively invariant for sufficiently small $\varepsilon$, $\frac{\tau}{\varepsilon}$, and $\frac{\mu}{\varepsilon}$. This is accomplished by showing that $\dot{V}_1 < 0$ on the boundary of $\Omega_1$, and $\dot{W} < 0$ on the boundary $W = \ell^2 c_2$.

At the initial time, $\big(\eta(0), v(0), z(0)\big)$ could be outside the set $\{W(\eta, z, v) < \ell^2 c_2\}$ but would move rapidly toward the set and will reach it within an interval $[0, T(\ell)]$, where $\lim_{\ell\to 0} T_1(\ell) = 0$. Since the initial states $\xi(0)$ are in the interior of $\Omega_1$, choosing $\ell$ small enough ensures $\xi$ does not leave $\Omega_1$, and by the end of this interval $(\xi, \eta, z, v)$ would be in the positively invariant set $\Omega$.

Now, the limit

$$|e_\omega{}^\star(t) - e_\omega(t)| \to 0 \; as \; \varepsilon \to 0, \frac{\tau}{\varepsilon} \to 0, \; and \; \frac{\mu}{\varepsilon} \to 0 \; for \; all \; t \geq 0$$

follows from the continuous dependence of the solutions of differential equations on parameters [34, Theorem 9.1] and exponential stability of the subsystems

$$\dot{\xi} = A_1\xi, \varepsilon\dot{\eta} = A_2\eta + B_1S_1 + B_2S_2, \tau\dot{z} = -z, \text{ and } \mu\dot{v} = A_3v + \frac{r_2k_m}{J}B_3z. \quad \blacksquare$$

### 3.3 Simulations and Experimental Results

The proposed control method is tested in two ways to assess its performance and its feasibility in practical settings. Firstly, the closed loop system is tested in simulation using MATLAB Simulink. Secondly, the closed loop system is tested in an experiment for further validation of the control method. The experimental setup is exactly the same as what was described in Section 2.3.1. The position measurement is only used here for the purpose of comparison and is not used in any way or form in the feedback controller. Table 3.1 shows the nominal parameters of the used surface mount PMSM.

For all simulations and experiments, the following controller parameters are used. However, we have to first determine a lower bound of $\frac{k_m}{\hat{k}_m}\frac{\omega}{\omega_{ref}}$ before we choose the controller parameters. According to [3], $\hat{k}_m$ can vary as much as 20%. Therefore, we set $\frac{k_m}{\hat{k}_m} = \frac{5}{6}$. Additionally, we allow $\omega$ to vary around $\omega_{ref}$ by 25% which sets $\frac{\omega}{\omega_{ref}} = \frac{3}{4}$. We choose the parameters of the Q-PLL extended high-gain observer $\rho_1 = 3$, $\rho_2 = 3$, and $\rho_3 = 1$, and they are

| Parameter | Value |
|---|---|
| Rated Voltage | 200 $VAC_{L-L}$ |
| Rated Current | 5.1 A |
| Rated Torque | 3.18 N.m |
| Rated Speed | 3000RPM |
| Inductance $\boldsymbol{L}$ | 4.47 mH |
| Per Phase Winding Resistance $\boldsymbol{R}$ | 0.835 Ω |
| Torque Constant $\boldsymbol{k_m}$ | 0.41 $V \cdot s$ |
| Number of Pole Pairs $\boldsymbol{n_p}$ | 4 |
| Viscosity Coefficient $\boldsymbol{B}$ | 0.0011 $\frac{N \cdot m \cdot s}{rad}$ |
| Moment of Inertia $\boldsymbol{J}$ | 0.0022 $Kg \cdot m^2$ |

Table 3.1. Nominal parameters of the used PMSM.

chosen such that the linearized boundary layer of the Q-PLL extended high-gain observer with no parameters perturbation and $\omega = \omega_{ref}$ has negative real roots at $-1$. We also choose $\left|\theta - \hat{\theta}\right| \le \frac{\pi}{8}$. Now, $\beta$ is within the following inequality

$$\frac{\rho_2}{\frac{k_m}{\hat{k}_m} \frac{\omega}{\omega_{ref}} {\rho_1}^2} < \beta < \frac{sin\left(n_p\left[\theta - \hat{\theta}\right]\right)}{n_p\left[\theta - \hat{\theta}\right]}$$

$$0.533 < \beta < 0.637$$

which was obtained using the inequalities ( 3.35 ). The current transient response is needed to be relatively fast. Therefore, the proportional and integral gains of the PI current controllers are chosen as: $k_p = 25$, and $k_i = 2500$, respectively, which makes $\tau = 1.73 \times 10^{-4}$. The parameters of the back-EMF observer are: $h_1 = 2$ and $h_2 = 1$, and they are chosen such that the matrix $A_3$ has negative real eigenvalues at $-1$. In addition, with $\tau = 1.73 \times 10^{-4}$, $\mu = 0.0001$ was found in the simulation and the experiment to provide relatively fast estimation of the back-emf signals as well as providing low noise amplification. Once $\mu$ has been determined, $\varepsilon = 0.0085$ was found to have the best compromise between fast estimation of the Q-PLL variables and low noise amplification in both the simulation and experiment. Now, the ratios $\frac{\tau}{\varepsilon} = 0.02$ and

$\frac{\mu}{\varepsilon^2} = 1.38$ are within the recommended values that are provided by Theorem 3.1. For fast speed error decay we choose $k_\omega = 60$.

The speed profile that is used for both the simulations and the experiments is given by

$$\omega_{ref} = \begin{cases} \frac{1}{2} z_1 t^2 & for \quad 0 \le t < t_1 \\ a_f t + C_1 & for \quad t_1 \le t < t_2 \\ -\frac{1}{2} z_1 t^2 + z_2 t + C_2 & for \quad t_2 \le t < t_3 \\ C_3 & for \quad t_3 \le t \end{cases}$$

where $z_1 = 310719,\ z_2 = 21554,\ a_f = 1554,\ C_1 = -3.884,\ C_2 = -647.6,\ C_3 = 100,$ $t_1 = 0.005,\ t_2 = 0.0644,$ and $t_3 = 0.0694$. The speed profile is designed to be relatively fast and the maximum required acceleration does not exceed the motor's capability. Since this speed controller is not designed to operate in low speeds so the initial condition $\omega_{ref}(0) = 50\frac{rad}{s}$. The speed profile is designed to show that the proposed controller performs well with fast speed reference transitions.

### 3.3.1 Simulations

There are three simulation cases that will be shown and discussed. The first case of the simulations will be conducted using the nominal parameters of the motor and the speed reference profile $\omega_{ref}$. This simulation is intended to show the response of the closed loop system using the controller parameters that we have come up with in the previous section. The second case will show the response of the closed loop system when the initial condition of the term $\theta - \hat{\theta}$ is set just under the edge of the sector. The third case will show the response of the closed loop system when an external load is applied.

#### 3.3.1.1 First Simulation Case

This simulation case will show the response of the closed loop system to the fast changing speed reference profile $\omega_{ref}$. In this case the motor's initial speed as well as the estimated speed are set to $50\frac{rad}{s}$. Then, $\omega_{ref}(t)$ is applied at $t = 0.1$. The nominal parameters in Table 3.1 are used. In addition, the motor in this case is not externally loaded.

Figure 3.2(a) shows the speed reference profile $\omega_{ref}$, the speed of the motor $\omega$, and the estimated speed of the motor $\widehat{\omega}$. It can be seen that, to a great extent, the speed trajectory of the motor under the proposed controller overlaps that of the speed profile $\omega_{ref}$. This shows the high performance of the proposed control method to closely follow the reference speed. In addition, Figure 3.2(b) gives a closer look at how the speed trajectory of the motor under the proposed controller deviates from the speed reference. The maximum speed error is less than $0.7\%$ and it occurs during transient.

Figure 3.2(c) show the position estimation error. It can be seen that the maximum position estimation error is less than $2^{\circ}$ during transient and less than $1.6^{\circ}$ during steady state. This shows accurate position estimation which is needed for the use of field oriented control technique.

#### 3.3.1.2 Second Simulation Case

This simulation case will show the response of the closed loop system when the initial position estimation error is large .In this case the motor's initial speed, estimated speed, and reference speed are set to $100\frac{rad}{s}$. Also, the initial error between the position of the rotor and the estimated position is set to $\theta(0) - \hat{\theta}(0) = \frac{9\pi}{80}$ which is just inside the border of the sector. The nominal parameters in Table 3.1 are used. In addition, the motor in this case is not externally loaded.

Figure 3.3(a) shows the speed reference profile $\omega_{ref}$, the speed of the motor $\omega$, and the estimated speed of the motor $\hat{\omega}$ when $\theta(0) - \hat{\theta}(0) = \frac{9\pi}{80}$. It can be seen that, initially, the speed trajectory of the motor as well as the speed estimation has deviated from each other and also deviated from the reference speed which is due to the initial position estimation error not being at its equilibrium point. However, the proposed controller was able to quickly close the gap between the motor's speed and its estimate and also regulate the speed of the motor to the speed reference. Simultaneously, the proposed controller was also able to quickly bring the position estimation error down from $\frac{9\pi}{80}$ to its equilibrium point which can be seen in Figure 3.3(c).

#### 3.3.1.3 Third Simulation Case

This simulation case will show the response of the closed loop system when an external load is applied. In this case the motor's initial speed, estimated speed, and reference speed are set to $100\,\frac{rad}{s}$. The nominal parameters in Table 3.1 are used. In addition, the motor in this cases is loaded with a step of external load of 2 $N.m$ applied at $t = 0.3s$ and removed at $t = 0.7s$. This will test the robustness of the proposed control method against external loads.

The speed trajectory of the motor under the proposed controller dropped about 12% when the external load was applied at $\mathrm{t} = 0.3\mathrm{s}$, which can be seen in Figures 3.2(a) and 3.2(b). Similar behavior can be observed at the moment when the external load is removed at $t = 0.7s$. The proposed controller was able to recover the speed quickly in both cases and that is due to estimating the disturbance and canceling it in the feedback.

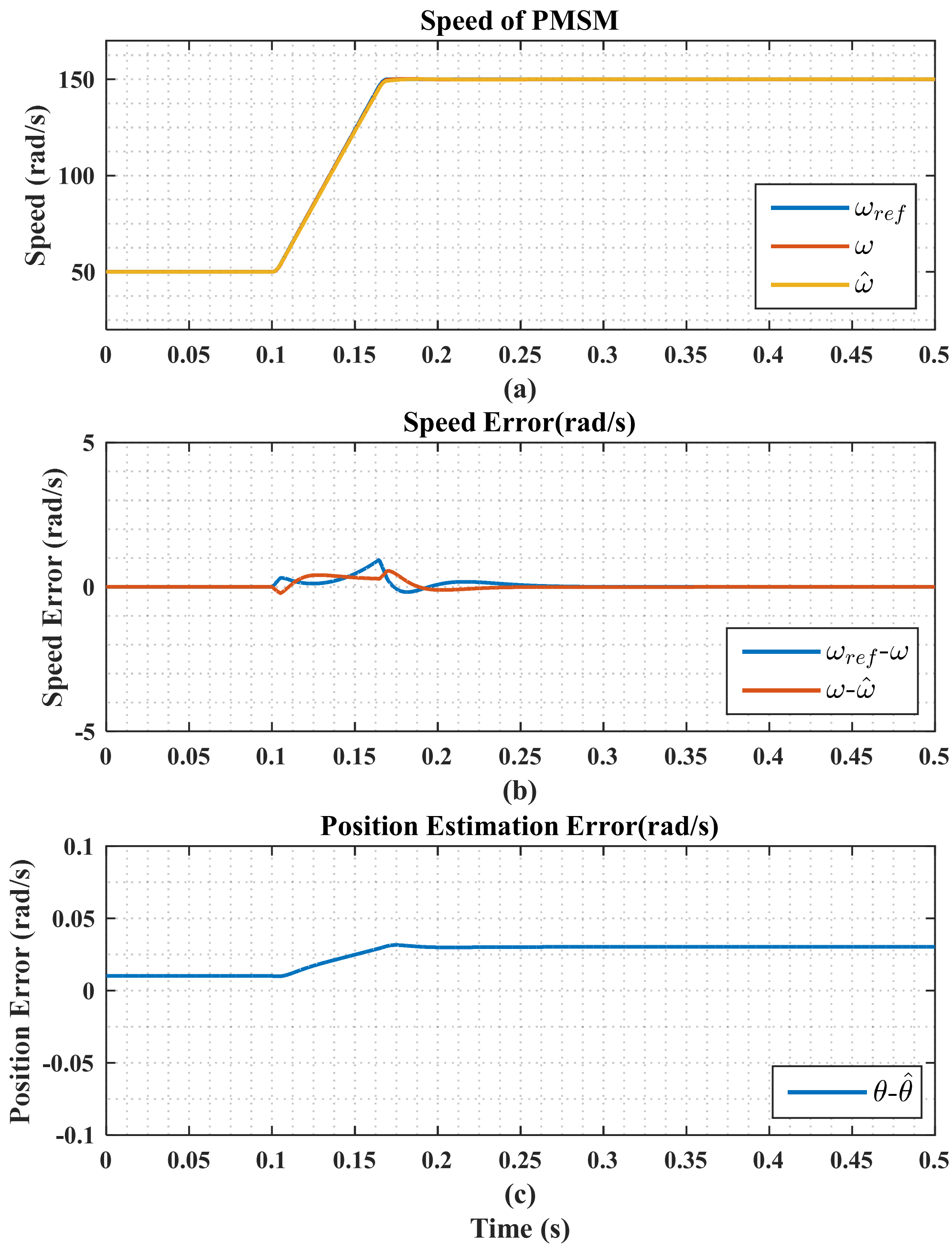


Figure 3.2. (a) Reference speed, speed of PMSM, and estimated speed, (b) Speed error from reference speed and speed estimation error, (c) Position estimation error.

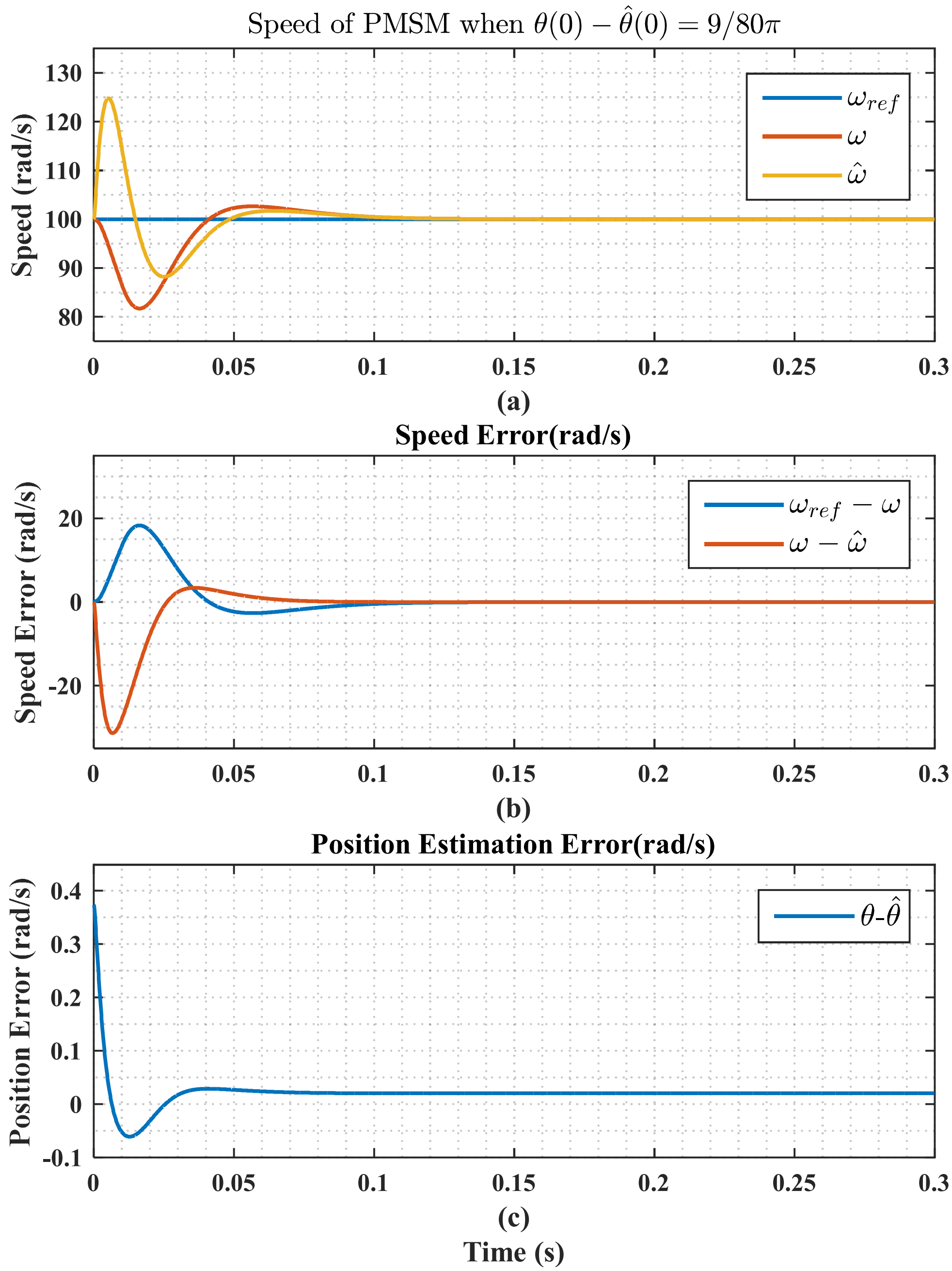


Figure 3.3. (a) Reference speed, speed of PMSM, and estimated speed, (b) Speed error from reference speed and speed estimation error, (c) Position estimation error.

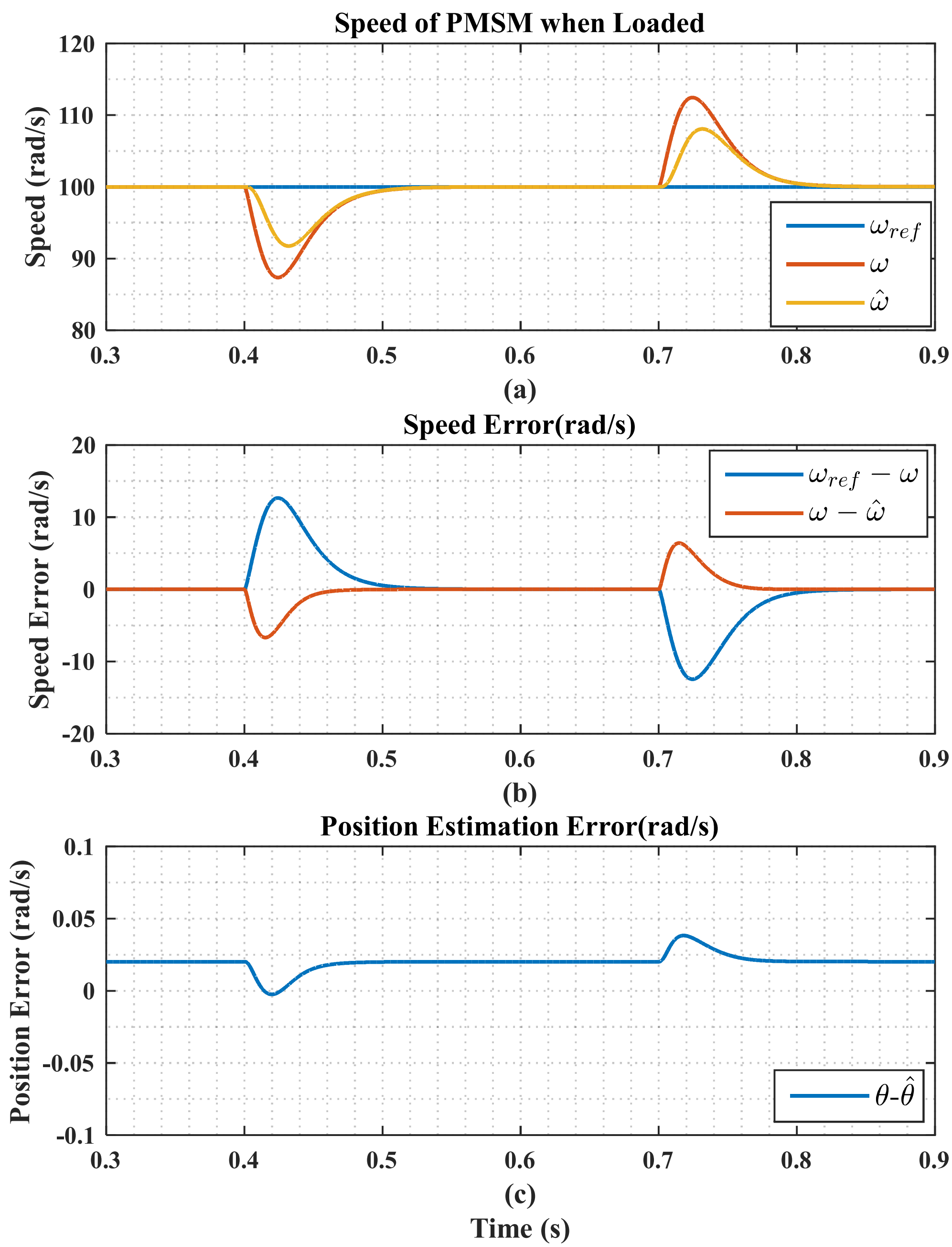


Figure 3.4. (a) Reference speed, speed of PMSM, and estimated speed, (b) Speed error from reference speed and speed estimation error, (c) Position estimation error.

### 3.3.2 Experiments

To show that the proposed controller can work in practical setting with excellent performance we conducted multiple experiments. The first experiment will be conducted using the nominal parameters of the motor and the speed reference profile $\omega_{ref}$. This experiment is intended to show the response of the closed loop system to the fast changing speed reference profile $\omega_{ref}$. The second experiment will show the response of the closed loop system when an external load is applied. The remaining experiments will be conducted to test the robustness of the proposed control method when the parameters of the motor are perturbed.

#### 3.3.2.1 First Experiment

The first experiment will be conducted to test the proposed controller in practical settings. The speed of the motor in this case is brought to $50\ \frac{\text{rad}}{\text{s}}$ using the position sensor. Then, the controller is switched to operate without the position sensor. This way the initial speed of the motor is $50\ \frac{\text{rad}}{\text{s}}$. The speed profile $\omega_{ref}$ is then applied at $t = 0.1$. The nominal parameters in Table 3.1 are used. In addition, the motor in this case is not externally loaded.

Figure 3.5 shows the results of this experiment. It can be seen in Figure 3.5(a) that an excellent transient response is achieved. In addition, the proposed controller was able to quickly regulate the speed after the transient period has passed. Figure 3.5(b) gives a closer look at how the speed trajectory of the motor under the proposed controller deviates from the speed reference. The maximum speed error is less than 5% and it occurs during transient.

Figure 3.5(c) show the position estimation error. It can be seen that the maximum position estimation error is less than $4^\circ$ during transient and less than $1.5^\circ$ during steady state. This shows accurate position estimation which is needed for the use of field oriented control technique.

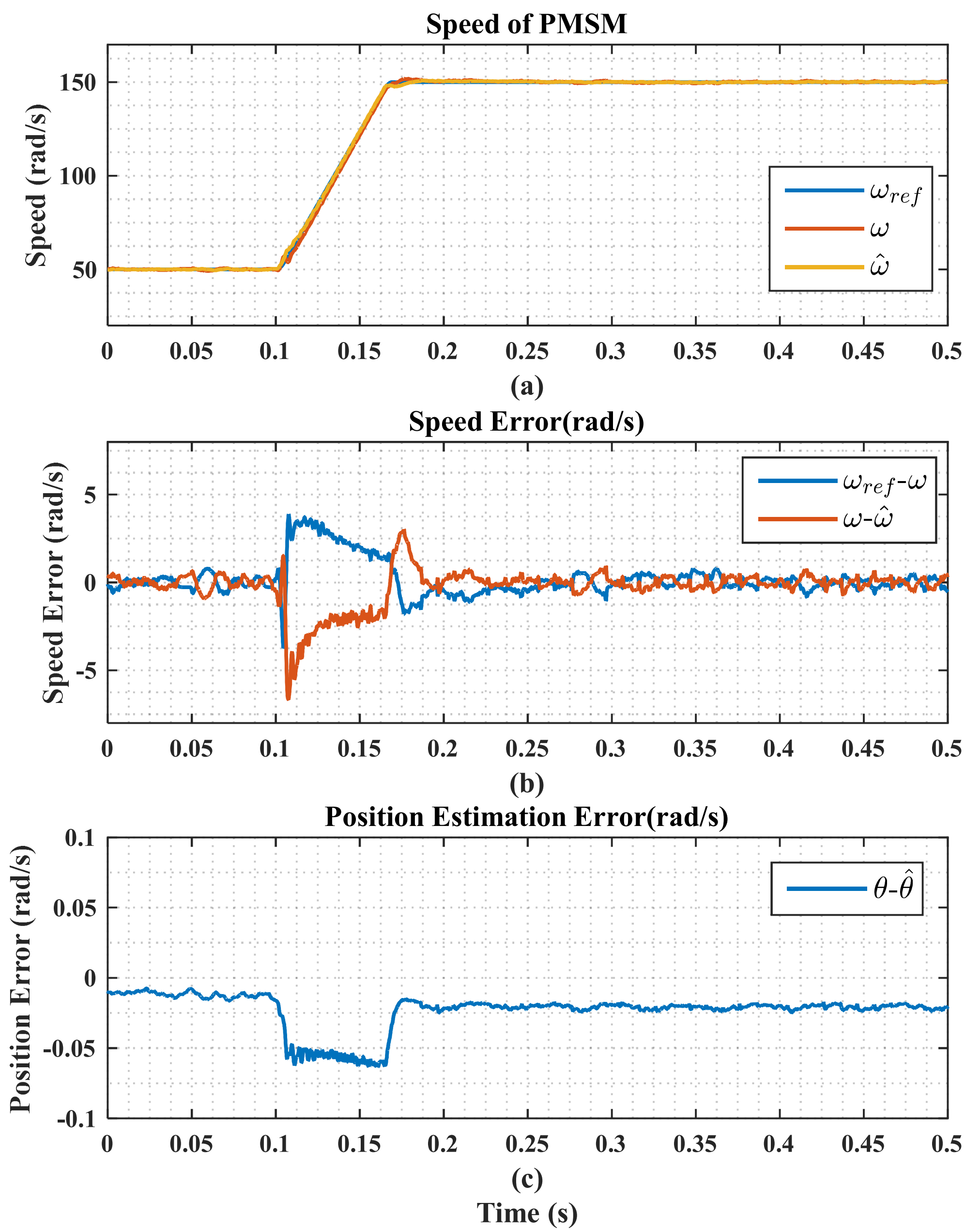


Figure 3.5. (a) Reference speed, speed of PMSM, and estimated speed, (b) Speed error from reference speed and speed estimation error, (c) Position estimation error.

### 3.3.2.2 Second Experiment

This experiment will test the robustness of the proposed control method against external loads. The motor in this case is running at 100 $\frac{\mathrm{rad}}{\mathrm{s}}$ when an external load of about2 $\mathrm{N.m}$ is applied at $\mathrm{t} = 0.2\mathrm{s}$ and removed at $\mathrm{t} = 0.8\mathrm{s}$. Figure 3.6(a) shows the speed reference profile

$\omega_{ref}$, the speed of the motor $\omega$, and the estimated speed of the motor $\widehat{\omega}$ when the load is applied and removed. It can be seen that the speed of the motor dropped about 12% once the motor is externally loaded at $\mathrm{t} = 0.2\mathrm{s}$. However, the proposed controller was able to overcome the external load and quickly recover the speed of the motor. Similar behavior can be observed when the load was removed at $\mathrm{t} = 0.8\mathrm{s}$. Figure 3.3(c) shows the position estimation error which shows a maximum deviation of about $4^{\circ}$.

**3.3.2.3 Third Experiment**

In this section we investigate the effects of perturbing the motor's parameters on performance. We have conducted ten experiments each of which we perturbed a parameter at a time. The nominal motor parameters $L$, $J$, and $B$ are perturbed by $\pm 25\%$ while $k_m$ is perturbed by $\pm 20\%$. The parameter $R$ is one time perturbed by setting it to zero and a second time perturbed by doubling its nominal value. The motor parameters are perturbed in the controller and not physical. Because of the number of the large number of figures associated with this section, we have moved the figures to Appendix B5. The motor in all of these cases is running at $50 \ \frac{\mathrm{rad}}{\mathrm{s}}$ when the speed reference profile $\omega_{ref}$ is applied at $\mathrm{t} = 0.1\mathrm{s}$.

Overall, the resulting performance of the proposed control method is excellent given these extreme motor's parameters perturbation. Looking at the figures in Appendix B5 one can see that some of the perturbed parameters have more effects on the performance than others. For example, decreasing $J$ by $25\%$ caused about $10\%$ speed error deviation during transient. Similarly, increasing $k_m$ by $20\%$ resulted in a speed deviation error of about 7.5% during transient. On the other hand, perturbing $R$, $B$, and $L$ have an unnoticeable effect in comparison to the case where the nominal motor parameters were used. It is expected that perturbing $R$ would not have a noticeable effect on perfornace because at moderate to high speed the term $Ri_\alpha$ and $Ri_\beta$ that appear in equations ( 3.1 ) and ( 3.2 ) respectively are negligible when compared to other terms in the equation. On the other hand, we expect a noticeable effect when $J$ and $k_m$ are perturbed because they appear as the coefficients of the speed control input $i_{q_{ref}}$ in the speed equation of the motor. Overall, given these extreme motor's parameters perturbation, the resulting performance of the proposed control method is excellent.

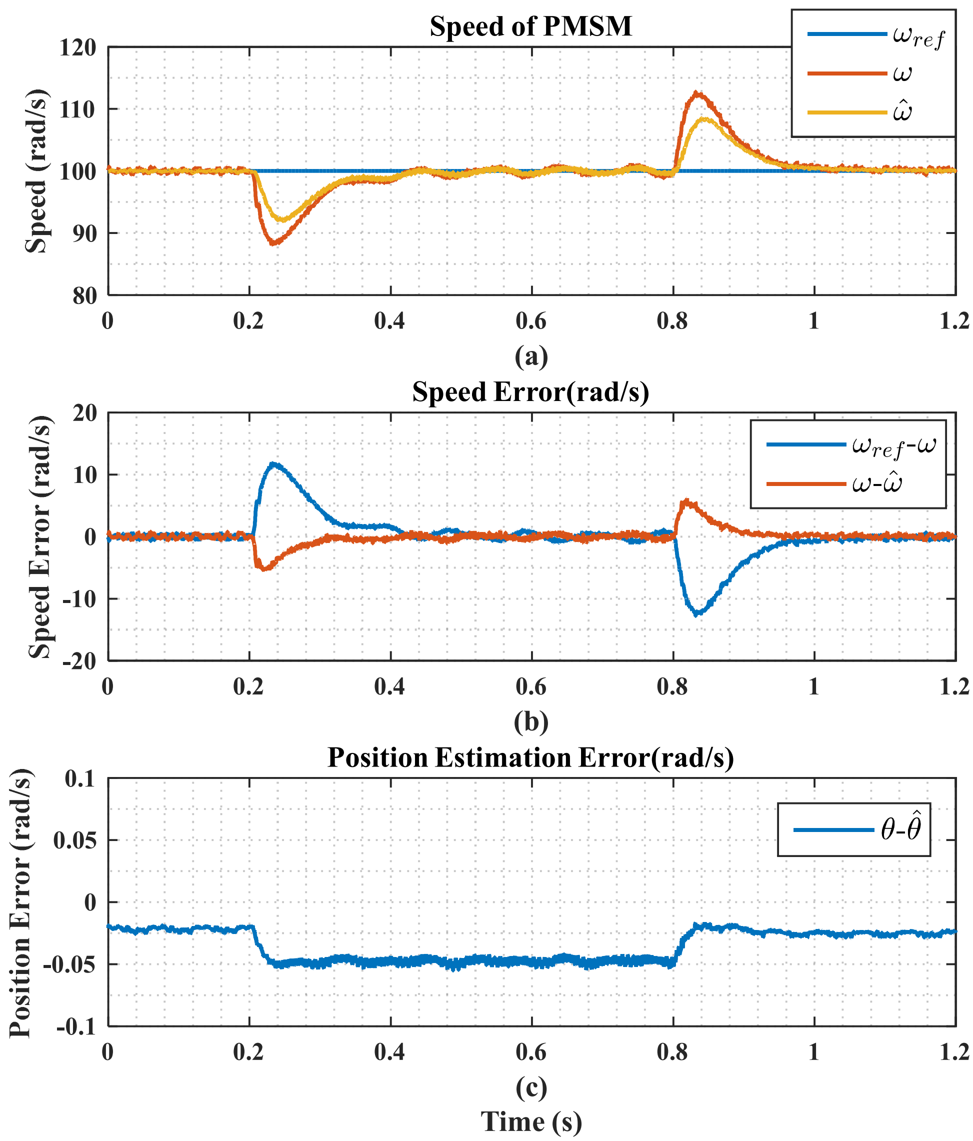


Figure 3.6. (a) Reference speed, speed of PMSM, and estimated speed, (b) Speed error from reference speed and speed estimation error, (c) Position estimation error.

### 3.4 Conclusion

In this Chapter, a back-EMF based speed sensorless control of a PMSM has been presented. The back-EMF signals are estimated using two extended high gain observers that are designed in the α-β model of the PMSM. The back-EMF estimates are then fed to a Q-PLL that is designed based on a reduced model of the system and also made to operate as an extended high-gain observer. The Q-PLL estimates rotor position and speed, and also estimates the disturbance. The estimated rotor's position is used for the field oriented control technique. On the other hand, the estimates of rotor speed and disturbance are used in a feedback linearization law to regulate speed of the motor. In the development of the proposed controller, we only assumed knowledge of the nominal parameters of the PMSM. Moreover, the external load is assumed to be time-varying and unknown but bounded. In addition, we have provided a nonlinear closed loop analysis of the output feedback controller.

The control method was successfully tested in simulations and in experiments under multiple operating conditions. The results confirmed the high performance of the proposed output feedback controller despite the application of unknown external load and parameters uncertainty.

There is, however, performance degradation in comparison to the sensor case that is presented in Chapter 2. The most noticeable performance degradation is that the proposed sensorless controller cannot reliably be used in low and zero speeds. This limitation is inherent to the back-EMF based sensorless control technique. Performance degradation can also be observed in other aspects. For example, one can compare between the robustness of the proposed sensor and sensorless cases against external load. Figure 2.12 shows that the speed dropped about 2.5% when the proposed sensor case was used and an external load of 2 $\mathrm{N.m}$ was applied. Figure 3.6, on the other hand, shows that the speed dropped about $12\%$ when the proposed sensorless case was used and the same external load was applied. In both cases the speed recovered to the reference speed but the proposed sensor case recovered faster. Note that $\varepsilon = 0.001$ was used in the sensor case while $\varepsilon = 0.0085$, which is much larger, was used in the sensorless case. When the position sensor is removed from the output feedback controller and replaced by the back-EMF observer and the Q-PLL, $\varepsilon$ cannot be reduced in practical settings as much as what was used in the sensor case to avoid noise amplification that would render the closed loop system unstable. In practice, noise is present in the current measurement which is directly used to drive the back-EMF observer and indirectly used in the Q-PLL. Therefore, in the sensorless case, we were only able to reduce $\varepsilon$ to $0.0085$ in the experiment and beyond which the system becomes unstable. On the other hand, in the sensor case, we were able to push $\varepsilon$ to $0.001$. This practical limitation of the sensorless case leads to degraded performance when compared to the sensor case.

We would like to note that this proposed sensorless control method is our second attempt at solving the problem of sensorless control of PMSM. In our first attempt, we used a back-EMF based sensorless speed control technique which is the same technique that we used in the second attempt. The main difference between our first and second attempts is that in our first attempt we used algebraic expressions to estimate the back-EMF signals, while in our second attempt we used extended high-gain observers to estimate the back-EMF signals. The algebraic expressions; that were used for the estimation of the back-EMF signals, were obtained after reducing the α-β model of the PMSM using singular perturbation theory. The reduction of the α-β model was achieved by setting $\mathrm{L} = 0$ and solving for the back-EMF signals which yielded the algebraic expressions. The consequence of this reduction is that for the equilibrium point of the closed loop system to be exponentially stable $\frac{L}{\varepsilon^2}$ must be sufficiently small which in some cases it might not be possible because L is a fixed parameter. Therefore, we have sought a second solution to the problem of sensorless speed control of PMSM such that it does have the limitation of $\frac{L}{\varepsilon^2}$ being sufficiently small. A detailed description, development, and simulation and experimental results of our first attempt can be found in [35].

# CHAPTER 4

## Future Work

We have seen in the simulations and the experiments that the proposed sensorless controller was able to steer the motor's speed to follow a fast changing reference speed. However, the proposed sensorless control method is designed to only operate in intermediate to high motor speeds and not for low speeds since the back-EMF signals become increasingly corrupted by noise as the motor's speed approaches zero and eventually these signals vanish at zero speed. This is because the back-EMF signals are proportional to the speed of the rotor. In the experiment, we have attempted both operating the motor in very low speeds and reversing the speed of the motor but the system sometimes becomes unstable as the motor's speed approaches zero. This result is not surprising for the back-EMF approach because it is unreliable for low and zero speeds. Therefore, in the future work, we will try combining a different sensorless control method with our proposed controller to deal with low and zero speeds.

The signal injection method is a very reliable sensorless control approach that has been successfully implemented to control the motor in zero and low rotor speeds. The signal injection approach uses high frequency signals, ideally much higher than the fundamental frequency, that are injected in a predetermined fashion such that the saliency features of the rotor are excited then exploited revealing estimates of position and speed. This approach works very well in zero and low speeds, but, practically; it is limited by the speed of the inverter's switches. This limitation puts a restriction on the frequency of the injected signal which imposes a rotor speed limit. In fact, there is a more restrictive factor on the frequency of the injected signal. As the switching frequency increases so does the heat of the inverter's switches which might cause damage to the switches. Therefore, the best solution to the problem of sensorless control of PMSM is to use both approaches, the signal injection method for zero and low motor speeds and the back-EMF method for intermediate to high motor speeds.

It can be easily observed that combining two controllers in the same control scheme requires switching between the two controllers. The switching law should include a mechanism that prevents it from trapping itself switching back and forth between the two controllers. Such mechanism could be as simple as using two speed thresholds. When the speed of the motor is below the low threshold, the signal injection method is used to control the motor. On the other hand, when the speed of the motor is above the high threshold, the back-EMF method approach is used. For speeds that fall within the two thresholds, the current control method is kept unchanged. Hence, the two controllers must be designed such that both of them can reliably function in the speeds above and below the two thresholds. In addition, the transition from one controller to the other must be done in such a way that prevents unwanted observer behavior from occurring at and just after the moment of switching. Therefore, passing the current controller's values of the estimated variables such as position and speed to the next controller should greatly smooth the transition.

In addition, a very important piece to our future work is to evaluate our proposed sensorless speed controller against existing control method. Preferably, those control methods that are mostly used in the industry. It seems to us from some drives systems manufactures' advertisements and catalogues that they primarily use a PI-based control scheme which is similar to the sensorless speed control method that is presented in [16]. Therefore, in our future work we will compare our proposed sensorless speed controller with the sensorless speed control method that is presented in [16]. For a fair comparison, we will follow the same comparison steps as the comparison that we have done in chapter 2.

# APPENDICES

# APPENDIX A

## Definition of Equations for Theorem 2.1

### A.1 Definition of Functions $f_1(\cdot)$ to $f_4(\cdot)$, and $g_1(\cdot)$ and $g_2(\cdot)$ For the Closed-Loop Equations ( 2.30 )-( 2.32 )

$$f_1 = M\left[sat\left(\frac{\psi(\hat{\cdot})}{M}\right) - sat\left(\frac{\psi(\cdot)}{M}\right)\right]$$

$$f_2 = \frac{M}{\varepsilon}\left[\phi_\varepsilon\left(\frac{\psi(\hat{\cdot})}{M}\right) - sat\left(\frac{\psi(\hat{\cdot})}{M}\right)\right]$$

$$f_3 = \frac{\alpha - \hat{\alpha}}{\hat{\alpha}}\Lambda - \left((\gamma - \hat{\gamma})\frac{k_m}{J} + (\mu - \hat{\mu})\right)\left(z_2 + \frac{1}{R + k_p}\left[\xi_2 + \bar{x}_q + Mk_p\phi_\varepsilon\left(\frac{\psi(\hat{\cdot})}{M}\right)\right]\right)$$
$$+\left(\left[(\gamma - \hat{\gamma})\frac{k_m}{J} + (\mu - \hat{\mu})\right]\frac{k_m}{R + k_p} + \frac{B}{J}(\gamma - \hat{\gamma})\right)(\omega_{ref} - \xi_3)$$
$$+(\mu - \hat{\mu})Msat\left(\frac{\psi(\hat{\cdot})}{M}\right) + \frac{1}{J}(\gamma - \hat{\gamma})T_L - \frac{1}{J}\frac{dT_L}{dt}$$

$$f_4 = -\frac{\hat{\alpha}M}{\varepsilon}\left[sat\left(\frac{\psi(\hat{\cdot})}{M}\right) - \phi_\varepsilon\left(\frac{\psi(\hat{\cdot})}{M}\right)\right] - \hat{\gamma}\eta_2$$

$$g_1 = n_p(\omega_{ref} - \xi_3)\left[z_2 + \frac{1}{R + k_p}\left(k_pM\phi_\varepsilon\left(\frac{\psi(\hat{\cdot})}{M}\right) - k_m(\omega_{ref} - \xi_3) + \xi_2 + \bar{x}_q\right)\right]$$
$$+\frac{k_i}{R + k_p}\left(z_1 + \frac{1}{R + k_p}\xi_1\right)$$

$$g_2 = -n_p(\omega_{ref} - \xi_3)\left[z_1 + \frac{1}{R + k_p}\xi_1 + i_{d_{ref}}\right] + \frac{1}{R + k_p}\left(\frac{{k_m}^2}{J} + k_i\right)z_2$$
$$-\frac{k_m}{R + k_p}\left(\frac{k_i}{R + k_p} + \gamma\right)(\omega_{ref} - \xi_3) + \frac{1}{(R + k_p)^2}\left(\frac{{k_m}^2}{J} + k_i\right)(\xi_2 + \bar{x}_q)$$
$$+\frac{k_pM}{(R + k_p)^2}\left(\frac{{k_m}^2}{J} + k_i\right)\phi_\varepsilon\left(\frac{\psi(\hat{\cdot})}{M}\right) - \frac{k_iM}{R + k_p}sat\left(\frac{\psi(\hat{\cdot})}{M}\right) - \frac{k_m}{J(R + k_p)}T_L$$
$$-\frac{k_p}{\hat{\alpha}(R + k_p)}\Lambda$$

Where $\psi(\hat{\cdot}) = \psi\left(\hat{e}_\omega, x_q, \hat{\sigma}, \omega_{ref}, \frac{d\omega_{ref}}{dt}\right)$, $\psi(\cdot) = \psi\left(e_\omega, x_q, \sigma, \omega_{ref}, \frac{d\omega_{ref}}{dt}\right)$, and

$$\Lambda = \phi'_\varepsilon\left(\frac{\psi(\hat{\cdot})}{M}\right)\left[\frac{d^2\omega_{ref}}{dt^2} + k_\omega\frac{d\omega_{ref}}{dt} + \hat{\mu}z_2 - \hat{\mu}Msat\left(\frac{\psi(\hat{\cdot})}{M}\right)\right.$$

$$+\left(\frac{\hat{\mu}}{R+k_p}-\mu(k_\omega-\hat{\gamma})\right)(\xi_2+\bar{x}_q)+\left((k_\omega-\hat{\gamma})\gamma-\frac{\hat{\mu}k_m}{R+k_p}\right)(\omega_{ref}-\xi_3)$$

$$-(k_\omega-\hat{\gamma})\left(\rho_2\eta_1+\hat{\gamma}\varepsilon\eta_2-\eta_3-\frac{1}{J}T_L\right)-(k_\omega-\hat{\gamma})\hat{\alpha}M\left(sat\left(\frac{\psi(\hat{\cdot})}{M}\right)-\phi_\varepsilon\left(\frac{\psi(\hat{\cdot})}{M}\right)\right)$$

$$+\left(\frac{\hat{\mu}k_p}{R+k_p}-(k_\omega-\hat{\gamma})\alpha\right)M\,\phi_\varepsilon\left(\frac{\psi(\hat{\cdot})}{M}\right)\Bigg].$$

# APPENDIX B

## Derivation and Definition of Equations for Theorem 3.1

## B1. Derivation of PMSM dq Model Using $T(\hat{\theta})$

The transformation from the αβ-coordinates to the dq-coordinates is given by

$$\begin{bmatrix} i_d \\ i_q \end{bmatrix} = T(\hat{\theta}) \begin{bmatrix} i_\alpha \\ i_\beta \end{bmatrix} \tag{B1.1}$$

$$\begin{bmatrix} u_d \\ u_q \end{bmatrix} = T(\hat{\theta}) \begin{bmatrix} u_\alpha \\ u_\beta \end{bmatrix} \tag{B1.2}$$

where $T(\hat{\theta}) = \begin{bmatrix} \cos(n_p\hat{\theta}) & \sin(n_p\hat{\theta}) \\ -\sin(n_p\hat{\theta}) & \cos(n_p\hat{\theta}) \end{bmatrix}$. First, we take the time derivative of $i_d$ and $i_q$ to obtain

$$\frac{di_d}{dt} = \frac{di_\alpha}{dt}\cos(n_p\hat{\theta}) + \frac{di_\beta}{dt}\sin(n_p\hat{\theta}) + n_p\dot{\hat{\theta}}\left[-i_\alpha\, sin(n_p\hat{\theta}) + i_\beta\, cos(n_p\hat{\theta})\right] \tag{B1.3}$$

$$\frac{di_q}{dt} = -\frac{di_\alpha}{dt}\sin(n_p\hat{\theta}) + \frac{di_\beta}{dt}\cos(n_p\hat{\theta}) - n_p\dot{\hat{\theta}}\left[i_\alpha\, cos(n_p\hat{\theta}) + i_\beta\, sin(n_p\hat{\theta})\right] \tag{B1.4}$$

Substitute ( 1.1 ) and ( 1.2 ) for $\frac{di_\alpha}{dt}$ and $\frac{di_\beta}{dt}$; respectively, in equations (B1.3) and (B1.4) to obtain

$$\begin{aligned} \frac{di_d}{dt} &= -\frac{R}{L}\left[i_\alpha\, cos(n_p\hat{\theta}) + i_\beta\, sin(n_p\hat{\theta})\right] + \frac{k_m}{L}\omega\left[sin(n_p\theta)\, cos(n_p\hat{\theta}) - cos(n_p\theta)\, sin(n_p\hat{\theta})\right] \\ &+n_p\dot{\hat{\theta}}\left[-i_\alpha\, sin(n_p\hat{\theta}) + i_\beta\, cos(n_p\hat{\theta})\right] + \frac{1}{L}\left[u_\alpha\, cos(n_p\hat{\theta}) + u_\beta\, sin(n_p\hat{\theta})\right] \end{aligned} \tag{B1.5}$$

$$\begin{aligned} \frac{di_q}{dt} &= -\frac{R}{L}\left[-i_\alpha\, sin(n_p\hat{\theta}) + i_\beta\, cos(n_p\hat{\theta})\right] - \frac{k_m}{L}\omega\left[sin(n_p\theta)\, sin(n_p\hat{\theta}) + cos(n_p\theta)\, cos(n_p\hat{\theta})\right] \\ &-n_p\dot{\hat{\theta}}\left[i_\alpha\, cos(n_p\hat{\theta}) + i_\beta\, sin(n_p\hat{\theta})\right] + \frac{1}{L}\left[-u_\alpha\, sin(n_p\hat{\theta}) + u_\beta\, cos(n_p\hat{\theta})\right] \end{aligned} \tag{B1.6}$$

Now, using the definitions

$i_d = i_\alpha\, cos(n_p\hat{\theta}) + i_\beta\, sin(n_p\hat{\theta}),\ i_q = -i_\alpha\, sin(n_p\hat{\theta}) + i_\beta\, cos(n_p\hat{\theta})$ ,

$u_d = u_\alpha\, cos(n_p\hat{\theta}) + u_\beta\, sin(n_p\hat{\theta}),\ u_q = -u_\alpha\, sin(n_p\hat{\theta}) + u_\beta\, cos(n_p\hat{\theta})$, and the trigonometric sum-difference identities

$$sin(x)\, cos(y) - cos(x)\, sin(y) = sin(x - y) \tag{B1.7}$$

$$sin(x)\,sin(y) + cos(x)\,cos(y) = cos(x - y) \tag{B1.8}$$

equations (B1.5) and (B1.6) simplify to

$$\frac{di_d}{dt} = -\frac{R}{L} i_d + \frac{k_m}{L} \omega\, sin\big(n_p[\theta - \hat{\theta}]\big) + n_p \dot{\hat{\theta}} i_q + \frac{1}{L} u_d$$

$$\frac{di_q}{dt} = -\frac{R}{L} i_q - \frac{k_m}{L} \omega\, cos\big(n_p[\theta - \hat{\theta}]\big) - n_p \dot{\hat{\theta}} i_d + \frac{1}{L} u_q$$

The speed equation in the αβ-coordinates is given by

$$\frac{d\omega}{dt} = \frac{k_m}{J}\big(-i_\alpha \sin(n_p\theta) + i_\beta \cos(n_p\theta)\big) - \frac{B}{J}\omega - \frac{1}{J} T_L \tag{B1.9}$$

We can transform (B1.9) into the dq-coordinates by substituting

$i_\alpha = i_d\, cos\big(n_p\hat{\theta}\big) - i_q\, sin\big(n_p\hat{\theta}\big)$

$i_\beta = i_d\, sin\big(n_p\hat{\theta}\big) + i_q\, cos\big(n_p\hat{\theta}\big)$;

which were obtained by solving (B1.1) for $i_\alpha$ and $i_\beta$, into (B1.9) to obtain

$$\begin{aligned}\frac{d\omega}{dt} = &-\frac{k_m}{J}\big[sin(n_p\theta)\, cos\big(n_p\hat{\theta}\big) - cos(n_p\theta)\, sin\big(n_p\hat{\theta}\big)\big] i_d \\ &+ \frac{k_m}{J}\big[sin(n_p\theta)\, sin\big(n_p\hat{\theta}\big) + cos(n_p\theta)\, cos\big(n_p\hat{\theta}\big)\big] i_q - \frac{B}{J}\omega - \frac{1}{J} T_L\end{aligned} \tag{B1.10}$$

Now, equation (B1.10) can be simplified using the trigonometric sum-difference identities (B1.7) and (B1.8), which yields

$$\frac{d\omega}{dt} = \frac{k_m}{J}\big(-i_d \sin\big(n_p[\theta - \hat{\theta}]\big) + i_q \cos\big(n_p[\theta - \hat{\theta}]\big)\big) - \frac{B}{J}\omega - \frac{1}{J} T_L.$$

**B2. Derivation of the Equilibrium Point**

The closed loop system is given by

$\dot{x}_d = -k_i i_d$

$$\dot{x}_q = k_i\left(\frac{1}{k_p\alpha_1}\left[k_\omega\omega_{ref} - (k_\omega - \alpha_2)\widehat{\omega} - \alpha_1 x_q - \hat{\sigma}\right] - i_q\right)$$

$$\dot{\omega} = \frac{k_m}{J}\left(-i_d\sin(n_p\tilde{\theta}) + i_q\cos(n_p\tilde{\theta})\right) - \frac{B}{J}\omega - \frac{1}{J}T_L$$

$$\dot{\tilde{\theta}} = \omega - \widehat{\omega} - \frac{\rho_1 L}{\varepsilon n_p \hat{k}_m \omega^\star}\hat{\sigma}_d$$

$$\dot{\widehat{\omega}} = k_\omega\omega_{ref} - k_\omega\widehat{\omega} + \frac{\rho_2 L}{\varepsilon^2 n_p \hat{k}_m \omega^\star}\hat{\sigma}_d$$

$$\dot{\hat{\sigma}} = \frac{\rho_3 L}{\varepsilon^3 n_p \hat{k}_m \omega^\star}\hat{\sigma}_d$$

$$\tau\frac{di_d}{dt} = -i_d + \frac{k_m}{R+k_p}\omega\, sin(n_p\tilde{\theta}) + \frac{1}{R+k_p}x_d + \tau n_p\widehat{\omega} i_q + \frac{\tau\rho_1 L}{\varepsilon\hat{k}_m\omega^\star}\hat{\sigma}_d i_q$$

$$\tau\frac{di_q}{dt} = -i_q + \frac{J}{k_m}\left[k_\omega\omega_{ref} - (k_\omega - \alpha_2)\widehat{\omega} - \hat{\sigma}\right] - \frac{k_m}{R+k_p}\omega\, cos(n_p\tilde{\theta})$$
$$-\tau\left[n_p\widehat{\omega} + \frac{\rho_1 L}{\varepsilon\hat{k}_m\omega^\star}\hat{\sigma}_d\right]i_d$$

$$\dot{\hat{\imath}}_d = -\frac{R}{L}\hat{\imath}_d - \frac{k_p}{L}i_d + \frac{1}{L}x_d + \hat{\sigma}_d + \frac{h_1}{\mu}(i_d - \hat{\imath}_d) + n_p\widehat{\omega}\hat{\imath}_q + \frac{\rho_1 L}{\varepsilon\hat{k}_m\omega^\star}\hat{\sigma}_d\hat{\imath}_q$$

$$\dot{\hat{\imath}}_q = -\frac{R}{L}\hat{\imath}_q - \frac{k_p}{L}i_q + \frac{1}{L\alpha_1}\left[k_\omega\omega_{ref} - (k_\omega - \alpha_2)\widehat{\omega} - \hat{\sigma}\right] + \hat{\sigma}_q + \frac{h_1}{\mu}\left(i_q - \hat{\imath}_q\right) - n_p\widehat{\omega}\hat{\imath}_d$$
$$-\frac{\rho_1 L}{\varepsilon\hat{k}_m\omega^\star}\hat{\sigma}_d\hat{\imath}_d$$

$$\dot{\hat{\sigma}}_d = \frac{h_2}{\mu^2}(i_d - \hat{\imath}_d) + n_p\widehat{\omega}\hat{\sigma}_q + \frac{\rho_1 L}{\varepsilon\hat{k}_m\omega^\star}\hat{\sigma}_d\hat{\sigma}_q$$

$$\dot{\hat{\sigma}}_q = \frac{h_2}{\mu^2}\left(i_q - \hat{\imath}_q\right) - n_p\widehat{\omega}\hat{\sigma}_d - \frac{\rho_1 L}{\varepsilon\hat{k}_m\omega^\star}\hat{\sigma}_d{}^2$$

Set the time derivatives to 0

$$0 = -k_i i_d \tag{B2.1}$$

$$0 = k_i\left(\frac{1}{k_p\alpha_1}\left[k_\omega\omega_{ref} - (k_\omega - \alpha_2)\widehat{\omega} - \alpha_1 x_q - \hat{\sigma}\right] - i_q\right) \tag{B2.2}$$

$$0 = \frac{k_m}{J}\left(-i_d \sin\left(n_p\tilde{\theta}\right) + i_q \cos\left(n_p\tilde{\theta}\right)\right) - \frac{B}{J}\omega - \frac{1}{J}T_L \tag{B2.3}$$

$$0 = \omega - \widehat{\omega} - \frac{\rho_1 L}{\varepsilon n_p \hat{k}_m \omega^\star}\hat{\sigma}_d \tag{B2.4}$$

$$0 = k_\omega \omega_{ref} - k_\omega \widehat{\omega} + \frac{\rho_2 L}{\varepsilon^2 n_p \hat{k}_m \omega^\star}\hat{\sigma}_d \tag{B2.5}$$

$$0 = \frac{\rho_3 L}{\varepsilon^3 n_p \hat{k}_m \omega^\star}\hat{\sigma}_d \tag{B2.6}$$

$$0 = -i_d + \frac{k_m}{R + k_p}\omega\, sin\left(n_p\tilde{\theta}\right) + \frac{1}{R + k_p}x_d + \tau n_p \widehat{\omega} i_q + \frac{\tau\rho_1 L}{\varepsilon \hat{k}_m \omega^\star}\hat{\sigma}_d i_q \tag{B2.7}$$

$$\begin{aligned} 0 = {} & -i_q + \frac{J}{k_m}\left[k_\omega \omega_{ref} - (k_\omega - \alpha_2)\widehat{\omega} - \hat{\sigma}\right] - \frac{k_m}{R + k_p}\omega\, cos\left(n_p\tilde{\theta}\right) \\ & -\tau\left[n_p\widehat{\omega} + \frac{\rho_1 L}{\varepsilon \hat{k}_m \omega^\star}\hat{\sigma}_d\right] i_d \end{aligned} \tag{B2.8}$$

$$0 = -\frac{R}{L}\hat{\imath}_d - \frac{k_p}{L}i_d + \frac{1}{L}x_d + \hat{\sigma}_d + \frac{h_1}{\mu}(i_d - \hat{\imath}_d) + n_p\widehat{\omega}\hat{\imath}_q + \frac{\rho_1 L}{\varepsilon \hat{k}_m \omega^\star}\hat{\sigma}_d \hat{\imath}_q \tag{B2.9}$$

$$\begin{aligned} 0 = {} & -\frac{R}{L}\hat{\imath}_q - \frac{k_p}{L}i_q + \frac{1}{L\alpha_1}\left[k_\omega \omega_{ref} - (k_\omega - \alpha_2)\widehat{\omega} - \hat{\sigma}\right] + \hat{\sigma}_q + \frac{h_1}{\mu}\left(i_q - \hat{\imath}_q\right) \\ & -n_p\widehat{\omega}\hat{\imath}_d - \frac{\rho_1 L}{\varepsilon \hat{k}_m \omega^\star}\hat{\sigma}_d \hat{\imath}_d \end{aligned} \tag{B2.10}$$

$$0 = \frac{h_2}{\mu^2}(i_d - \hat{\imath}_d) + n_p\widehat{\omega}\hat{\sigma}_q + \frac{\rho_1 L}{\varepsilon \hat{k}_m \omega^\star}\hat{\sigma}_d\hat{\sigma}_q \tag{B2.11}$$

$$0 = \frac{h_2}{\mu^2}\left(i_q - \hat{\imath}_q\right) - n_p\widehat{\omega}\hat{\sigma}_d - \frac{\rho_1 L}{\varepsilon \hat{k}_m \omega^\star}{\hat{\sigma}_d}^2 \tag{B2.12}$$

It can be seen from (B2.1) and (B2.6) that $i_d = \hat{\sigma}_d = 0$, therefore set $i_d = 0$ and $\hat{\sigma}_d = 0$

$$0 = \frac{1}{k_p\alpha_1}\left[k_\omega \omega_{ref} - (k_\omega - \alpha_2)\widehat{\omega} - \alpha_1 x_q - \hat{\sigma}\right] - i_q \tag{B2.13}$$

$$0 = k_m i_q\, cos\left(n_p\tilde{\theta}\right) - B\omega - T_L \tag{B2.14}$$

$$0 = \omega - \widehat{\omega} \tag{B2.15}$$

$$0 = \omega_{ref} - \widehat{\omega} \tag{B2.16}$$

$$0 = k_m\omega\, sin\left(n_p\tilde{\theta}\right) + x_d + L n_p \widehat{\omega} i_q \tag{B2.17}$$

$$0 = -i_q + \frac{J}{k_m}\left[k_\omega \omega_{ref} - (k_\omega - \alpha_2)\widehat{\omega} - \hat{\sigma}\right] - \frac{k_m}{R + k_p}\omega \cos\left(n_p \tilde{\theta}\right) \tag{B2.18}$$

$$0 = -\left(\frac{R}{L} + \frac{h_1}{\mu}\right)\hat{\imath}_d + \frac{1}{L}x_d + n_p \widehat{\omega}\hat{\imath}_q \tag{B2.19}$$

$$0 = -\frac{R}{L}\hat{\imath}_q - \frac{k_p}{L}i_q + \frac{1}{L\alpha_1}\left[k_\omega \omega_{ref} - (k_\omega - \alpha_2)\widehat{\omega} - \hat{\sigma}\right] + \hat{\sigma}_q + \frac{h_1}{\mu}\left(i_q - \hat{\imath}_q\right) - n_p \widehat{\omega}\hat{\imath}_d \tag{B2.20}$$

$$0 = -\frac{h_2}{\mu^2}\hat{\imath}_d + n_p \widehat{\omega}\hat{\sigma}_q \tag{B2.21}$$

$$0 = \frac{h_2}{\mu^2}\left(i_q - \hat{\imath}_q\right) \tag{B2.22}$$

It can be seen from (B2.14) and (B2.22) that $i_q = \hat{\imath}_q = \frac{B\omega_{ref} + T_L}{k_m \cos\left(n_p \tilde{\theta}\right)}$, and from (B2.15) and (B2.16) that $\omega = \widehat{\omega} = \omega_{ref}$, therefore set $\hat{\imath}_q = i_q$, $\omega = \omega_{ref}$, and $\widehat{\omega} = \omega_{ref}$

$$0 = \frac{1}{k_p \alpha_1}\left[\alpha_2 \omega_{ref} - \alpha_1 x_q - \hat{\sigma}\right] - i_q \tag{B2.23}$$

$$0 = k_m \omega_{ref} \sin\left(n_p \tilde{\theta}\right) + x_d + L n_p \omega_{ref} i_q \tag{B2.24}$$

$$0 = -i_q + \frac{J}{k_m}\left[\alpha_2 \omega_{ref} - \hat{\sigma}\right] - \frac{k_m}{R + k_p}\omega_{ref} \cos\left(n_p \tilde{\theta}\right) \tag{B2.25}$$

$$0 = -\left(\frac{R}{L} + \frac{h_1}{\mu}\right)\hat{\imath}_d + \frac{1}{L}x_d + n_p \omega_{ref} i_q \tag{B2.26}$$

$$0 = -\frac{R + k_p}{L}i_q + \frac{1}{L\alpha_1}\left[\alpha_2 \omega_{ref} - \hat{\sigma}\right] + \hat{\sigma}_q - n_p \omega_{ref}\hat{\imath}_d \tag{B2.27}$$

$$0 = -\frac{h_2}{\mu^2}\hat{\imath}_d + n_p \omega_{ref}\hat{\sigma}_q \tag{B2.28}$$

Solving (B2.24) for $x_d$ yields $x_d = -k_m \omega_{ref} \sin\left(n_p \tilde{\theta}\right) - L n_p \omega_{ref} i_q$, and solving (B2.25) for $\hat{\sigma}$ gives $\hat{\sigma} = -\frac{k_m}{J}i_q + \alpha_2 \omega_{ref} - \frac{{k_m}^2}{J(R + k_p)}\omega_{ref} \cos\left(n_p \tilde{\theta}\right) = -\frac{k_m}{J}i_q + \left[\alpha_2 - k_m \alpha_1 \cos\left(n_p \tilde{\theta}\right)\right]\omega_{ref}$;

therefore, set $x_d = -k_m \omega_{ref} \sin\left(n_p \tilde{\theta}\right) - L n_p \omega_{ref} i_q$, and $\hat{\sigma} = -\frac{k_m}{J}i_q + \left[\alpha_2 - k_m \alpha_1 \cos\left(n_p \tilde{\theta}\right)\right]\omega_{ref}$

$$0 = -x_q + k_m \omega_{ref} \cos\left(n_p \tilde{\theta}\right) + R i_q \tag{B2.29}$$

$$0 = -\left(\frac{R}{L} + \frac{h_1}{\mu}\right)\hat{\imath}_d - \frac{k_m \omega_{ref}}{L} sin\left(n_p \tilde{\theta}\right) \tag{B2.30}$$

$$0 = k_m \omega_{ref} \, cos\left(n_p \tilde{\theta}\right) + L\hat{\sigma}_q - n_p L \omega_{ref} \hat{\imath}_d \tag{B2.31}$$

$$0 = -\frac{h_2}{\mu^2}\hat{\imath}_d + n_p \omega_{ref} \hat{\sigma}_q \tag{B2.32}$$

Now, solving (B2.29) for $x_q$ gives us $x_q = Ri_q + k_m \omega_{ref} \, cos\left(n_p \tilde{\theta}\right)$, and solving (B2.30) for $\hat{\imath}_d$ we obtain $\hat{\imath}_d = -\frac{\mu k_m \omega_{ref}}{\mu R + L h_1} sin\left(n_p \tilde{\theta}\right)$. Substituting $\hat{\imath}_d$ into (B2.32) and solving for $\hat{\sigma}_q$ we arrive at $\hat{\sigma}_q = -\frac{k_m h_2}{\mu n_p (\mu R + L h_1)} sin\left(n_p \tilde{\theta}\right)$. Finally, substitute both $\hat{\imath}_d$ and $\hat{\sigma}_q$ into (B2.31) to arrive at

$$0 = \omega_{ref} \, cos\left(n_p \tilde{\theta}\right) + \frac{L\left[\mu^2 {n_p}^2 {\omega_{ref}}^2 - h_2\right]}{\mu n_p (\mu R + L h_1)} sin\left(n_p \tilde{\theta}\right)$$

rearranging to obtain

$$\frac{sin\left(n_p \tilde{\theta}\right)}{cos\left(n_p \tilde{\theta}\right)} = tan\left(n_p \tilde{\theta}\right) = -\frac{\mu(\mu R + L h_1) n_p \omega_{ref}}{L\left[\mu^2 {n_p}^2 {\omega_{ref}}^2 - h_2\right]}$$

and solving for $\tilde{\theta}$ yields

$$\tilde{\theta} = \frac{1}{n_p} tan^{-1}\left[-\frac{\mu(\mu R + L h_1) n_p \omega_{ref}}{L\left(\mu^2 {n_p}^2 {\omega_{ref}}^2 - h_2\right)}\right]$$

In summary, the equilibrium points are given by

$$\bar{\imath}_q = \bar{\hat{\imath}}_q = \frac{B\omega_{ref} + T_L}{k_m \cos\left(n_p \bar{\tilde{\theta}}\right)}$$

$$\bar{x}_d = -k_m \omega_{ref} \sin\left(n_p \bar{\tilde{\theta}}\right) - n_p L \omega_{ref} \bar{\imath}_q$$

$$\bar{x}_q = R\bar{\imath}_q + k_m \omega_{ref} \cos\left(n_p \bar{\tilde{\theta}}\right)$$

$$\bar{\omega} = \omega_{ref}$$

$$\bar{\tilde{\theta}} = \frac{1}{n_p} arctan\left[-\frac{\mu(\mu R + Lh_1)n_p\omega_{ref}}{L\left(\mu^2 {n_p}^2 {\omega_{ref}}^2 - h_2\right)}\right]$$

$$\bar{\hat{\omega}} = \omega_{ref}$$

$$\bar{\hat{\sigma}} = -\frac{k_m}{J}\bar{\iota}_q + \left[\alpha_2 - k_m\alpha_1 \cos\left(n_p\bar{\tilde{\theta}}\right)\right]\omega_{ref}$$

$$\bar{\iota}_d = 0$$

$$\bar{\hat{\iota}}_d = -\frac{\mu k_m\omega_{ref}}{\mu R + Lh_1} sin\left(n_p\bar{\tilde{\theta}}\right)$$

$$\bar{\hat{\sigma}}_d = 0$$

$$\bar{\hat{\sigma}}_q = -\frac{k_m h_2}{\mu n_p(\mu R + Lh_1)} sin\left(n_p\bar{\tilde{\theta}}\right)$$

where $\bar{\tilde{\theta}}$, $\bar{\iota}_q$, $\bar{\hat{\iota}}_q$, $\bar{x}_d$, $\bar{x}_q$, $\bar{\omega}$, $\bar{\hat{\omega}}$, $\bar{\hat{\sigma}}$, $\bar{\iota}_d$, $\bar{\hat{\iota}}_d$, $\bar{\hat{\sigma}}_d$, and $\bar{\hat{\sigma}}_q$ are the equilibrium values of $\tilde{\theta}$, $i_q$, $\hat{\iota}_q$, $x_d$, $x_q$, $\omega$, $\hat{\omega}$, $\hat{\sigma}$, $i_d$, $\hat{\iota}_d$, $\hat{\sigma}_d$, and $\hat{\sigma}_q$; respectively. The $sin\left(n_p\bar{\tilde{\theta}}\right)$ and $cos\left(n_p\bar{\tilde{\theta}}\right)$ satisfy

$$sin\left(n_p\bar{\tilde{\theta}}\right) = \frac{-\frac{\mu(\mu R+Lh_1)n_p\omega_{ref}}{L\left(\mu^2{n_p}^2{\omega_{ref}}^2-h_2\right)}}{\sqrt{1+\left[\frac{\mu(\mu R+Lh_1)n_p\omega_{ref}}{L\left(\mu^2{n_p}^2{\omega_{ref}}^2-h_2\right)}\right]^2}}, \text{ and } cos\left(n_p\bar{\tilde{\theta}}\right) = \frac{1}{\sqrt{1+\left[\frac{\mu(\mu R+Lh_1)n_p\omega_{ref}}{L\left(\mu^2{n_p}^2{\omega_{ref}}^2-h_2\right)}\right]^2}}$$

and they were obtained using the following trigonometric identities

$sin(tan^{-1}(x)) = \frac{x}{\sqrt{1+x^2}}$ and $cos^2(x) + sin^2(x) = 1$.

**B3. Derivation of the inequalities in ( 3.35 )**

The transfer function

$$\Gamma(s) = \frac{\frac{k_m}{\hat{k}_m}\frac{\omega}{\omega_{ref}}(\rho_1 s^2 + \rho_2 s + \rho_3)}{s^3 + \frac{k_m}{\hat{k}_m}\frac{\omega}{\omega_{ref}}\beta(\rho_1 s^2 + \rho_2 s + \rho_3)} = \frac{\gamma_1 s^2 + \gamma_2 s + \gamma_3}{s^3 + \beta\gamma_1 s^2 + \beta\gamma_2 s + \beta\gamma_3}$$

where $\beta > 0, \gamma_1 = \frac{k_m}{\hat{k}_m}\frac{\omega}{\omega_{ref}}\rho_1, \gamma_2 = \frac{k_m}{\hat{k}_m}\frac{\omega}{\omega_{ref}}\rho_2, \gamma_3 = \frac{k_m}{\hat{k}_m}\frac{\omega}{\omega_{ref}}\rho_3$, is Strictly Positive Real (SPR) if and only if

1) $\Gamma(s)$ is Hurwitz

2) $\Re\{\Gamma(j\omega)\} > 0, \forall\ \omega \in [0, \infty)$

3) $\Gamma(s) > 0$ or $\lim_{\omega \to \infty} \omega^2 \Re\{\Gamma(j\omega)\} > 0$

The first condition can be checked using Routh-Hurwitz criterion. The Routh's tabulation of the characteristic equation of $\Gamma(s)$ is given by

| | | |
|---|---|---|
| $s^3$ | $1$ | $\beta\gamma_2$ |
| $s^2$ | $\beta\gamma_1$ | $\beta\gamma_3$ |
| $s^1$ | $\frac{\beta^2\gamma_1\gamma_2 - \beta\gamma_3}{\beta\gamma_1}$ | 0 |
| $s^0$ | $\beta\gamma_3$ | 0 |

Table B3.1 Routh's tabulation of the characteristic equation.

So, for $\Gamma(s)$ to be Hurwitz we need to satisfy the following inequalities

$$\beta\gamma_1 > 0$$

$$\beta\gamma_3 > 0$$

$$\frac{\beta^2\gamma_1\gamma_2 - \beta\gamma_3}{\beta\gamma_1} = \beta\gamma_2 - \frac{\gamma_3}{\gamma_1} > 0$$

For the second condition, we need $\Re\{\Gamma(j\omega)\} > 0, \forall\ \omega \in [0, \infty)$; that is,

$$\Re\left\{\frac{\gamma_1(j\omega)^2 + \gamma_2(j\omega) + \gamma_3}{(j\omega)^3 + \beta\gamma_1(j\omega)^2 + \beta\gamma_2(j\omega) + \beta\gamma_3}\right\} > 0$$

$$\Re\left\{\frac{(\gamma_3 - \gamma_1\omega^2) + j\gamma_2\omega}{\beta(\gamma_3 - \gamma_1\omega^2) + j(\beta\gamma_2\omega - \omega^3)}\right\} > 0$$

$$\Re\left\{\frac{(\gamma_3 - \gamma_1\omega^2) + j\gamma_2\omega}{\beta(\gamma_3 - \gamma_1\omega^2) + j(\beta\gamma_2\omega - \omega^3)} \times \frac{\beta(\gamma_3 - \gamma_1\omega^2) - j(\beta\gamma_2\omega - \omega^3)}{\beta(\gamma_3 - \gamma_1\omega^2) - j(\beta\gamma_2\omega - \omega^3)}\right\} > 0$$

$$\Re\left\{\frac{[\beta(\gamma_3 - \gamma_1\omega^2)(\gamma_3 - \gamma_1\omega^2) + \gamma_2(\beta\gamma_2\omega - \omega^3)\omega] + j[\beta\gamma_2(\gamma_3 - \gamma_1\omega^2)\omega - (\gamma_3 - \gamma_1\omega^2)(\beta\gamma_2\omega - \omega^3)]}{[\beta(\gamma_3 - \gamma_1\omega^2)]^2 + [\beta\gamma_2\omega - \omega^3]^2}\right\} > 0$$

The real part is given by

$$\frac{\beta(\gamma_3 - \gamma_1\omega^2)(\gamma_3 - \gamma_1\omega^2) + \gamma_2(\beta\gamma_2\omega - \omega^3)\omega}{[\beta(\gamma_3 - \gamma_1\omega^2)]^2 + [\beta\gamma_2\omega - \omega^3]^2} > 0$$

which is rewritten as

$$\frac{(\beta{\gamma_1}^2 - \gamma_2)\omega^4 + \beta({\gamma_2}^2 - 2\gamma_1\gamma_3)\omega^2 + \beta{\gamma_3}^2}{[\beta(\gamma_3 - \gamma_1\omega^2)]^2 + [\beta\gamma_2\omega - \omega^3]^2} > 0$$

To satisfy the inequality we need

$$\beta{\gamma_1}^2 - \gamma_2 \geq 0$$

$$\gamma_2{}^2 - 2\gamma_1\gamma_3 \geq 0$$

For the third condition, we have

$$\lim_{\omega \to \infty} \omega^2 \Re\{\Gamma(j\omega)\} > 0$$

$$\lim_{\omega \to \infty} \omega^2 \left( \frac{(\beta\gamma_1{}^2 - \gamma_2)\omega^4 + \beta(\gamma_2{}^2 - 2\gamma_1\gamma_3)\omega^2 + \beta\gamma_3{}^2}{[\beta(\gamma_3 - \gamma_1\omega^2)]^2 + [\beta\gamma_2\omega - \omega^3]^2} \right) > 0$$

$$\lim_{\omega \to \infty} \left( \frac{(\beta\gamma_1{}^2 - \gamma_2)\omega^6 + \beta(\gamma_2{}^2 - 2\gamma_1\gamma_3)\omega^4 + \beta\gamma_3{}^2\omega^2}{\omega^6 + \beta(\beta\gamma_1{}^2 - 2\gamma_2)\omega^4 + \beta^2(\gamma_2{}^2 - 2\gamma_1\gamma_3)\omega^2 + \beta^2\gamma_3{}^2} \right) > 0$$

which yields

$$\beta\gamma_1{}^2 - \gamma_2 > 0$$

So, in total, there are five conditions to satisfy and they are

$$\beta\gamma_1 > 0$$

$$\beta\gamma_3 > 0$$

$$\beta\gamma_2 - \frac{\gamma_3}{\gamma_1} > 0$$

$$\gamma_2{}^2 - 2\gamma_1\gamma_3 \geq 0$$

$$\beta\gamma_1{}^2 - \gamma_2 > 0$$

Let $\gamma_1 = \frac{a}{\beta}$, $\gamma_2 = \frac{b}{\beta}$, and $\gamma_3 = \frac{c}{\beta}$; then the inequalities reduce to

$$a > 0$$

$$c > 0$$

$$b - \frac{c}{a} > 0 \Rightarrow b > \frac{c}{a}$$

$$b^2 - 2ac \geq 0 \Rightarrow b^2 \geq 2ac$$

$$a^2 - b > 0 \Rightarrow b < a^2$$

Let $b_1(a,c) = \frac{c}{a}$, $b_2(a,c) = \sqrt{2ac}$, and $b_3(a,c) = a^2$. Figure B3.1 shows the plot of $b_1$, $b_2$, and $b_3$ that is used to determine the valid values of $a$ and $c$.

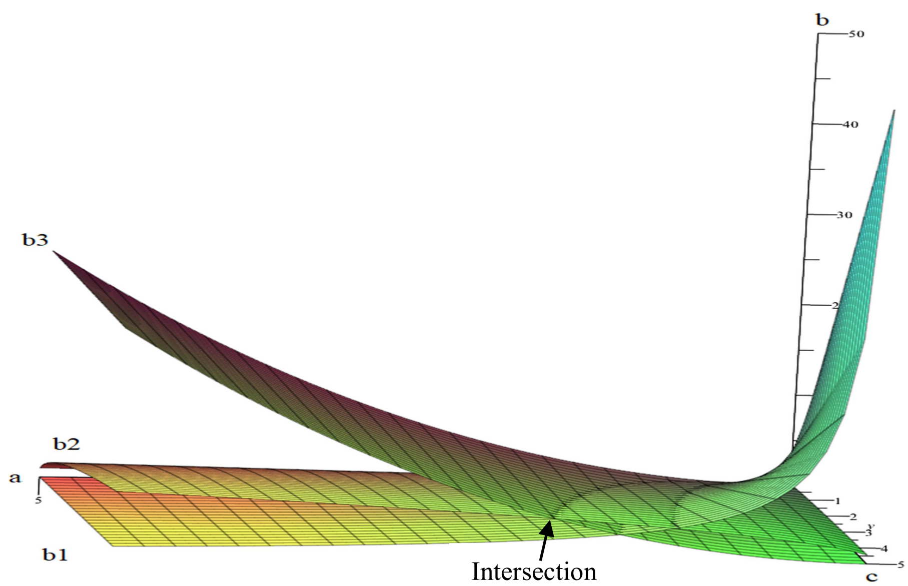


Figure B3.1 Plot of the functions $b_1$, $b_2$, and $b_3$.

It can be seen from Figure B3.1 that the inequalities are valid beyond the intersection $b_2 = b_3$; that is, $\sqrt{2ac} = a^2 \Rightarrow c = \frac{1}{2}a^3$. Now, $a$, $b$, and $c$ can be chosen according to the following

$$a > 0$$

$$0 < c < \frac{1}{2}a^3$$

$$\sqrt{2ac} \leq b < a^2$$

Substitute back $a = \frac{k_m}{\hat{k}_m}\frac{\omega}{\omega_{re}}\beta\rho_1,\ b = \frac{k_m}{\hat{k}_m}\frac{\omega}{\omega_{ref}}\beta\rho_2$, and $c = \frac{k_m}{\hat{k}_m}\frac{\omega}{\omega_{ref}}\beta\rho_3$; then we arrive at the following inequalities

$$\beta\frac{k_m}{\hat{k}_m}\frac{\omega}{\omega^\star}\rho_1 > 0$$

$$0 < \rho_3 < \frac{1}{2}\beta^2\left(\frac{k_m}{\hat{k}_m}\frac{\omega}{\omega^\star}\right)^2 {\rho_1}^3$$

$$\sqrt{2\rho_1\rho_3} \leq \rho_2 < \beta\frac{k_m}{\hat{k}_m}\frac{\omega}{\omega^\star}{\rho_1}^2$$

which reduce to

$$\rho_2 < a{\rho_1}^2$$

$$\rho_3 \leq \frac{{\rho_2}^2}{2\rho_1}$$

## B4. Definition of Functions $f_1(\cdot)$ to $f_{12}(\cdot)$ For the Closed-Loop Equations ( 3.47 )-( 3.50 )

$$f_1(\cdot)=\begin{bmatrix} -\frac{k_i k_m}{R+k_p}(\omega_{ref}-\xi_3)\,sin\left(\varepsilon^2 n_p(\eta_1+\check{\eta}_1)\right)+k_i z_\alpha\,cos\left(n_p\left(\theta-\varepsilon^2(\eta_1+\check{\eta}_1)\right)\right)+k_i z_\beta\,sin\left(n_p\left(\theta-\varepsilon^2(\eta_1+\check{\eta}_1)\right)\right) \\ -k_i z_\alpha\,sin\left(n_p\left(\theta-\varepsilon^2(\eta_1+\check{\eta}_1)\right)\right)+k_i z_\beta\,cos\left(n_p\left(\theta-\varepsilon^2(\eta_1+\check{\eta}_1)\right)\right)+\frac{k_i RM}{R+k_p}\left[sat\left(\frac{\psi(\hat{\cdot})}{M}\right)-sat\left(\frac{\bar{\psi}(\cdot)}{M}\right)\right]-\frac{k_i k_m}{R+k_p}\left[1-cos\left(\varepsilon^2 n_p(\eta_1+\check{\eta}_1)\right)\right](\omega_{ref}-\xi_3) \\ \alpha_1\xi_1\,sin\left(\varepsilon^2 n_p(\eta_1+\check{\eta}_1)\right)-\frac{k_m}{J}\left[z_\alpha\,sin(n_p\theta)-z_\beta\,cos(n_p\theta)\right]-\alpha_1 k_p M\left[sat\left(\frac{\psi(\hat{\cdot})}{M}\right)-sat\left(\frac{\bar{\psi}(\cdot)}{M}\right)\right]cos\left(\varepsilon^2 n_p(\eta_1+\check{\eta}_1)\right)+\left[1-cos\left(\varepsilon^2 n_p(\eta_1+\check{\eta}_1)\right)\right]\left[(k_\omega-\alpha_2)\xi_3+\alpha_2\omega_{ref}+\dot{\omega}_{ref}+\frac{1}{J}T_L\right] \end{bmatrix}$$

$$f_2(\cdot)=\frac{Mk_p}{\varepsilon(R+k_p)}\begin{bmatrix} 0 \\ k_i\left[sat\left(\frac{\psi(\hat{\cdot})}{M}\right)-\phi_\varepsilon\left(\frac{\psi(\hat{\cdot})}{M}\right)\right] \\ \frac{k_m}{J}\left[sat\left(\frac{\psi(\hat{\cdot})}{M}\right)-\phi_\varepsilon\left(\frac{\psi(\hat{\cdot})}{M}\right)\right]cos\left(\varepsilon^2 n_p(\eta_1+\check{\eta}_1)\right) \end{bmatrix}$$

$$f_3(\cdot)=\begin{bmatrix} \frac{\rho_1 k_m}{n_p\hat{k}_m\omega^\star}\left[v_{\alpha 2}cos\left(n_p\left(\theta-\varepsilon^2(\eta_1+\check{\eta}_1)\right)\right)+v_{\beta 2}\,sin\left(n_p\left(\theta-\varepsilon^2(\eta_1+\check{\eta}_1)\right)\right)\right] \\ \frac{k_m}{J}\left[z_\alpha\,sin(n_p\theta)-z_\beta\,cos(n_p\theta)\right]+\frac{\rho_2 k_m}{n_p\hat{k}_m\omega^\star}\left[v_{\alpha 2}cos\left(n_p\left(\theta-\varepsilon^2(\eta_1+\check{\eta}_1)\right)\right)+v_{\beta 2}\,sin\left(n_p\left(\theta-\varepsilon^2(\eta_1+\check{\eta}_1)\right)\right)\right] \\ \frac{\rho_3 k_m}{n_p\hat{k}_m\omega^\star}\left[1+\left(\frac{\alpha_1}{\hat{\alpha}_1}-1\right)\phi_\varepsilon'\left(\frac{\psi(\hat{\cdot})}{M}\right)\right]\left[v_{\alpha 2}cos\left(n_p\left(\theta-\varepsilon^2(\eta_1+\check{\eta}_1)\right)\right)+v_{\beta 2}\,sin\left(n_p\left(\theta-\varepsilon^2(\eta_1+\check{\eta}_1)\right)\right)\right] \end{bmatrix}$$

$$f_4(\cdot)=\begin{bmatrix} -\frac{h_1}{h_2\sqrt{1-\left(\mu n_p\frac{h_1}{h_2}(\omega_{ref}-e_\omega)\right)^2}}\left(-\alpha_1\xi_1\,sin\left(\varepsilon^2 n_p(\eta_1+\check{\eta}_1)\right)+\alpha_1(\xi_2+\bar{x}_q)\,cos\left(\varepsilon^2 n_p(\eta_1+\check{\eta}_1)\right)-\alpha_2(\omega_{ref}-\xi_3)+\frac{k_m}{J}\left[z_\alpha\,sin(n_p\theta)-z_\beta\,cos(n_p\theta)\right]+\alpha_1 k_p M\phi_\varepsilon\left(\frac{\psi(\hat{\cdot})}{M}\right)cos\left(\varepsilon^2 n_p(\eta_1+\check{\eta}_1)\right)-\frac{1}{J}T_L\right) \\ 0 \\ 0 \end{bmatrix}$$

$$f_5(\cdot)=\begin{bmatrix} \frac{\varepsilon\rho_1 r_2 k_m h_1}{\hat{k}_m\omega^\star h_2}\left(\alpha_1(\xi_2+\bar{x}_q)-\alpha_2(\omega_{ref}-\xi_3)+\alpha_1 k_p M\phi_\varepsilon\left(\frac{\psi(\hat{\cdot})}{M}\right)-\frac{1}{J}T_L\right)\frac{sin\left(\varepsilon^2 n_p(\eta_1+\check{\eta}_1)\right)}{\varepsilon^2 n_p} \\ \varepsilon\left[\frac{\rho_2 r_2 k_m h_1}{n_p\hat{k}_m\omega^\star h_2}\left(\alpha_1(\xi_2+\bar{x}_q)-\alpha_2(\omega_{ref}-\xi_3)+\alpha_1 k_p M\phi_\varepsilon\left(\frac{\psi(\hat{\cdot})}{M}\right)-\frac{1}{J}T_L\right)-\alpha_1\xi_1\right]\frac{sin\left(\varepsilon^2 n_p(\eta_1+\check{\eta}_1)\right)}{\varepsilon^2 n_p}-\hat{\alpha}_2\eta_2-\frac{\hat{\alpha}_1 k_p M}{\varepsilon}\left[sat\left(\frac{\psi(\hat{\cdot})}{M}\right)-\phi_\varepsilon\left(\frac{\psi(\hat{\cdot})}{M}\right)\right]+\frac{\alpha_1}{\varepsilon}\left[cos(\varepsilon^2 n_p\eta_1)-1\right]\left[k_p M\phi_\varepsilon\left(\frac{\psi(\hat{\cdot})}{M}\right)+(\xi_2+\bar{x}_q)\right] \\ f_{5a} \end{bmatrix}$$

$$\begin{aligned} f_{5a}=&\frac{\rho_3 r_2 k_m h_1}{\varepsilon n_p\hat{k}_m\omega^\star h_2}\left[1+\left(\frac{\alpha_1}{\hat{\alpha}_1}-1\right)\phi_\varepsilon'\left(\frac{\psi(\hat{\cdot})}{M}\right)\right]\left(\alpha_1(\xi_2+\bar{x}_q)-\alpha_2(\omega_{ref}-\xi_3)+\alpha_1 k_p M\phi_\varepsilon\left(\frac{\psi(\hat{\cdot})}{M}\right)-\frac{1}{J}T_L\right)sin\left(\varepsilon^2 n_p(\eta_1+\check{\eta}_1)\right) \\ &-\frac{\alpha_1-\hat{\alpha}_1}{\hat{\alpha}_1}(k_\omega-\hat{\alpha}_2)\phi_\varepsilon'\left(\frac{\psi(\hat{\cdot})}{M}\right)\left(\frac{\rho_2 k_m}{\varepsilon^2 n_p\hat{k}_m\omega^\star}(\omega_{ref}-\xi_3)\,sin\left(\varepsilon^2 n_p(\eta_1+\check{\eta}_1)\right)-\eta_3-\alpha_2(\omega_{ref}-\xi_3)+\alpha_1\left[k_p M\phi_\varepsilon\left(\frac{\psi(\hat{\cdot})}{M}\right)+(\xi_2+\bar{x}_q)\right]\right) \\ &-\frac{\alpha_1-\hat{\alpha}_1}{\hat{\alpha}_1}(k_\omega-\hat{\alpha}_2)\phi_\varepsilon'\left(\frac{\psi(\hat{\cdot})}{M}\right)\left(-\frac{\rho_2 k_m}{n_p\hat{k}_m\omega^\star}\left[v_{\alpha 2}cos\left(n_p\left(\theta-\varepsilon^2(\eta_1+\check{\eta}_1)\right)\right)+v_{\beta 2}\,sin\left(n_p\left(\theta-\varepsilon^2(\eta_1+\check{\eta}_1)\right)\right)\right]+\varepsilon\hat{\alpha}_2\eta_2+\hat{\alpha}_1 k_p M\left[sat\left(\frac{\psi(\hat{\cdot})}{M}\right)-\phi_\varepsilon\left(\frac{\psi(\hat{\cdot})}{M}\right)\right]-\frac{1}{J}T_L\right) \\ &-\frac{\alpha_1-\hat{\alpha}_1}{\hat{\alpha}_1}(k_\omega-\hat{\alpha}_2)\phi_\varepsilon'\left(\frac{\psi(\hat{\cdot})}{M}\right)\left(-\frac{\rho_2 r_2 k_m h_1}{n_p\hat{k}_m\omega^\star h_2}\left[\left(\alpha_1(\xi_2+\bar{x}_q)-\alpha_2(\omega_{ref}-\xi_3)+\alpha_1 k_p M\phi_\varepsilon\left(\frac{\psi(\hat{\cdot})}{M}\right)-\frac{1}{J}T_L\right)sin\left(\varepsilon^2 n_p(\eta_1+\check{\eta}_1)\right)+n_p(\omega_{ref}-\xi_3)^2 cos\left(\varepsilon^2 n_p(\eta_1+\check{\eta}_1)\right)\right]\right) \\ &+(\alpha_1-\hat{\alpha}_1)\left[1-\phi_\varepsilon'\left(\frac{\psi(\hat{\cdot})}{M}\right)\right]\left(-\frac{k_i}{R+k_p}(\xi_2+\bar{x}_q)+\frac{k_i k_m}{R+k_p}(\omega_{ref}-\xi_3)\,cos\left(\varepsilon^2 n_p(\eta_1+\check{\eta}_1)\right)-k_i z_\alpha\,sin\left(n_p\left(\theta-\varepsilon^2(\eta_1+\check{\eta}_1)\right)\right)+k_i z_\beta\,cos\left(n_p\left(\theta-\varepsilon^2(\eta_1+\check{\eta}_1)\right)\right)+k_i M sat\left(\frac{\psi(\hat{\cdot})}{M}\right)-\frac{k_i k_p M}{R+k_p}\phi_\varepsilon\left(\frac{\psi(\hat{\cdot})}{M}\right)\right) \\ &-(\alpha_2-\hat{\alpha}_2)\left(-\alpha_1\xi_1\,sin\left(\varepsilon^2 n_p(\eta_1+\check{\eta}_1)\right)+\alpha_1(\xi_2+\bar{x}_q)\,cos\left(\varepsilon^2 n_p(\eta_1+\check{\eta}_1)\right)-\alpha_2(\omega_{ref}-\xi_3)+\frac{k_m}{J}\left[z_\alpha\,sin(n_p\theta)-z_\beta\,cos(n_p\theta)\right]+\alpha_1 k_p M\phi_\varepsilon\left(\frac{\psi(\hat{\cdot})}{M}\right)cos\left(\varepsilon^2 n_p(\eta_1+\check{\eta}_1)\right)-\frac{1}{J}T_L\right) \\ &+\frac{\alpha_1-\hat{\alpha}_1}{\hat{\alpha}_1}\phi_\varepsilon'\left(\frac{\psi(\hat{\cdot})}{M}\right)\left[\ddot{\omega}_{ref}+k_\omega\dot{\omega}_{ref}\right]-\frac{1}{J}\dot{T}_L \end{aligned}$$

$$f_6(\cdot)=\begin{bmatrix} -\frac{\rho_1 r_2 n_p k_m {h_1}^2}{\hat{k}_m\omega^\star {h_2}^2}(\omega_{ref}-\xi_3)^3 sin(\varepsilon^2 n_p\eta_1)-\frac{\rho_1 k_m(\omega_{ref}-\xi_3)}{\mu\hat{k}_m\omega^\star}\left[1-\sqrt{1-\left(\mu n_p\frac{h_1}{h_2}(\omega_{ref}-e_\omega)\right)^2}\right]\left[\frac{r_2 h_1}{h_2}(\omega_{ref}-\xi_3)\,cos(\varepsilon^2 n_p\eta_1)-\frac{sin(\varepsilon^2 n_p\eta_1)}{\varepsilon^2 n_p}\right] \\ f_{6a} \\ \left[1+\left(\frac{\alpha_1}{\hat{\alpha}_1}-1\right)\phi_\varepsilon'\left(\frac{\psi(\hat{\cdot})}{M}\right)\right]\left(-\frac{\rho_2 r_2 n_p k_m {h_1}^2}{\hat{k}_m\omega^\star {h_2}^2}(\omega_{ref}-\xi_3)^3 sin(\varepsilon^2 n_p\eta_1)-\frac{\rho_3 k_m(\omega_{ref}-\xi_3)}{\mu\hat{k}_m\omega^\star}\left[1-\sqrt{1-\left(\mu n_p\frac{h_1}{h_2}(\omega_{ref}-\xi_3)\right)^2}\right]\left[\frac{r_2 h_1}{h_2}(\omega_{ref}-\xi_3)\,cos(\varepsilon^2 n_p\eta_1)-\frac{sin(\varepsilon^2 n_p\eta_1)}{\varepsilon^2 n_p}\right]\right) \end{bmatrix}$$

$$\begin{aligned} f_{6a}=&-\frac{n_p h_1}{h_2}\left(\frac{\rho_2 r_2 k_m h_1}{\hat{k}_m\omega^\star h_2}(\omega_{ref}-\xi_3)^2+\alpha_1\left[k_p M\phi_\varepsilon\left(\frac{\psi(\hat{\cdot})}{M}\right)+(\xi_2+\bar{x}_q)\right]\right)(\omega_{ref}-\xi_3)\,sin(\varepsilon^2 n_p\eta_1) \\ &-\frac{1}{\mu}\left[1-\sqrt{1-\left(\mu n_p\frac{h_1}{h_2}(\omega_{ref}-\xi_3)\right)^2}\right]\left(\frac{\rho_2 k_m(\omega_{ref}-\xi_3)}{\hat{k}_m\omega^\star}\left[\frac{r_2 h_1}{h_2}(\omega_{ref}-\xi_3)\,cos(\varepsilon^2 n_p\eta_1)-\frac{sin(\varepsilon^2 n_p\eta_1)}{\varepsilon^2 n_p}\right]+\alpha_1\left[k_p M\phi_\varepsilon\left(\frac{\psi(\hat{\cdot})}{M}\right)+(\xi_2+\bar{x}_q)\right]cos(\varepsilon^2 n_p\eta_1)\right) \end{aligned}$$

$$\begin{aligned} f_7(\cdot)=&\frac{1}{(R+k_p)\hat{\alpha}_1}\phi_\varepsilon'\left(\frac{\psi(\hat{\cdot})}{M}\right)\begin{bmatrix} sin\left(n_p\left(\theta-\varepsilon^2(\eta_1+\check{\eta}_1)\right)\right) \\ -cos\left(n_p\left(\theta-\varepsilon^2(\eta_1+\check{\eta}_1)\right)\right) \end{bmatrix}\left(\frac{\rho_3 k_m}{\varepsilon^2 n_p\hat{k}_m\omega^\star}(\omega_{ref}-\xi_3)\,sin\left(\varepsilon^2 n_p(\eta_1+\check{\eta}_1)\right)-\frac{\rho_3 k_m}{n_p\hat{k}_m\omega^\star}\left[v_{\alpha 2}cos\left(n_p\left(\theta-\varepsilon^2(\eta_1+\check{\eta}_1)\right)\right)+v_{\beta 2}\,sin\left(n_p\left(\theta-\varepsilon^2(\eta_1+\check{\eta}_1)\right)\right)\right]\right. \\ &\left.-\frac{\rho_3 r_2 k_m h_1}{n_p\hat{k}_m\omega^\star h_2}\left[\left(\alpha_1(\xi_2+\bar{x}_q)-\alpha_2(\omega_{ref}-\xi_3)+\alpha_1 k_p M\phi_\varepsilon\left(\frac{\psi(\hat{\cdot})}{M}\right)-\frac{1}{J}T_L\right)sin\left(\varepsilon^2 n_p(\eta_1+\check{\eta}_1)\right)+n_p(\omega_{ref}-\xi_3)^2 cos\left(\varepsilon^2 n_p(\eta_1+\check{\eta}_1)\right)\right]\right) \end{aligned}$$

$$f_8(\cdot)=\frac{k_p M}{\varepsilon(R+k_p)}\begin{bmatrix} sin\left(n_p\left(\theta-\varepsilon^2(\eta_1+\check{\eta}_1)\right)\right) \\ -cos\left(n_p\left(\theta-\varepsilon^2(\eta_1+\check{\eta}_1)\right)\right) \end{bmatrix}\left[sat\left(\frac{\psi(\hat{\cdot})}{M}\right)-\phi_\varepsilon\left(\frac{\psi(\hat{\cdot})}{M}\right)\right]$$

$$f_9(\cdot)=\begin{bmatrix} f_{9a}(\cdot) \\ f_{9b}(\cdot) \end{bmatrix}$$

$$\begin{aligned} f_{9a}(\cdot)=&\frac{k_m}{R+k_p}\left(-\alpha_1\xi_1\,sin\left(\varepsilon^2 n_p(\eta_1+\check{\eta}_1)\right)+\alpha_1(\xi_2+\bar{x}_q)\,cos\left(\varepsilon^2 n_p(\eta_1+\check{\eta}_1)\right)-\alpha_2(\omega_{ref}-\xi_3)+\frac{k_m}{J}\left[z_\alpha\,sin(n_p\theta)-z_\beta\,cos(n_p\theta)\right]+\alpha_1 k_p M\phi_\varepsilon\left(\frac{\psi(\hat{\cdot})}{M}\right)cos\left(\varepsilon^2 n_p(\eta_1+\check{\eta}_1)\right)-\frac{1}{J}T_L\right)sin(n_p\theta) \\ &+\frac{1}{R+k_p}\left(-\frac{k_i}{R+k_p}\xi_1-\frac{k_i k_m}{R+k_p}(\omega_{ref}-\xi_3)\,sin\left(\varepsilon^2 n_p(\eta_1+\check{\eta}_1)\right)+k_i z_\alpha\,cos\left(n_p\left(\theta-\varepsilon^2(\eta_1+\check{\eta}_1)\right)\right)+k_i z_\beta\,sin\left(n_p\left(\theta-\varepsilon^2(\eta_1+\check{\eta}_1)\right)\right)\right)cos\left(n_p\left(\theta-\varepsilon^2(\eta_1+\check{\eta}_1)\right)\right) \end{aligned}$$

$$-\frac{1}{R+k_p}\left[1-\phi_\varepsilon'\left(\frac{\psi(\cdot)}{M}\right)\right]\left(-\frac{k_i}{R+k_p}\left[(\xi_2+\bar{x}_q)-k_m(\omega_{ref}-\xi_3)\cos\left(\varepsilon^2 n_p(\eta_1+\check{\eta}_1)\right)\right]-k_i\left[z_\alpha\sin\left(n_p\left(\theta-\varepsilon^2(\eta_1+\check{\eta}_1)\right)\right)-z_\beta\cos\left(n_p\left(\theta-\varepsilon^2(\eta_1+\check{\eta}_1)\right)\right)\right]+k_iMsat\left(\frac{\psi(\cdot)}{M}\right)-\frac{k_ik_pM}{R+k_p}\phi_\varepsilon\left(\frac{\psi(\cdot)}{M}\right)\right)$$
$$*\sin\left(n_p\left(\theta-\varepsilon^2(\eta_1+\check{\eta}_1)\right)\right)$$
$$+\frac{n_p}{R+k_p}\left[-\xi_1\sin\left(n_p\left(\theta-\varepsilon^2(\eta_1+\check{\eta}_1)\right)\right)-\left[(\xi_2+\bar{x}_q)+k_pM\phi_\varepsilon\left(\frac{\psi(\cdot)}{M}\right)\right]\cos\left(n_p\left(\theta-\varepsilon^2(\eta_1+\check{\eta}_1)\right)\right)\right]$$
$$*\left[\omega_{ref}-\xi_3-\varepsilon\eta_2+\frac{\rho_1k_m}{\varepsilon n_p\hat{k}_m\omega^\star}\left((\omega_{ref}-\xi_3)\sin\left(\varepsilon^2n_p(\eta_1+\check{\eta}_1)\right)-\varepsilon^2\left[v_{\alpha2}\cos\left(n_p\left(\theta-\varepsilon^2(\eta_1+\check{\eta}_1)\right)\right)+v_{\beta2}\sin\left(n_p\left(\theta-\varepsilon^2(\eta_1+\check{\eta}_1)\right)\right)\right]\right)\right]$$
$$+\frac{n_p}{R+k_p}\left[-\xi_1\sin\left(n_p\left(\theta-\varepsilon^2(\eta_1+\check{\eta}_1)\right)\right)-\left[(\xi_2+\bar{x}_q)+k_pM\phi_\varepsilon\left(\frac{\psi(\cdot)}{M}\right)\right]\cos\left(n_p\left(\theta-\varepsilon^2(\eta_1+\check{\eta}_1)\right)\right)\right]$$
$$*\left[-\frac{\varepsilon\rho_1r_2k_mh_1}{n_p\hat{k}_m\omega^\star h_2}\left[\left(\alpha_1(\xi_2+\bar{x}_q)-\alpha_2(\omega_{ref}-\xi_3)+\alpha_1k_pM\phi_\varepsilon\left(\frac{\psi(\cdot)}{M}\right)-\frac{1}{J}T_L\right)\sin\left(\varepsilon^2n_p(\eta_1+\check{\eta}_1)\right)+n_p(\omega_{ref}-\xi_3)^2\cos\left(\varepsilon^2n_p(\eta_1+\check{\eta}_1)\right)\right]\right]$$
$$+\frac{1}{(R+k_p)\hat{\alpha}_1}\phi_\varepsilon'\left(\frac{\psi(\cdot)}{M}\right)(k_\omega-\hat{\alpha}_2)\left(\frac{\rho_2k_m}{\varepsilon^2n_p\hat{k}_m\omega^\star}(\omega_{ref}-\xi_3)\sin\left(\varepsilon^2n_p(\eta_1+\check{\eta}_1)\right)-\eta_3-\alpha_2(\omega_{ref}-\xi_3)+\alpha_1\left[k_pM\phi_\varepsilon\left(\frac{\psi(\cdot)}{M}\right)+(\xi_2+\bar{x}_q)\right]\right)\sin\left(n_p\left(\theta-\varepsilon^2(\eta_1+\check{\eta}_1)\right)\right)$$
$$+\frac{1}{(R+k_p)\hat{\alpha}_1}\phi_\varepsilon'\left(\frac{\psi(\cdot)}{M}\right)(k_\omega-\hat{\alpha}_2)\left(-\frac{\rho_2k_m}{n_p\hat{k}_m\omega^\star}\left[v_{\alpha2}\cos\left(n_p\left(\theta-\varepsilon^2(\eta_1+\check{\eta}_1)\right)\right)+v_{\beta2}\sin\left(n_p\left(\theta-\varepsilon^2(\eta_1+\check{\eta}_1)\right)\right)\right]+\varepsilon\hat{\alpha}_2\eta_2+\hat{\alpha}_1k_pM\left[sat\left(\frac{\psi(\cdot)}{M}\right)-\phi_\varepsilon\left(\frac{\psi(\cdot)}{M}\right)\right]-\frac{1}{J}T_L\right)\sin\left(n_p\left(\theta-\varepsilon^2(\eta_1+\check{\eta}_1)\right)\right)$$
$$+\frac{1}{(R+k_p)\hat{\alpha}_1}\phi_\varepsilon'\left(\frac{\psi(\cdot)}{M}\right)(k_\omega-\hat{\alpha}_2)\left(-\frac{\rho_2r_2k_mh_1}{n_p\hat{k}_m\omega^\star h_2}\left[\left(\alpha_1(\xi_2+\bar{x}_q)-\alpha_2(\omega_{ref}-\xi_3)+\alpha_1k_pM\phi_\varepsilon\left(\frac{\psi(\cdot)}{M}\right)-\frac{1}{J}T_L\right)\sin\left(\varepsilon^2n_p(\eta_1+\check{\eta}_1)\right)+n_p(\omega_{ref}-\xi_3)^2\cos\left(\varepsilon^2n_p(\eta_1+\check{\eta}_1)\right)\right]\right)\sin\left(n_p\left(\theta-\varepsilon^2(\eta_1+\check{\eta}_1)\right)\right)$$
$$+\frac{n_pk_m}{R+k_p}(\omega_{ref}-\xi_3)^2\cos(n_p\theta)-\frac{1}{(R+k_p)\hat{\alpha}_1}\phi_\varepsilon'\left(\frac{\psi(\cdot)}{M}\right)\left[\ddot{\omega}_{ref}+k_\omega\dot{\omega}_{ref}\right]\sin\left(n_p\left(\theta-\varepsilon^2(\eta_1+\check{\eta}_1)\right)\right)$$

$$f_{9b}(\cdot)=-\frac{k_m}{R+k_p}\left(-\alpha_1\xi_1\sin\left(\varepsilon^2n_p(\eta_1+\check{\eta}_1)\right)+\alpha_1(\xi_2+\bar{x}_q)\cos\left(\varepsilon^2n_p(\eta_1+\check{\eta}_1)\right)-\alpha_2(\omega_{ref}-\xi_3)+\frac{k_m}{J}\left[z_\alpha\sin(n_p\theta)-z_\beta\cos(n_p\theta)\right]+\alpha_1k_pM\phi_\varepsilon\left(\frac{\psi(\cdot)}{M}\right)\cos\left(\varepsilon^2n_p(\eta_1+\check{\eta}_1)\right)-\frac{1}{J}T_L\right)\cos(n_p\theta)$$
$$+\frac{1}{R+k_p}\left(-\frac{k_i}{R+k_p}\xi_1-\frac{k_ik_m}{R+k_p}(\omega_{ref}-\xi_3)\sin\left(\varepsilon^2n_p(\eta_1+\check{\eta}_1)\right)+k_iz_\alpha\cos\left(n_p\left(\theta-\varepsilon^2(\eta_1+\check{\eta}_1)\right)\right)+k_iz_\beta\sin\left(n_p\left(\theta-\varepsilon^2(\eta_1+\check{\eta}_1)\right)\right)\right)\sin\left(n_p\left(\theta-\varepsilon^2(\eta_1+\check{\eta}_1)\right)\right)$$
$$+\frac{1}{R+k_p}\left[1-\phi_\varepsilon'\left(\frac{\psi(\cdot)}{M}\right)\right]\left(-\frac{k_i}{R+k_p}\left[(\xi_2+\bar{x}_q)-k_m(\omega_{ref}-\xi_3)\cos\left(\varepsilon^2n_p(\eta_1+\check{\eta}_1)\right)\right]-k_i\left[z_\alpha\sin\left(n_p\left(\theta-\varepsilon^2(\eta_1+\check{\eta}_1)\right)\right)-z_\beta\cos\left(n_p\left(\theta-\varepsilon^2(\eta_1+\check{\eta}_1)\right)\right)\right]+k_iMsat\left(\frac{\psi(\cdot)}{M}\right)-\frac{k_ik_pM}{R+k_p}\phi_\varepsilon\left(\frac{\psi(\cdot)}{M}\right)\right)$$
$$*\cos\left(n_p\left(\theta-\varepsilon^2(\eta_1+\check{\eta}_1)\right)\right)$$
$$+\frac{n_p}{R+k_p}\left[\xi_1\cos\left(n_p\left(\theta-\varepsilon^2(\eta_1+\check{\eta}_1)\right)\right)-\left[(\xi_2+\bar{x}_q)+k_pM\phi_\varepsilon\left(\frac{\psi(\cdot)}{M}\right)\right]\sin\left(n_p\left(\theta-\varepsilon^2(\eta_1+\check{\eta}_1)\right)\right)\right]$$
$$*\left[\omega_{ref}-\xi_3-\varepsilon\eta_2+\frac{\rho_1k_m}{\varepsilon n_p\hat{k}_m\omega^\star}\left((\omega_{ref}-\xi_3)\sin\left(\varepsilon^2n_p(\eta_1+\check{\eta}_1)\right)-\varepsilon^2\left[v_{\alpha2}\cos\left(n_p\left(\theta-\varepsilon^2(\eta_1+\check{\eta}_1)\right)\right)+v_{\beta2}\sin\left(n_p\left(\theta-\varepsilon^2(\eta_1+\check{\eta}_1)\right)\right)\right]\right)\right]$$
$$+\frac{n_p}{R+k_p}\left[\xi_1\cos\left(n_p\left(\theta-\varepsilon^2(\eta_1+\check{\eta}_1)\right)\right)-\left[(\xi_2+\bar{x}_q)+k_pM\phi_\varepsilon\left(\frac{\psi(\cdot)}{M}\right)\right]\sin\left(n_p\left(\theta-\varepsilon^2(\eta_1+\check{\eta}_1)\right)\right)\right]$$
$$*\left[-\frac{\varepsilon\rho_1r_2k_mh_1}{n_p\hat{k}_m\omega^\star h_2}\left[\left(\alpha_1(\xi_2+\bar{x}_q)-\alpha_2(\omega_{ref}-\xi_3)+\alpha_1k_pM\phi_\varepsilon\left(\frac{\psi(\cdot)}{M}\right)-\frac{1}{J}T_L\right)\sin\left(\varepsilon^2n_p(\eta_1+\check{\eta}_1)\right)+n_p(\omega_{ref}-e_\omega)^2\cos\left(\varepsilon^2n_p(\eta_1+\check{\eta}_1)\right)\right]\right]$$
$$-\frac{1}{(R+k_p)\hat{\alpha}_1}\phi_\varepsilon'\left(\frac{\psi(\cdot)}{M}\right)(k_\omega-\hat{\alpha}_2)\left(\frac{\rho_2k_m}{\varepsilon^2n_p\hat{k}_m\omega^\star}(\omega_{ref}-\xi_3)\sin\left(\varepsilon^2n_p(\eta_1+\check{\eta}_1)\right)-\eta_3-\alpha_2(\omega_{ref}-\xi_3)+\alpha_1\left[k_pM\phi_\varepsilon\left(\frac{\psi(\cdot)}{M}\right)+(\xi_2+\bar{x}_q)\right]\right)\cos\left(n_p\left(\theta-\varepsilon^2(\eta_1+\check{\eta}_1)\right)\right)$$
$$-\frac{1}{(R+k_p)\hat{\alpha}_1}\phi_\varepsilon'\left(\frac{\psi(\cdot)}{M}\right)(k_\omega-\hat{\alpha}_2)\left(-\frac{\rho_2k_m}{n_p\hat{k}_m\omega^\star}\left[v_{\alpha2}\cos\left(n_p\left(\theta-\varepsilon^2(\eta_1+\check{\eta}_1)\right)\right)+v_{\beta2}\sin\left(n_p\left(\theta-\varepsilon^2(\eta_1+\check{\eta}_1)\right)\right)\right]+\varepsilon\hat{\alpha}_2\eta_2+\hat{\alpha}_1k_pM\left[sat\left(\frac{\psi(\cdot)}{M}\right)-\phi_\varepsilon\left(\frac{\psi(\cdot)}{M}\right)\right]-\frac{1}{J}T_L\right)\cos\left(n_p\left(\theta-\varepsilon^2(\eta_1+\check{\eta}_1)\right)\right)$$
$$-\frac{1}{(R+k_p)\hat{\alpha}_1}\phi_\varepsilon'\left(\frac{\psi(\cdot)}{M}\right)(k_\omega-\hat{\alpha}_2)\left(-\frac{\rho_2r_2k_mh_1}{n_p\hat{k}_m\omega^\star h_2}\left[\left(\alpha_1(\xi_2+\bar{x}_q)-\alpha_2(\omega_{ref}-\xi_3)+\alpha_1k_pM\phi_\varepsilon\left(\frac{\psi(\cdot)}{M}\right)-\frac{1}{J}T_L\right)\sin\left(\varepsilon^2n_p(\eta_1+\check{\eta}_1)\right)+n_p(\omega_{ref}-\xi_3)^2\cos\left(\varepsilon^2n_p(\eta_1+\check{\eta}_1)\right)\right]\right)\cos\left(n_p\left(\theta-\varepsilon^2(\eta_1+\check{\eta}_1)\right)\right)$$
$$+\frac{n_pk_m}{R+k_p}(\omega_{ref}-\xi_3)^2\sin(n_p\theta)+\frac{1}{(R+k_p)\hat{\alpha}_1}\phi_\varepsilon'\left(\frac{\psi(\cdot)}{M}\right)\left[\ddot{\omega}_{ref}+k_\omega\dot{\omega}_{ref}\right]\cos\left(n_p\left(\theta-\varepsilon^2(\eta_1+\check{\eta}_1)\right)\right)$$

$$f_{10}(\cdot)=\begin{bmatrix}\sin(n_p\theta)\\ h_1\sin(n_p\theta)\\ -\cos(n_p\theta)\\ -h_1\cos(n_p\theta)\end{bmatrix}\frac{r_2\alpha_1}{h_2\hat{\alpha}_1}\phi_\varepsilon'\left(\frac{\psi(\cdot)}{M}\right)\left(\frac{\rho_3k_m}{\varepsilon^2n_p\hat{k}_m\omega^\star}(\omega_{ref}-\xi_3)\sin\left(\varepsilon^2n_p(\eta_1+\check{\eta}_1)\right)-\frac{\rho_3k_m}{n_p\hat{k}_m\omega^\star}\left[v_{\alpha2}\cos\left(n_p\left(\theta-\varepsilon^2(\eta_1+\check{\eta}_1)\right)\right)+v_{\beta2}\sin\left(n_p\left(\theta-\varepsilon^2(\eta_1+\check{\eta}_1)\right)\right)\right]\right.$$
$$\left.-\frac{\rho_3r_2k_mh_1}{n_p\hat{k}_m\omega^\star h_2}\left[\left(\alpha_1(\xi_2+\bar{x}_q)-\alpha_2(\omega_{ref}-\xi_3)+\alpha_1k_pM\phi_\varepsilon\left(\frac{\psi(\cdot)}{M}\right)-\frac{1}{J}T_L\right)\sin\left(\varepsilon^2n_p(\eta_1+\check{\eta}_1)\right)+n_p(\omega_{ref}-\xi_3)^2\cos\left(\varepsilon^2n_p(\eta_1+\check{\eta}_1)\right)\right]\right)$$

$$f_{11}(\cdot)=\frac{1}{\varepsilon}\begin{bmatrix}0\\ -\sin(n_p\theta)\\ 0\\ \cos(n_p\theta)\end{bmatrix}2r_2\sin^2\left(\frac{1}{2}\varepsilon^2n_p(\eta_1+\check{\eta}_1)\right)\left[\left(\alpha_1(\xi_2+\bar{x}_q)+\alpha_1k_pM\phi_\varepsilon\left(\frac{\psi(\cdot)}{M}\right)\right)+r_2\alpha_1\xi_1\sin\left(\varepsilon^2n_p(\eta_1+\check{\eta}_1)\right)\right]$$

$$f_{12}(\cdot)=\begin{bmatrix}f_{12_a}(\cdot)\\ f_{12_b}(\cdot)\\ f_{12_c}(\cdot)\\ f_{12_d}(\cdot)\end{bmatrix}$$

$$f_{12a}(\cdot)=-\mu\frac{R}{L}\left[v_{\alpha1}+\frac{r_2}{h_2}\left(\alpha_1(\xi_2+\bar{x}_q)-\alpha_2(\omega_{ref}-\xi_3)+\alpha_1k_pM\phi_\varepsilon\left(\frac{\psi(\cdot)}{M}\right)-\frac{1}{J}T_L\right)\sin(n_p\theta)-\frac{r_2n_p}{h_2}(\omega_{ref}-\xi_3)^2\cos(n_p\theta)\right]$$
$$-\frac{r_2\alpha_1}{h_2}\left[1-\phi_\varepsilon'\left(\frac{\psi(\cdot)}{M}\right)\right]\left(-\frac{k_i}{R+k_p}\left[(\xi_2+\bar{x}_q)-k_m(\omega_{ref}-\xi_3)\cos\left(\varepsilon^2n_p(\eta_1+\check{\eta}_1)\right)\right]-k_i\left[z_\alpha\sin\left(n_p\left(\theta-\varepsilon^2(\eta_1+\check{\eta}_1)\right)\right)-z_\beta\cos\left(n_p\left(\theta-\varepsilon^2(\eta_1+\check{\eta}_1)\right)\right)\right]+k_iMsat\left(\frac{\psi(\cdot)}{M}\right)-\frac{k_ik_pM}{R+k_p}\phi_\varepsilon\left(\frac{\psi(\cdot)}{M}\right)\right)\sin(n_p\theta)$$
$$+\frac{r_2\alpha_1}{h_2\hat{\alpha}_1}\phi_\varepsilon'\left(\frac{\psi(\cdot)}{M}\right)(k_\omega-\hat{\alpha}_2)\left(\frac{\rho_2k_m}{\varepsilon^2n_p\hat{k}_m\omega^\star}(\omega_{ref}-\xi_3)\sin\left(\varepsilon^2n_p(\eta_1+\check{\eta}_1)\right)-\eta_3-\alpha_2(\omega_{ref}-\xi_3)+\alpha_1\left[k_pM\phi_\varepsilon\left(\frac{\psi(\cdot)}{M}\right)+(\xi_2+\bar{x}_q)\right]\right)\sin(n_p\theta)$$
$$+\frac{r_2\alpha_1}{h_2\hat{\alpha}_1}\phi_\varepsilon'\left(\frac{\psi(\cdot)}{M}\right)(k_\omega-\hat{\alpha}_2)\left(-\frac{\rho_2k_m}{n_p\hat{k}_m\omega^\star}\left[v_{\alpha2}\cos\left(n_p\left(\theta-\varepsilon^2(\eta_1+\check{\eta}_1)\right)\right)+v_{\beta2}\sin\left(n_p\left(\theta-\varepsilon^2(\eta_1+\check{\eta}_1)\right)\right)\right]+\varepsilon\hat{\alpha}_2\eta_2+\hat{\alpha}_1k_pM\left[sat\left(\frac{\psi(\cdot)}{M}\right)-\phi_\varepsilon\left(\frac{\psi(\cdot)}{M}\right)\right]-\frac{1}{J}T_L\right)\sin(n_p\theta)$$
$$+\frac{\mu r_2\alpha_1}{h_2\hat{\alpha}_1}\phi_\varepsilon'\left(\frac{\psi(\cdot)}{M}\right)(k_\omega-\hat{\alpha}_2)\left(-\frac{\rho_2r_2k_mh_1}{n_p\hat{k}_m\omega^\star h_2}\left[\left(\alpha_1(\xi_2+\bar{x}_q)-\alpha_2(\omega_{ref}-\xi_3)+\alpha_1k_pM\phi_\varepsilon\left(\frac{\psi(\cdot)}{M}\right)-\frac{1}{J}T_L\right)\sin\left(\varepsilon^2n_p(\eta_1+\check{\eta}_1)\right)+n_p(\omega_{ref}-\xi_3)^2\cos\left(\varepsilon^2n_p(\eta_1+\check{\eta}_1)\right)\right]\right)\sin(n_p\theta)$$
$$+\frac{r_2}{h_2}\left[\alpha_2\sin(n_p\theta)-2n_p(\omega_{ref}-\xi_3)\cos(n_p\theta)\right]\left(-\alpha_1\xi_1\sin\left(\varepsilon^2n_p(\eta_1+\check{\eta}_1)\right)+\alpha_1(\xi_2+\bar{x}_q)\cos\left(\varepsilon^2n_p(\eta_1+\check{\eta}_1)\right)-\alpha_2(\omega_{ref}-\xi_3)+\frac{k_m}{J}\left[z_\alpha\sin(n_p\theta)-z_\beta\cos(n_p\theta)\right]+\alpha_1k_pM\phi_\varepsilon\left(\frac{\psi(\cdot)}{M}\right)\cos\left(\varepsilon^2n_p(\eta_1+\check{\eta}_1)\right)-\frac{1}{J}T_L\right)$$
$$-\frac{n_pr_2}{h_2}\left(\alpha_1(\xi_2+\bar{x}_q)-\alpha_2(\omega_{ref}-\xi_3)+\alpha_1k_pM\phi_\varepsilon\left(\frac{\psi(\cdot)}{M}\right)-\frac{1}{J}T_L\right)(\omega_{ref}-\xi_3)\cos(n_p\theta)+\frac{{n_p}^2r_2}{h_2}(\omega_{ref}-\xi_3)^3\sin(n_p\theta)-\frac{r_2\alpha_1}{h_2\hat{\alpha}_1}\phi_\varepsilon'\left(\frac{\psi(\cdot)}{M}\right)\left[\ddot{\omega}_{ref}+k_\omega\dot{\omega}_{ref}\right]\sin(n_p\theta)+\frac{r_2}{Jh_2}T_L\sin(n_p\theta)$$

$$f_{12}\ (\cdot)=-\frac{r_2\alpha_1h_1}{h_2}\left[1-\phi_\varepsilon'\left(\frac{\psi(\cdot)}{M}\right)\right]\left(-\frac{k_i}{R+k_p}\left[(\xi_2+\bar{x}_q)-k_m(\omega_{ref}-\xi_3)\cos\left(\varepsilon^2n_p(\eta_1+\check{\eta}_1)\right)\right]-k_i\left[z_\alpha\sin\left(n_p\left(\theta-\varepsilon^2(\eta_1+\check{\eta}_1)\right)\right)-z_\beta\cos\left(n_p\left(\theta-\varepsilon^2(\eta_1+\check{\eta}_1)\right)\right)\right]+k_iMsat\left(\frac{\psi(\cdot)}{M}\right)-\frac{k_ik_pM}{R+k_p}\phi_\varepsilon\left(\frac{\psi(\cdot)}{M}\right)\right)\sin(n_p\theta)$$
$$+\frac{r_2\alpha_1h_1}{h_2\hat{\alpha}_1}\phi_\varepsilon'\left(\frac{\psi(\cdot)}{M}\right)(k_\omega-\hat{\alpha}_2)\left(\frac{\rho_2k_m}{\varepsilon^2n_p\hat{k}_m\omega^\star}(\omega_{ref}-\xi_3)\sin\left(\varepsilon^2n_p(\eta_1+\check{\eta}_1)\right)-\eta_3-\alpha_2(\omega_{ref}-\xi_3)+\alpha_1\left[k_pM\phi_\varepsilon\left(\frac{\psi(\cdot)}{M}\right)+(\xi_2+\bar{x}_q)\right]\right)\sin(n_p\theta)$$
$$+\frac{r_2\alpha_1h_1}{h_2\hat{\alpha}_1}\phi_\varepsilon'\left(\frac{\psi(\cdot)}{M}\right)(k_\omega-\hat{\alpha}_2)\left(-\frac{\rho_2k_m}{n_p\hat{k}_m\omega^\star}\left[v_{\alpha2}\cos\left(n_p\left(\theta-\varepsilon^2(\eta_1+\check{\eta}_1)\right)\right)+v_{\beta2}\sin\left(n_p\left(\theta-\varepsilon^2(\eta_1+\check{\eta}_1)\right)\right)\right]+\varepsilon\hat{\alpha}_2\eta_2+\hat{\alpha}_1k_pM\left[sat\left(\frac{\psi(\cdot)}{M}\right)-\phi_\varepsilon\left(\frac{\psi(\cdot)}{M}\right)\right]-\frac{1}{J}T_L\right)\sin(n_p\theta)$$

$$+\frac{r_2\alpha_1 h_1}{h_2\hat{\alpha}_1}\phi_\varepsilon'\left(\frac{\psi(\cdot)}{M}\right)(k_\omega-\hat{\alpha}_2)\left(-\frac{\rho_2 r_2 k_m h_1}{n_p\hat{k}_m\omega^\star h_2}\left[\left(\alpha_1(\xi_2+\bar{x}_q)-\alpha_2(\omega_{ref}-\xi_3)+\alpha_1 k_p M\phi_\varepsilon\left(\frac{\psi(\cdot)}{M}\right)-\frac{1}{J}T_L\right)sin\left(\varepsilon^2 n_p(\eta_1+\check{\eta}_1)\right)+n_p(\omega_{ref}-\xi_3)^2 cos\left(\varepsilon^2 n_p(\eta_1+\check{\eta}_1)\right)\right]\right)sin(n_p\theta)$$
$$+\frac{r_2 h_1}{h_2}[\alpha_2\, sin(n_p\theta)\ -2n_p(\omega_{ref}-\xi_3)\,cos(n_p\theta)]\left(-\alpha_1\xi_1\, sin\left(\varepsilon^2 n_p(\eta_1+\check{\eta}_1)\right)+\alpha_1(\xi_2+\bar{x}_q)\,cos\left(\varepsilon^2 n_p(\eta_1+\check{\eta}_1)\right)-\alpha_2(\omega_{ref}-\xi_3)+\frac{k_m}{J}[z_\alpha\, sin(n_p\theta)-z_\beta\, cos(n_p\theta)]+\alpha_1 k_p M\phi_\varepsilon\left(\frac{\psi(\cdot)}{M}\right)cos\left(\varepsilon^2 n_p(\eta_1+\check{\eta}_1)\right)-\frac{1}{J}T_L\right)$$
$$-\frac{n_p r_2 h_1}{h_2}\left(\alpha_1(\xi_2+\bar{x}_q)-\alpha_2(\omega_{ref}-\xi_3)+\alpha_1 k_p M\phi_\varepsilon\left(\frac{\psi(\cdot)}{M}\right)-\frac{1}{J}T_L\right)(\omega_{ref}-\xi_3)\,cos(n_p\theta)+\frac{{n_p}^2 r_2 h_1}{h_2}(\omega_{ref}-\xi_3)^3 sin(n_p\theta)-\frac{r_2\alpha_1 h_1}{h_2\hat{\alpha}_1}\phi_\varepsilon'\left(\frac{\psi(\cdot)}{M}\right)[\ddot{\omega}_{ref}+k_\omega\dot{\omega}_{ref}]\,sin(n_p\theta)+\frac{r_2 h_1}{Jh_2}T_L\, sin(n_p\theta)$$

$$f_{12}\ (\cdot)=-\frac{R}{L}\left[v_{\beta 1}-\frac{r_2}{h_2}\left(\alpha_1(\xi_2+\bar{x}_q)-\alpha_2(\omega_{ref}-\xi_3)+\alpha_1 k_p M\phi_\varepsilon\left(\frac{\psi(\cdot)}{M}\right)-\frac{1}{J}T_L\right)cos(n_p\theta)+\frac{r_2 n_p}{h_2}(\omega_{ref}-\xi_3)^2 sin(n_p\theta)\right]$$
$$+\frac{r_2\alpha_1}{h_2}\left[1-\phi_\varepsilon'\left(\frac{\psi(\cdot)}{M}\right)\right]\left(-\frac{k_i}{R+k_p}\left[(\xi_2+\bar{x}_q)-k_m(\omega_{ref}-\xi_3)\,cos\left(\varepsilon^2 n_p(\eta_1+\check{\eta}_1)\right)\right]-k_i\left[z_\alpha\, sin\left(n_p\left(\theta-\varepsilon^2(\eta_1+\check{\eta}_1)\right)\right)-z_\beta\, cos\left(n_p\left(\theta-\varepsilon^2(\eta_1+\check{\eta}_1)\right)\right)\right]+k_i Msat\left(\frac{\psi(\cdot)}{M}\right)-\frac{k_i k_p M}{R+k_p}\phi_\varepsilon\left(\frac{\psi(\cdot)}{M}\right)\right)cos(n_p\theta)$$
$$-\frac{r_2\alpha_1}{h_2\hat{\alpha}_1}\phi_\varepsilon'\left(\frac{\psi(\cdot)}{M}\right)(k_\omega-\hat{\alpha}_2)\left(\frac{\rho_2 k_m}{\varepsilon^2 n_p\hat{k}_m\omega^\star}(\omega_{ref}-\xi_3)\,sin\left(\varepsilon^2 n_p(\eta_1+\check{\eta}_1)\right)-\eta_3-\alpha_2(\omega_{ref}-\xi_3)+\alpha_1\left[k_p M\phi_\varepsilon\left(\frac{\psi(\cdot)}{M}\right)+(\xi_2+\bar{x}_q)\right]\right)cos(n_p\theta)$$
$$-\frac{r_2\alpha_1}{h_2\hat{\alpha}_1}\phi_\varepsilon'\left(\frac{\psi(\cdot)}{M}\right)(k_\omega-\hat{\alpha}_2)\left(-\frac{\rho_2 k_m}{n_p\hat{k}_m\omega^\star}\left[v_{\alpha 2}cos\left(n_p\left(\theta-\varepsilon^2(\eta_1+\check{\eta}_1)\right)\right)+v_{\beta 2}\, sin\left(n_p\left(\theta-\varepsilon^2(\eta_1+\check{\eta}_1)\right)\right)\right]+\varepsilon\hat{\alpha}_2\eta_2+\hat{\alpha}_1 k_p M\left[sat\left(\frac{\psi(\cdot)}{M}\right)-\phi_\varepsilon\left(\frac{\psi(\cdot)}{M}\right)\right]-\frac{1}{J}T_L\right)cos(n_p\theta)$$
$$-\frac{r_2\alpha_1}{h_2\hat{\alpha}_1}\phi_\varepsilon'\left(\frac{\psi(\cdot)}{M}\right)(k_\omega-\hat{\alpha}_2)\left(-\frac{\rho_2 r_2 k_m h_1}{n_p\hat{k}_m\omega^\star h_2}\left[\left(\alpha_1(\xi_2+\bar{x}_q)-\alpha_2(\omega_{ref}-\xi_3)+\alpha_1 k_p M\phi_\varepsilon\left(\frac{\psi(\cdot)}{M}\right)-\frac{1}{J}T_L\right)sin\left(\varepsilon^2 n_p(\eta_1+\check{\eta}_1)\right)+n_p(\omega_{ref}-\xi_3)^2 cos\left(\varepsilon^2 n_p(\eta_1+\check{\eta}_1)\right)\right]\right)cos(n_p\theta)$$
$$-\frac{r_2}{h_2}[\alpha_2\, cos(n_p\theta)+2n_p(\omega_{ref}-\xi_3)\,sin(n_p\theta)]\left(-\alpha_1\xi_1\, sin\left(\varepsilon^2 n_p(\eta_1+\check{\eta}_1)\right)+\alpha_1(\xi_2+\bar{x}_q)\,cos\left(\varepsilon^2 n_p(\eta_1+\check{\eta}_1)\right)-\alpha_2(\omega_{ref}-\xi_3)+\frac{k_m}{J}[z_\alpha\, sin(n_p\theta)-z_\beta\, cos(n_p\theta)]+\alpha_1 k_p M\phi_\varepsilon\left(\frac{\psi(\cdot)}{M}\right)cos\left(\varepsilon^2 n_p(\eta_1+\check{\eta}_1)\right)-\frac{1}{J}T_L\right)$$
$$-\frac{n_p r_2}{h_2}\left(\alpha_1(\xi_2+\bar{x}_q)-\alpha_2(\omega_{ref}-\xi_3)+\alpha_1 k_p M\phi_\varepsilon\left(\frac{\psi(\cdot)}{M}\right)-\frac{1}{J}T_L\right)(\omega_{ref}-\xi_3)\,sin(n_p\theta)+\frac{{n_p}^2 r_2}{h_2}(\omega_{ref}-\xi_3)^3 sin(n_p\theta)+\frac{r_2\alpha_1}{h_2\hat{\alpha}_1}\phi_\varepsilon'\left(\frac{\psi(\cdot)}{M}\right)[\ddot{\omega}_{ref}+k_\omega\dot{\omega}_{ref}]\,cos(n_p\theta)-\frac{r_2}{Jh_2}T_L\, cos(n_p\theta)$$

$$f_{12d}(\cdot)=\frac{r_2\alpha_1 h_1}{h_2}\left[1-\phi_\varepsilon'\left(\frac{\psi(\cdot)}{M}\right)\right]\left(-\frac{k_i}{R+k_p}\left[(\xi_2+\bar{x}_q)-k_m(\omega_{ref}-\xi_3)\,cos\left(\varepsilon^2 n_p(\eta_1+\check{\eta}_1)\right)\right]-k_i\left[z_\alpha\, sin\left(n_p\left(\theta-\varepsilon^2(\eta_1+\check{\eta}_1)\right)\right)-z_\beta\, cos\left(n_p\left(\theta-\varepsilon^2(\eta_1+\check{\eta}_1)\right)\right)\right]+k_i Msat\left(\frac{\psi(\cdot)}{M}\right)-\frac{k_i k_p M}{R+k_p}\phi_\varepsilon\left(\frac{\psi(\cdot)}{M}\right)\right)cos(n_p\theta)$$
$$-\frac{r_2\alpha_1 h_1}{h_2\hat{\alpha}_1}\phi_\varepsilon'\left(\frac{\psi(\cdot)}{M}\right)(k_\omega-\hat{\alpha}_2)\left(\frac{\rho_2 k_m}{\varepsilon^2 n_p\hat{k}_m\omega^\star}(\omega_{ref}-\xi_3)\,sin\left(\varepsilon^2 n_p(\eta_1+\check{\eta}_1)\right)-\eta_3-\alpha_2(\omega_{ref}-\xi_3)+\alpha_1\left[k_p M\phi_\varepsilon\left(\frac{\psi(\cdot)}{M}\right)+(\xi_2+\bar{x}_q)\right]\right)cos(n_p\theta)$$
$$-\frac{r_2\alpha_1 h_1}{h_2\hat{\alpha}_1}\phi_\varepsilon'\left(\frac{\psi(\cdot)}{M}\right)(k_\omega-\hat{\alpha}_2)\left(-\frac{\rho_2 k_m}{n_p\hat{k}_m\omega^\star}\left[v_{\alpha 2}cos\left(n_p\left(\theta-\varepsilon^2(\eta_1+\check{\eta}_1)\right)\right)+v_{\beta 2}\, sin\left(n_p\left(\theta-\varepsilon^2(\eta_1+\check{\eta}_1)\right)\right)\right]+\varepsilon\hat{\alpha}_2\eta_2+\hat{\alpha}_1 k_p M\left[sat\left(\frac{\psi(\cdot)}{M}\right)-\phi_\varepsilon\left(\frac{\psi(\cdot)}{M}\right)\right]-\frac{1}{J}T_L\right)cos(n_p\theta)$$
$$-\frac{r_2\alpha_1 h_1}{h_2\hat{\alpha}_1}\phi_\varepsilon'\left(\frac{\psi(\cdot)}{M}\right)(k_\omega-\hat{\alpha}_2)\left(-\frac{\rho_2 r_2 k_m h_1}{n_p\hat{k}_m\omega^\star h_2}\left[\left(\alpha_1(\xi_2+\bar{x}_q)-\alpha_2(\omega_{ref}-\xi_3)+\alpha_1 k_p M\phi_\varepsilon\left(\frac{\psi(\cdot)}{M}\right)-\frac{1}{J}T_L\right)sin\left(\varepsilon^2 n_p(\eta_1+\check{\eta}_1)\right)+n_p(\omega_{ref}-\xi_3)^2 cos\left(\varepsilon^2 n_p(\eta_1+\check{\eta}_1)\right)\right]\right)cos(n_p\theta)$$
$$-\frac{r_2 h_1}{h_2}[\alpha_2\, cos(n_p\theta)+2n_p(\omega_{ref}-\xi_3)\,sin(n_p\theta)]\left(-\alpha_1\xi_1\, sin\left(\varepsilon^2 n_p(\eta_1+\check{\eta}_1)\right)+\alpha_1(\xi_2+\bar{x}_q)\,cos\left(\varepsilon^2 n_p(\eta_1+\check{\eta}_1)\right)-\alpha_2(\omega_{ref}-\xi_3)+\frac{k_m}{J}[z_\alpha\, sin(n_p\theta)-z_\beta\, cos(n_p\theta)]+\alpha_1 k_p M\phi_\varepsilon\left(\frac{\psi(\cdot)}{M}\right)cos\left(\varepsilon^2 n_p(\eta_1+\check{\eta}_1)\right)-\frac{1}{J}T_L\right)$$
$$-\frac{n_p r_2 h_1}{h_2}\left(\alpha_1(\xi_2+\bar{x}_q)-\alpha_2(\omega_{ref}-\xi_3)+\alpha_1 k_p M\phi_\varepsilon\left(\frac{\psi(\cdot)}{M}\right)-\frac{1}{J}T_L\right)(\omega_{ref}-\xi_3)\,sin(n_p\theta)+\frac{{n_p}^2 r_2}{h_2}(\omega_{ref}-\xi_3)^3 sin(n_p\theta)+\frac{r_2\alpha_1}{h_2\hat{\alpha}_1}\phi_\varepsilon'\left(\frac{\psi(\cdot)}{M}\right)[\ddot{\omega}_{ref}+k_\omega\dot{\omega}_{ref}]\,cos(n_p\theta)-\frac{r_2}{Jh_2}T_L\, cos(n_p\theta)$$

**B5. Parameters Perturbation Figures**

We investigated the robustness of the proposed controller to the effect of parameter perturbation. The following figures show the experimental results of this investigation.

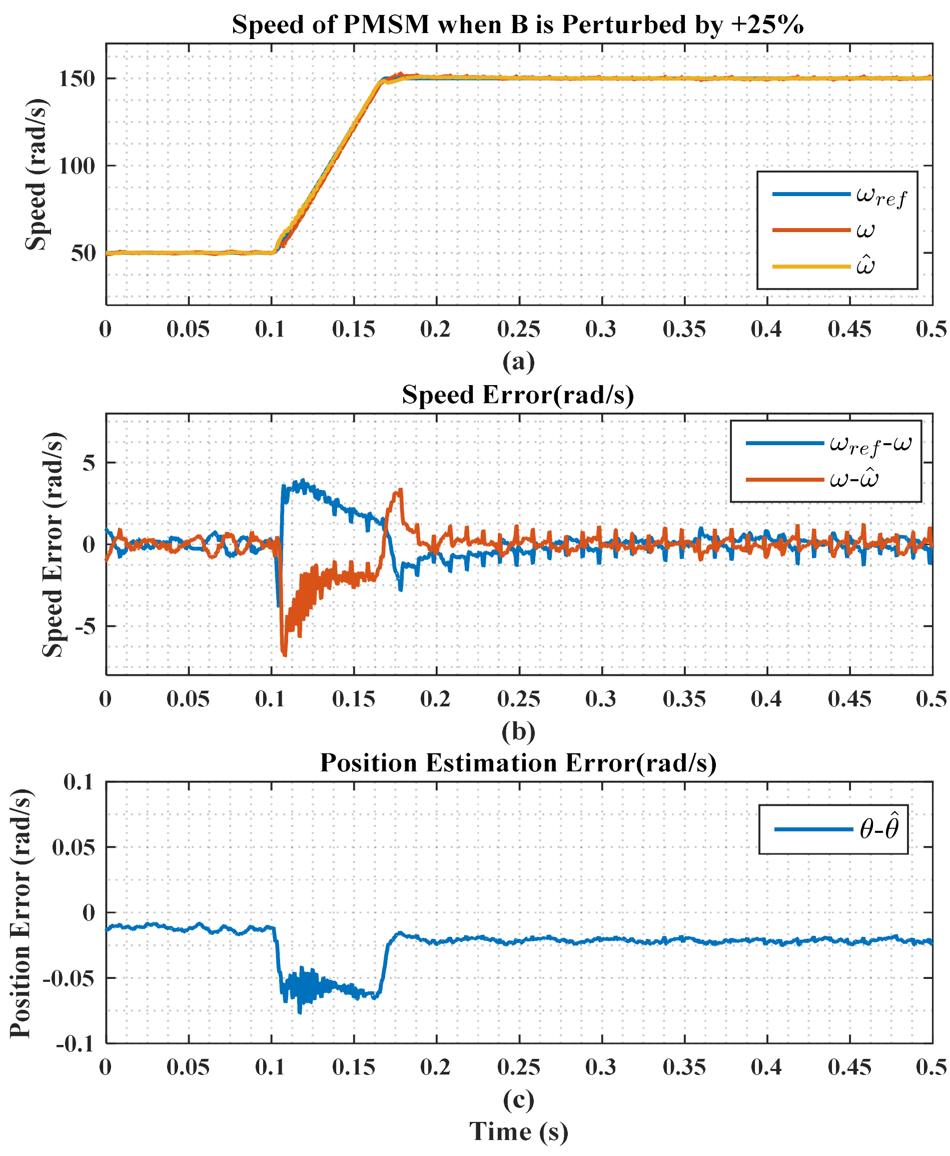


Figure B5.1 (a) Reference speed, speed of PMSM, and estimated speed, (b) Speed error from reference speed and speed estimation error, (c) Position estimation error.

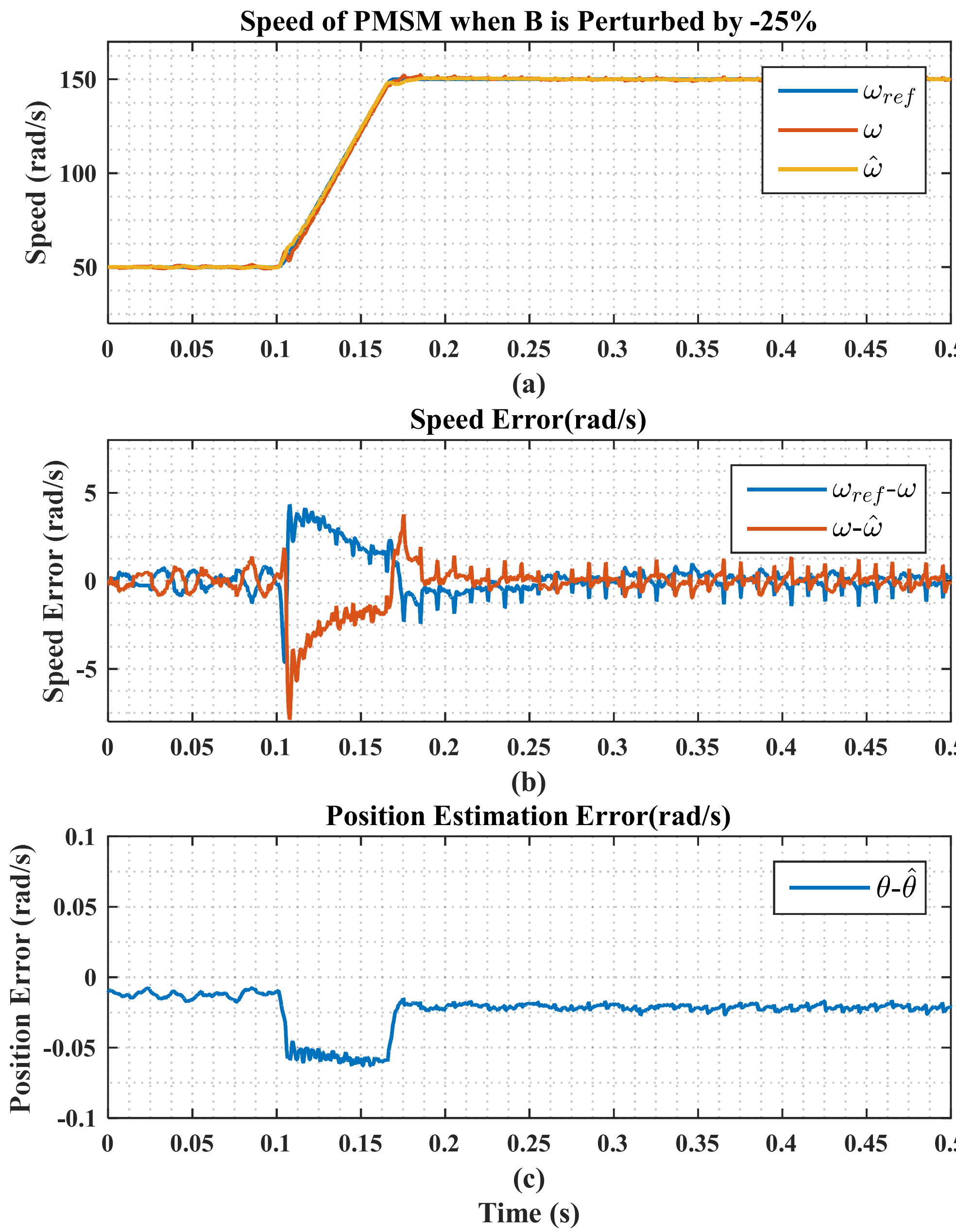


Figure B5.2 (a) Reference speed, speed of PMSM, and estimated speed, (b) Speed error from reference speed and speed estimation error, (c) Position estimation error.

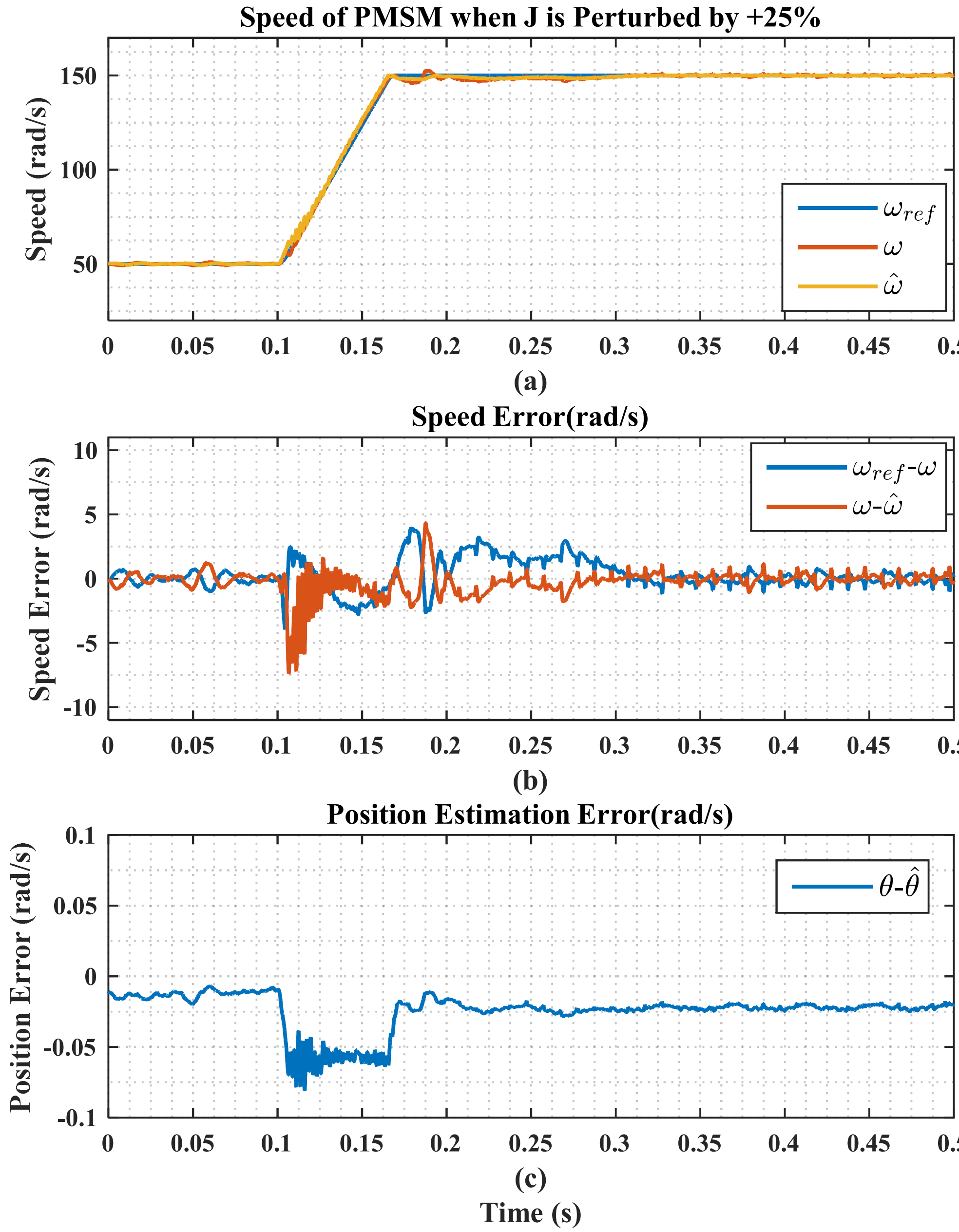


Figure B5.3 (a) Reference speed, speed of PMSM, and estimated speed, (b) Speed error from reference speed and speed estimation error, (c) Position estimation error.

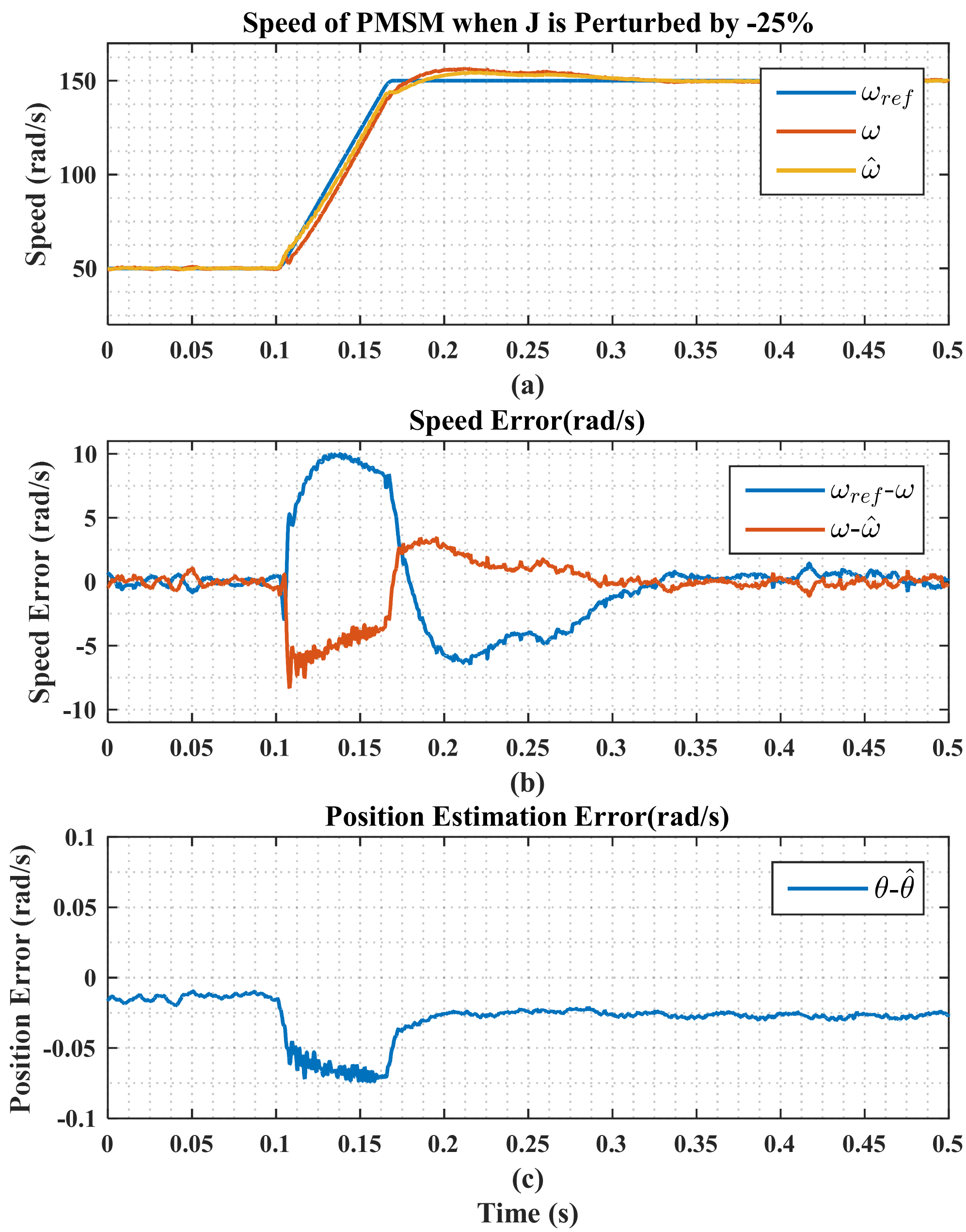


Figure B5.4 (a) Reference speed, speed of PMSM, and estimated speed, (b) Speed error from reference speed and speed estimation error, (c) Position estimation error.

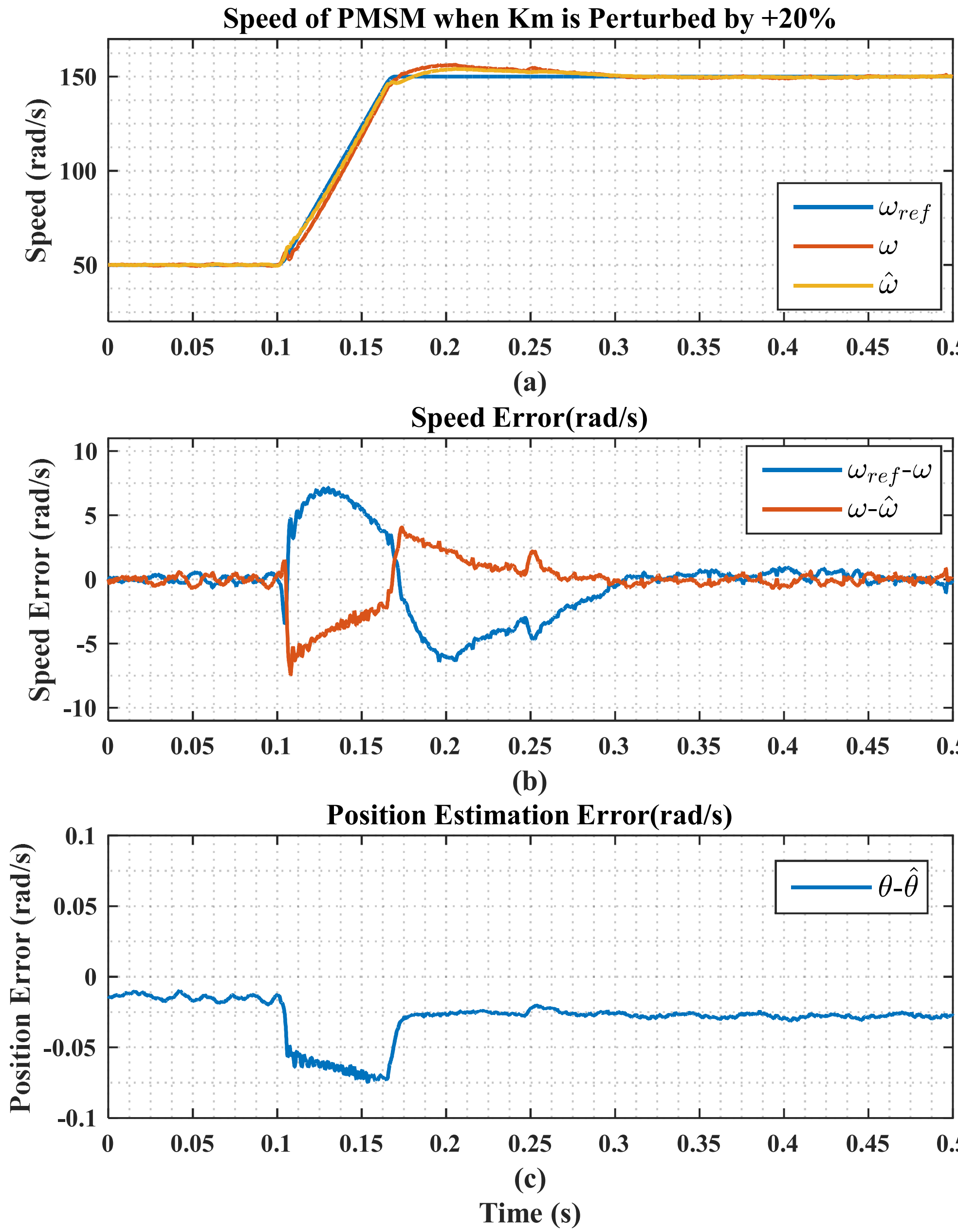


Figure B5.5 (a) Reference speed, speed of PMSM, and estimated speed, (b) Speed error from reference speed and speed estimation error, (c) Position estimation error.

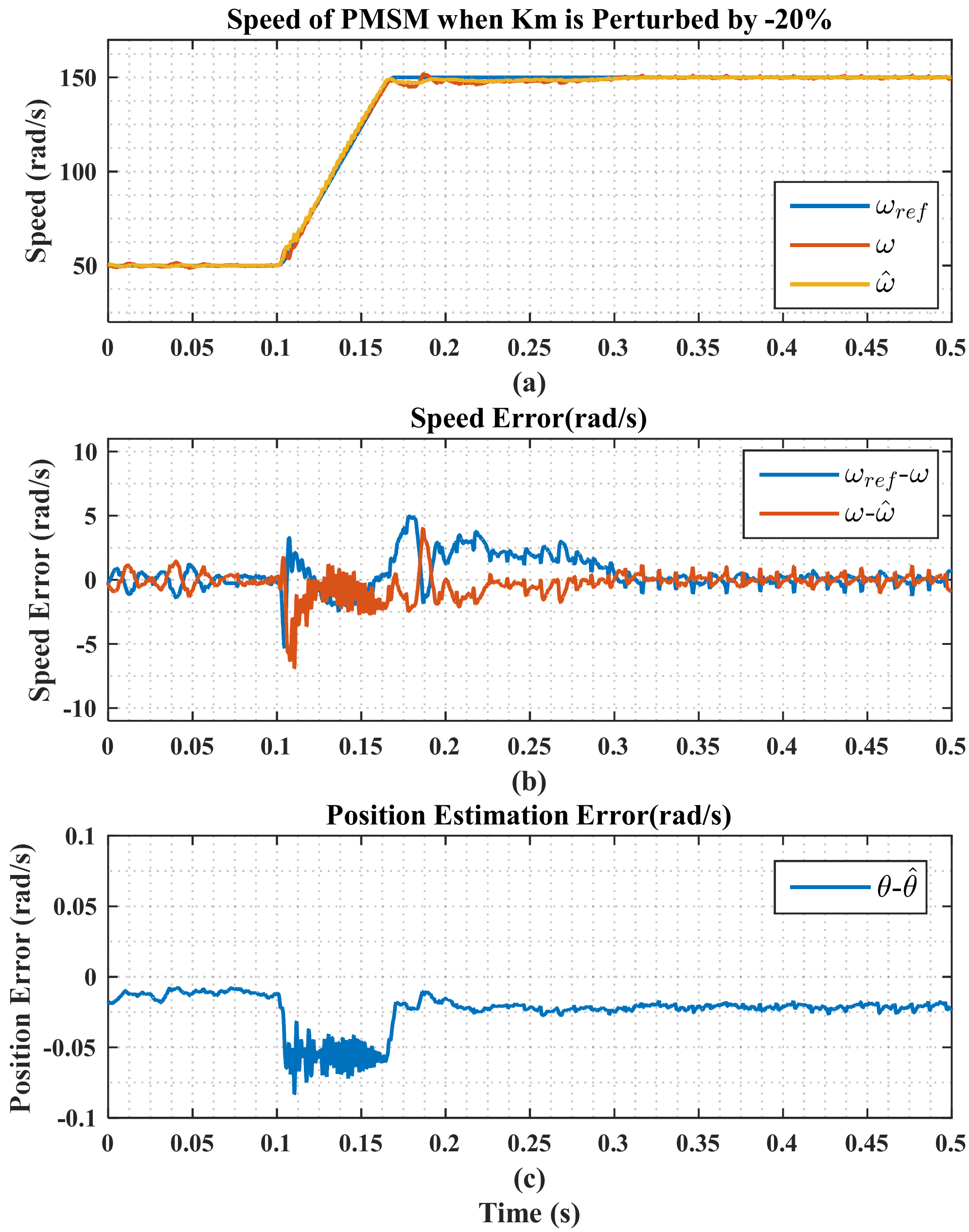


Figure B5.6 (a) Reference speed, speed of PMSM, and estimated speed, (b) Speed error from reference speed and speed estimation error, (c) Position estimation error.

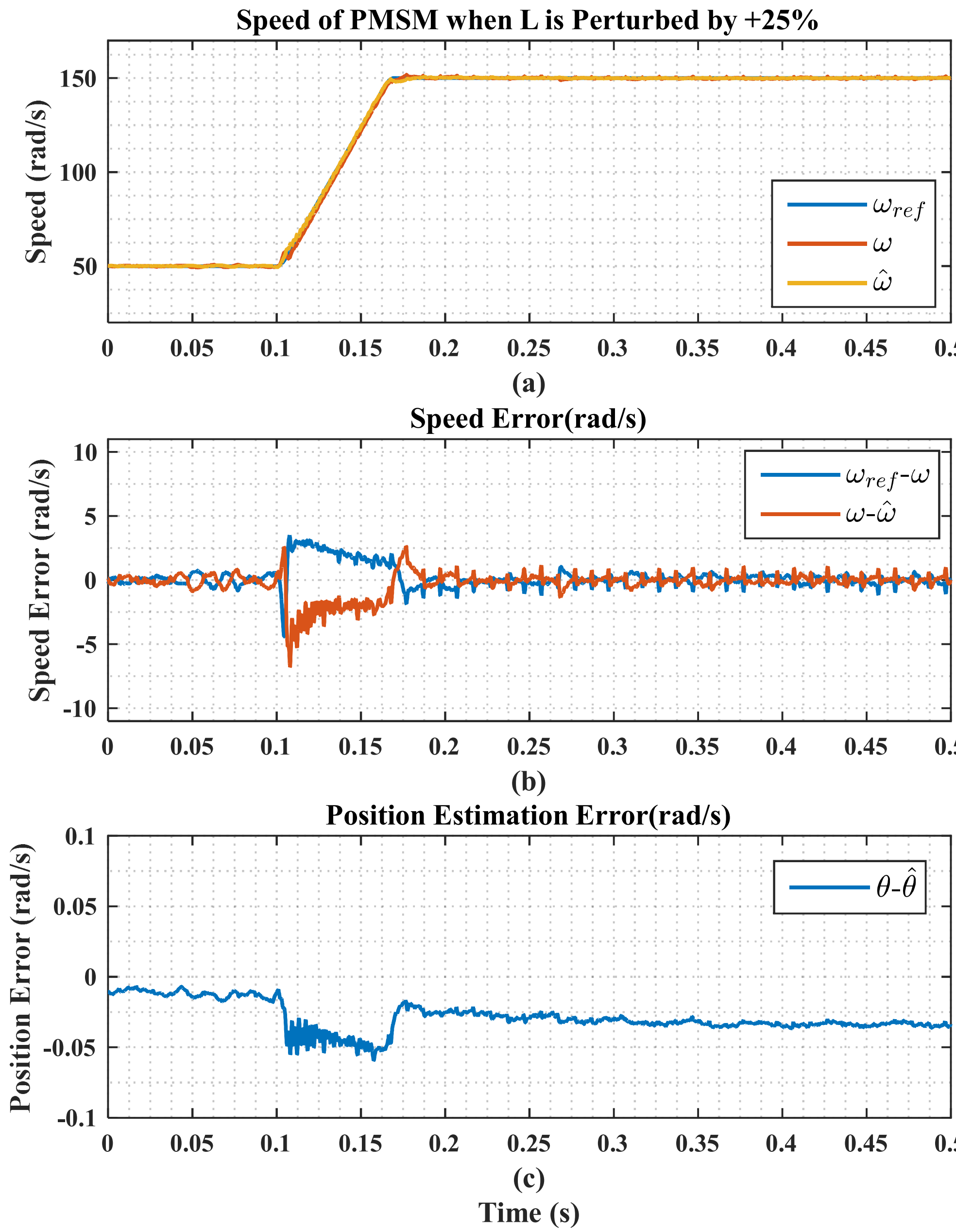


Figure B5.7 (a) Reference speed, speed of PMSM, and estimated speed, (b) Speed error from reference speed and speed estimation error, (c) Position estimation error.

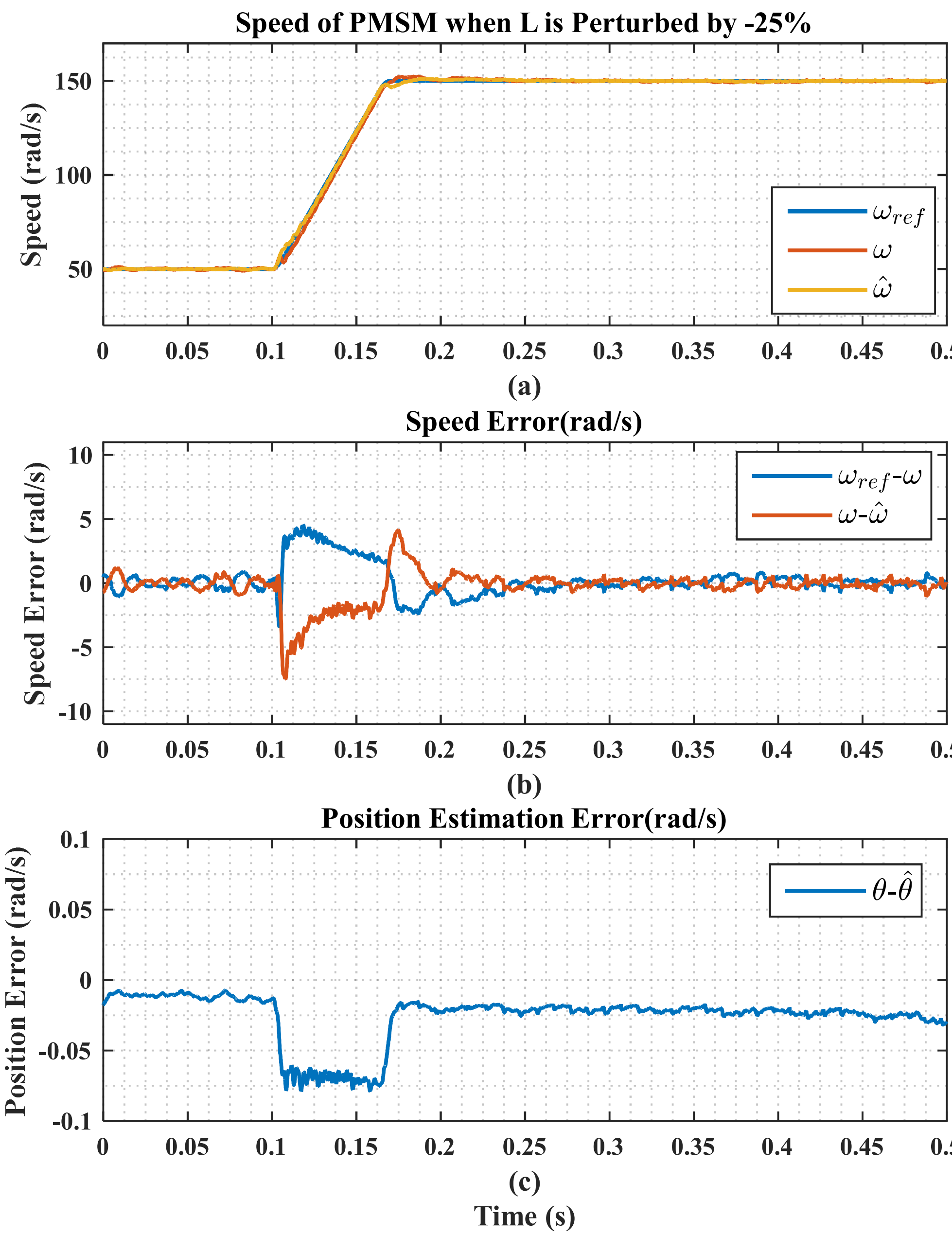


Figure B5.8 (a) Reference speed, speed of PMSM, and estimated speed, (b) Speed error from reference speed and speed estimation error, (c) Position estimation error.

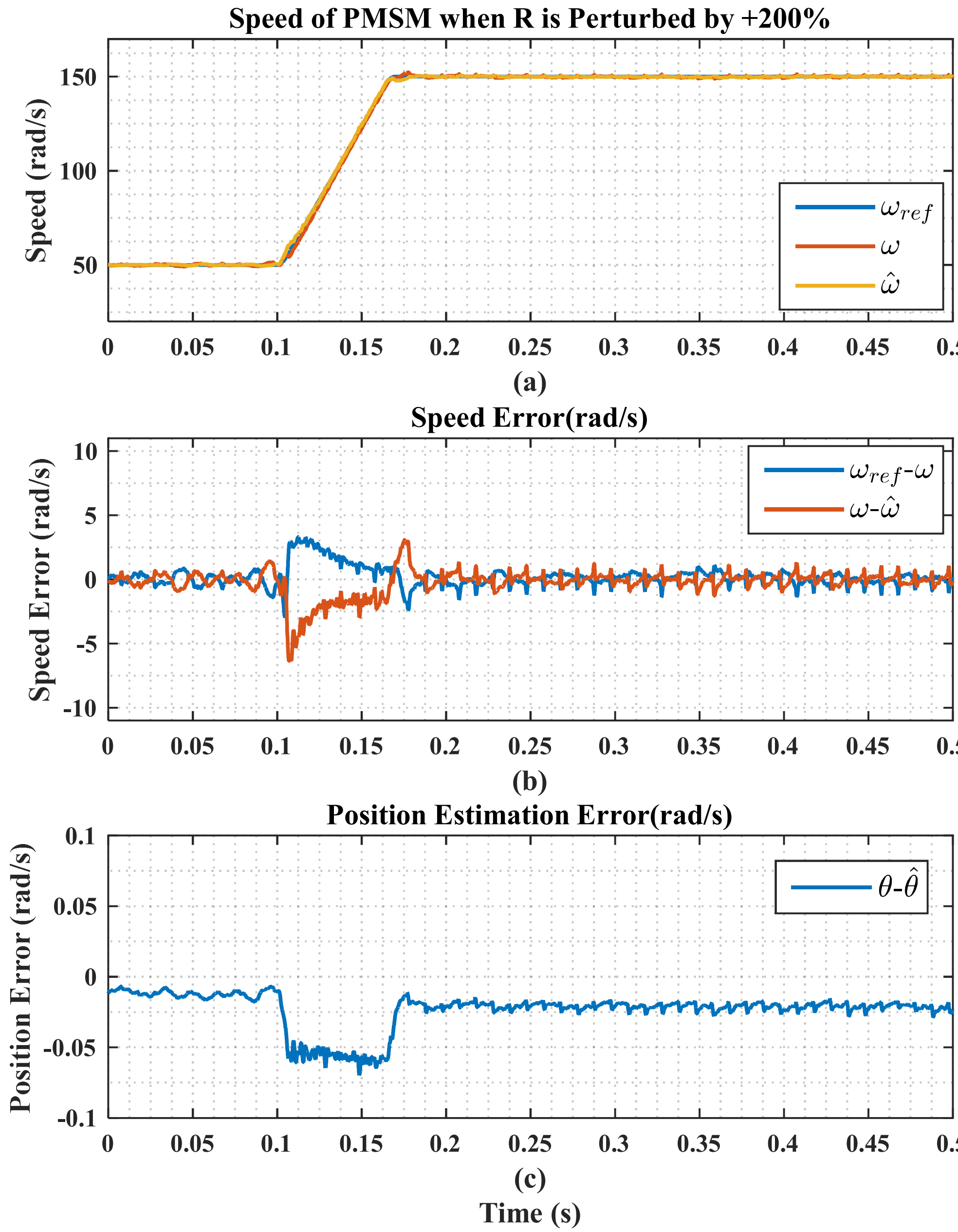


Figure B5.9 (a) Reference speed, speed of PMSM, and estimated speed, (b) Speed error from reference speed and speed estimation error, (c) Position estimation error.

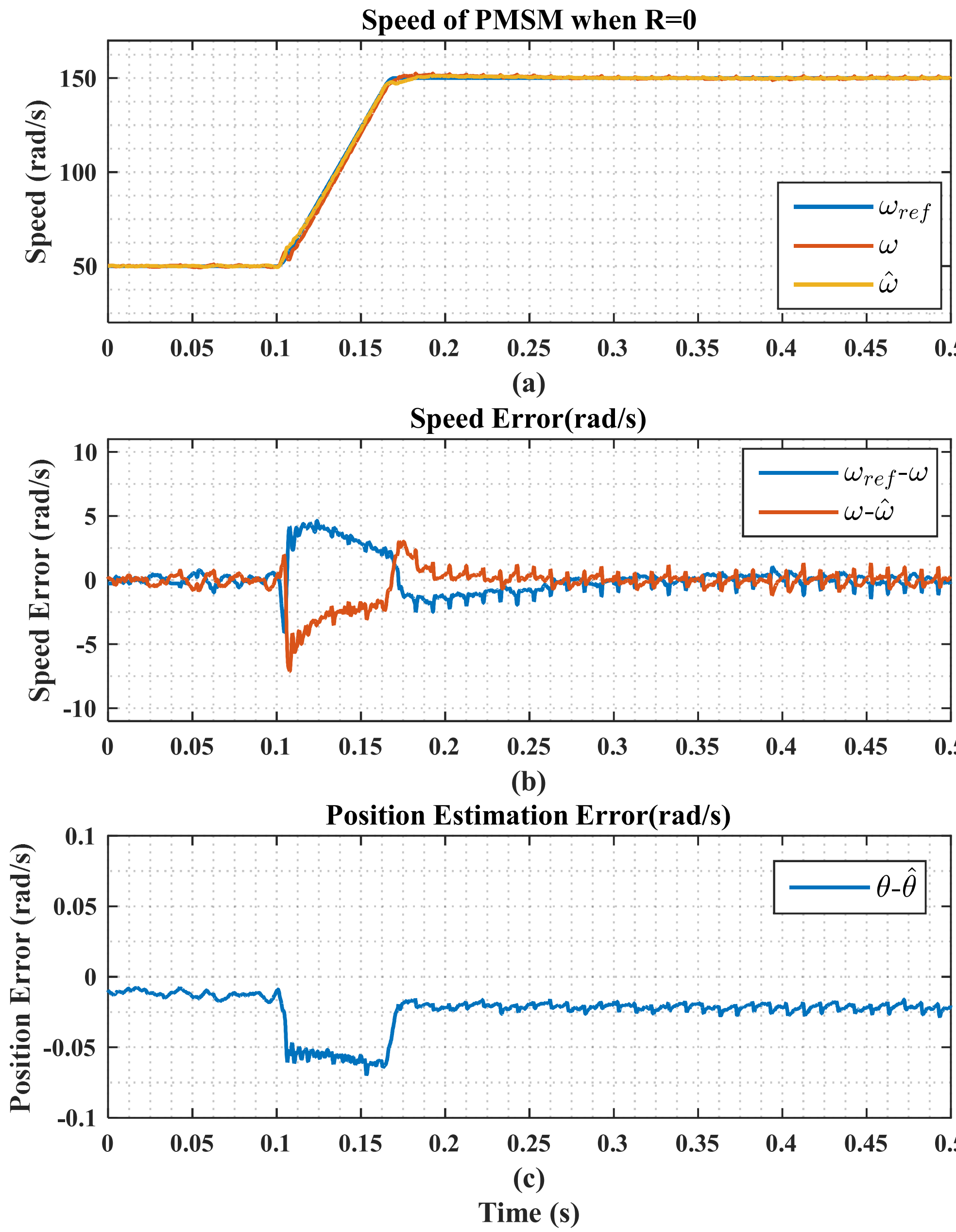


Figure B5.10 (a) Reference speed, speed of PMSM, and estimated speed, (b) Speed error from reference speed and speed estimation error, (c) Position estimation error.

# BIBLIOGRAPHY

## BIBLIOGRAPHY


[1] Werner Leonhard, “Control of Electrical Drive,” 3rd Edition. Springer 2001.

[2] Rik De Doncker, Duco W.J. Pulle, and Andre Veltman, “Advanced Electric Drives: analysis, modeling, and control.” Springer Dordrecht Heidelberg London New York 2011.

[3] R. Krishnan, “Electric Motor Drives: modeling, analysis, and control.” Upper Saddle River, New Jersey: Prentice Hall, 2001.

[4] L. Wang, S. Chai, D. Yoo, L. Gan, and K. Ng, “PID and Predictive Control of Electrical Drives and Power Converters Using MATLAB / Simulink.” Singapore Pte Ltd, Malaysia: John Wiley & Sons, 2015.

[5] X. G. Zhang, K. Zhao, and L. Sun, “A PMSMsliding mode control system based on a novel reaching law,” in Proc. Int. Conf. Electr. Mach. Syst., 2011, pp. 1–5.

[6] Z. Xiaoguang, S. Lizhi, Z. Ke, and S. Li, “Nonlinear speed control for PMSM system using sliding-mode control and disturbance compensation techniques,” IEEE Trans. Power Electron., vol. 28, no. 3, pp. 1358–1365, Mar. 2013.

[7] Li Xiaodi; Li Shihua, "Extended state observer based adaptive control scheme for PMSM system," in *Control Conference (CCC), 2014 33rd Chinese* , vol., no., pp.8074-8079, 28-30 July 2014.

[8] Jun Zhang; Zhaojun Meng; Rui Chen; Changzhi Sun; Yuejun An, "Decoupling control of PMSM based on exact linearization," in *Electronic and Mechanical Engineering and Information Technology (EMEIT), 2011 International Conference on* , vol.3, no., pp.1458-1461, 12-14 Aug. 2011.

[9] G. Zhu, L.-A. Dessaint, O. Akhrif and A. Kaddouri, "Speed tracking control of a permanent-magnet synchronous motor with state and load torque observer," Industrial Electronics, IEEE, vol. 47, no. 2, pp. 346-355, 2000.

[10] H. Sira-Ramirez, J. Linares-Flores, C. Garcia-Rodriguez and M. A. Contreras-Ordaz, "On the Control of the Permanent Magnet Synchronous Motor: An Active Disturbance Rejection Control Approach," in *IEEE Transactions on Control Systems Technology*, vol. 22, no. 5, pp. 2056-2063, Sept. 2014.

[11] N. T. T. Vu, H. H. Choi, R. Y. Kim and J. W. Jung, "Robust speed control method for permanent magnet synchronous motor," in IET Electric Power Applications, vol. 6, no. 7, pp. 399-411, August 2012.

[12] J. Chen, J. Zhang and R. Huang, "Disturbance observer based fuzzy speed regulator for permanent magnet synchronous motor," 2016 35th Chinese Control Conference (CCC), Chengdu, 2016, pp. 148-153.

[13] H. Liu and S. Li, "Speed Control for PMSM Servo System Using Predictive Functional Control and Extended State Observer," in *IEEE Transactions on Industrial Electronics*, vol. 59, no. 2, pp. 1171-1183, Feb. 2012.

[14] S. Li, J. Yang, W.-H. Chen, and X. Chen, Disturbance Observer-Based Control: Methods and Applications. Boca Raton, Florida: CRC Press, 2014.

[15] Z. Gao, "On the centrality of disturbance rejection in automatic control," ISA Transactions, Volume 53, Issue 4, July 2014, Pages 850-857.

[16] S. Bolognani, S. Calligaro and R. Petrella, "Design Issues and Estimation Errors Analysis of Back-EMF-Based Position and Speed Observer for SPM Synchronous Motors," in IEEE Journal of Emerging and Selected Topics in Power Electronics, vol. 2, no. 2, pp. 159-170, June 2014.

[17] C. Olivieri and M. Tursini, "A novel PLL scheme for a sensorless PMSM drive overcoming common speed reversal problems," International Symposium on Power Electronics Power Electronics, Electrical Drives, Automation and Motion, Sorrento, 2012, pp. 1051-1056.

[18] L. Harnefors and H. -. Nee, "A general algorithm for speed and position estimation of AC motors," in IEEE Transactions on Industrial Electronics, vol. 47, no. 1, pp. 77-83, Feb. 2000.

[19] R. Ortega, L. Praly, A. Astolfi, J. Lee and K. Nam, "Estimation of Rotor Position and Speed of Permanent Magnet Synchronous Motors With Guaranteed Stability," in IEEE Transactions on Control Systems Technology, vol. 19, no. 3, pp. 601-614, May 2011.

[20] J. Solsona, M. I. Valla and C. Muravchik, "Nonlinear control of a permanent magnet synchronous motor with disturbance torque estimation," in *IEEE Transactions on Energy Conversion*, vol. 15, no. 2, pp. 163-168, June 2000.

[21] S. A. A. Rizvi, A. Y. Memon "An extended observer based robust nonlinear speed sensorless controller for a PMSM," International Journal of Control, Jan 2018.

[22] A. Y. Memon and S. A. A. Rizvi, "Robust output feedback linearizing speed sensorless control of PMSM," 2015 IEEE Conference on Control Applications (CCA), Sydney, NSW, 2015, pp. 359-364.

[23] S. Po-ngam and S. Sangwongwanich, "Stability and Dynamic Performance Improvement of Adaptive Full-Order Observers for Sensorless PMSM Drive," in *IEEE Transactions on Power Electronics*, vol. 27, no. 2, pp. 588-600, Feb. 2012.

[24] D. Bao, X. Pan, Y. Wang, X. Wang and K. Li, "Adaptive Synchronous-Frequency Tracking-Mode Observer for the Sensorless Control of a Surface PMSM," in *IEEE Transactions on Industry Applications*, vol. 54, no. 6, pp. 6460-6471, Nov.-Dec. 2018.

[25] D. Liang, J. Li and R. Qu, "Sensorless Control of Permanent Magnet Synchronous Machine Based on Second-Order Sliding-Mode Observer With Online Resistance Estimation," in *IEEE Transactions on Industry Applications*, vol. 53, no. 4, pp. 3672-3682, July-Aug. 2017.

[26] Yongchang Zhang and Jiali Liu, "An improved Q-PLL to overcome the speed reversal problems in sensorless PMSM drive," 2016 IEEE 8th International Power Electronics and Motion Control Conference (IPEMC-ECCE Asia), Hefei, 2016, pp. 1884-1888.

[27] Ji-Hoon Jang; Seung-Ki Sul; Jung-Ik Ha; Ide, K.; Sawamura, M., "Sensorless drive of surface-mounted permanent-magnet motor by high-frequency signal injection based on magnetic saliency," in Industry Applications, IEEE Transactions on , vol.39, no.4, pp.1031-1039, July-Aug. 2003.

[28] G. Zhang, G. Wang and D. Xu, "Saliency-based position sensorless control methods for PMSM drives - A review," in Chinese Journal of Electrical Engineering, vol. 3, no. 2, pp. 14-23, September 2017.

[29] G. Wang, R. Yang, and D. Xu, "DSP-Based Control of Sensorless IPMSM Drives for Wide-Speed-Range Operation," IEEE Trans. Ind. Electron., vol. 60, no. 2, pp. 720–727, Feb. 2013.

[30] M. Seilmeier and B. Piepenbreier, "Sensorless control of PMSM for the whole speed range using two-degree-of-freedom current control and HF test current injection for low-speed range," IEEE Trans. Power Electron., vol. 30, no. 8, pp. 4394–4403, Aug. 2015.

[31] X. Jin, R. Ni, W. Chen, F. Blaabjerg and D. Xu, "High-Frequency Voltage-Injection Methods and Observer Design for Initial Position Detection of Permanent Magnet Synchronous Machines," in IEEE Transactions on Power Electronics, vol. 33, no. 9, pp. 7971-7979, Sept. 2018.

[32] L.B. Freidovich and H.K. Khalil, "Performance recovery of feedback linearization-based designs", IEEE Trans. Automat. Control, 53(2008), 2324-2334.

[33] John Chiasson, Modeling and high-Performance Control of Electric Machines. Hoboken, New Jersey: John Wiley & Sons, Inc, 2005. Ch9.

[34] Hassan K. Khalil, Nonlinear Systems. Upper Saddle River, New Jersey: Prentice Hall, 2002.

[35] A. A. Alfehaid, E. G. Strangas and H. K. Khalil, "Sensorless Speed Control of PMSM Using Extended High-Gain Observers,"*2019 American Control Conference (ACC)*, Philadelphia, PA, USA, 2019, pp. 2576-2581.

[36] N.P Quang and J.-A Dittrich, “Vector Control of Three-Phase AC Machines,” 2nd editon. Springer-Verlag Berlin Heidelberg 2015.

[37] Jing Lei and H. K. Khalil, "High-gain observers in the presence of sensor nonlinearities,"*2017 American Control Conference (ACC)*, Seattle, WA, 2017, pp. 3282-3287.